

Organic Photorefractives: Mechanisms, Materials, and Applications

Oksana Ostroverkhova^{*,†} and W. E. Moerner[‡]

Department of Physics, University of Alberta, Edmonton, Alberta, Canada T6G 2J1, and Department of Chemistry, Stanford University, Stanford, California 94305-5080

Received September 10, 2003

Contents

1. Introduction	3267	6.7. Other Materials Directions	3298
2. Necessary Elements for Photorefractivity: Materials Design	3269	6.7.1. Hybrid Organic–Inorganic Composites and Glasses	3298
3. Theoretical Description of the Photorefractive Effect in Organic Materials	3271	6.7.2. Electron-Transporting and Bipolar Organic Materials	3299
3.1. Space-Charge Field Formation	3271	6.7.3. Sol-Gels	3299
3.2. Orientational Enhancement Effect	3274	7. Applications and Novel Effects	3300
4. Experimental Techniques	3275	7.1. Applications	3300
4.1. Photorefractive Measurements	3275	7.1.1. Data Storage	3300
4.1.1. Two-Beam Coupling	3275	7.1.2. Image Processing	3302
4.1.2. Four-Wave Mixing	3277	7.1.3. Nondestructive Testing	3305
4.1.3. Photoelectromotive Force	3278	7.2. Novel Optical Effects	3306
4.1.4. Photorefractive Gratings Written via Two-Photon Excitation	3278	7.2.1. Spatial Solitons	3306
4.2. Experimental Techniques for Probing Various Processes Relevant to Photorefractivity	3279	7.2.2. Other Space-Charge Field Related Effects	3307
4.2.1. Photoconductive Properties	3279	8. Conclusions and Outlook	3308
4.2.2. Orientational Properties	3279	9. Abbreviations	3309
5. Physical Studies	3279	10. Acknowledgment	3310
5.1. Materials Study of Key Components	3279	11. References	3310
5.1.1. Sensitizers	3279		
5.1.2. Photoconductors	3282		
5.1.3. Chromophores	3283		
5.1.4. Plasticizers	3284		
5.1.5. Other Dopants	3284		
5.2. Improving the Photorefractive Performance by Tuning the Experimental Conditions	3284		
5.2.1. Fine-Tuning the Temperature	3285		
5.2.2. Preillumination Effects	3285		
5.3. Characterization Issues and Caveats	3287		
5.3.1. Photorefractive Response Speed: Photoconductivity or Orientationally Limited?	3287		
5.3.2. Traps and Grating Dark Decay	3288		
5.3.3. Other Concerns	3288		
6. New Photorefractive Materials	3289		
6.1. Polymer Composites	3289		
6.2. Organic Amorphous Glasses	3292		
6.3. Fully Functionalized Polymers	3294		
6.4. Polymer-Dispersed Liquid Crystals	3295		
6.5. Other Liquid Crystal-Containing Materials	3296		
6.6. Near-Infrared-Sensitive Materials	3297		

1. Introduction

For many years, considerable research efforts have been directed toward exploring the interaction between light and matter for the prospective replacement of electronic devices with faster, more sensitive, and more reliable optical devices. Therefore, materials whose optical properties are sensitive to light, including nonlinear optical (NLO) materials, have attracted attention. An important subset of NLO materials are materials that exhibit the photorefractive (PR) effect, or PR materials. The PR effect refers to spatial modulation of the index of refraction under nonuniform illumination via space-charge-field formation and electro-optic nonlinearity. The effect arises when charge carriers, photogenerated by a spatially modulated light intensity, separate by drift and/or diffusion processes and become trapped to produce a nonuniform space-charge distribution. The resulting internal space-charge electric field then modulates the refractive index to create a phase grating, or hologram, which can diffract a light beam. Because such a hologram can typically be erased by uniform optical illumination, PR holograms are dynamic, that is, they may be erased and rewritten, one of many properties that distinguish PR materials from other mechanisms for hologram formation.¹ The PR effect was first observed in 1966 in a LiNbO₃ crystal,² a discovery that launched extensive studies of the effect in inorganics. Until 1990, all PR materi-

* To whom correspondence should be addressed.

† University of Alberta, phone: 780-492-3960; fax: 780-492-0714; e-mail: oksanao@ualberta.ca.

‡ Stanford University, phone: 650-723-1727; fax: 650-725-0259; e-mail: wmoerner@stanford.edu.



Oksana Ostroverkhova (Franchuk) was born in 1973 in Kiev, Ukraine. After receiving Diploma with Honors in Physics and Optical Engineering from Kiev Shevchenko University (Kiev, Ukraine) in 1996, she pursued graduate study in physics, specializing in the photoconductive and nonlinear optical properties of polymers and liquid crystals, at Case Western Reserve University (Cleveland, USA) in the group of Prof. K. D. Singer and obtained a Ph.D. in Physics in 2001. Her postdoctoral work at the Department of Chemistry at Stanford University (Stanford, USA) in the group of Prof. W. E. Moerner involved physics and applications of photorefractive organic materials. Currently, Dr. Ostroverkhova is a Killam Memorial Fellow in the group of Prof. F. A. Hegmann at the Department of Physics at the University of Alberta (Edmonton, Canada). Her current research utilizes THz spectroscopy for probing transient photoconductivity in organic semiconductors.



William Esco (W. E.) Moerner was born in 1953 in Pleasanton, CA. After receiving three bachelor's degrees (Physics, Electrical Engineering, and Mathematics) in 1975 from Washington University, St. Louis, he obtained the M.S. (1978) and Ph.D. (1982) in Physics from Cornell University in the group of Prof. A. J. Sievers III. He then spent 13 years as a Research Staff Member, Project Leader, and Manager at the IBM Almaden Research Center in San Jose, California. After an appointment as Visiting Guest Professor of Physical Chemistry at ETH-Zuerich (1993–1994), he assumed the Distinguished Chair in Physical Chemistry in the Department of Chemistry and Biochemistry at the University of California, San Diego, in 1995. His research group moved to Stanford University, where he became Professor of Chemistry in 1998 and Harry S. Mosher Professor in 2003. He received the Earle K. Plyler Prize for Molecular Spectroscopy in 2001, and is a Fellow of the American Physical Society, the Optical Society of America, the American Academy of Arts and Sciences, and the American Association for the Advancement of Science. Since joining academia, Dr. Moerner's group has explored mechanisms of photorefractivity in polymers as well as room-temperature single-molecule spectroscopy and microscopy in crystals, polymers, and biomolecules, where the single molecule is a nanoscale object interacting with light.

als were inorganic crystals such as LiNbO_3 , KNbO_3 , BaTiO_3 , $\text{Bi}_{12}\text{SiO}_{20}$ (BSO), $\text{Sr}_x\text{Ba}_{1-x}\text{NbO}_3$, InP:Fe , GaAs , multiple-quantum-well semiconductors, and several others.^{3–5} Many potentially important applications

have been proposed and demonstrated for PR inorganics, including high-density optical data storage, image processing (correlation, pattern recognition), phase conjugation, optical limiting, simulations of neural networks and associative memories, and programmable optical interconnection. However, the difficult crystal growth and sample preparation required for inorganic PR crystals has limited their use in these applications. In contrast, organic PR materials and, in particular, polymeric and/or glassy PR materials, offer ease and flexibility of fabrication and control over the properties, which serves as one of the reasons for pursuing the development of organic PR materials. Another motivation comes from a consideration of a particular figure-of-merit that compares the refractive index change possible in different materials (assuming equal densities of trapped charges). This figure-of-merit may be defined as $Q = n^3 r_e / \epsilon_r$, where n is the optical index of refraction, r_e is the effective electro-optic coefficient, and ϵ_r is the relative dielectric constant. Q approximately measures the ratio of the optical nonlinearity to the screening of the internal space-charge distribution by medium polarization. For inorganics, it is well-known that Q does not vary much from material to material, which is a result of the fact that the optical nonlinearity is driven chiefly by the large ionic polarizability. For organics, however, the nonlinearity is a molecular property arising from the asymmetry of the electronic charge distributions in the ground and excited states.⁶ For this reason, in organics large electro-optic coefficients are not accompanied by large dc dielectric constants; thus, a potential improvement in performance of up to a factor of 10 or more in Q is possible with organic PR materials.

It is important to avoid confusing the PR effect with the large number of other local mechanisms which can modify the index of refraction of a material (n) in response to an optical beam, such as photochromism, thermochromism, thermorefractive, generation of excited states, conventional electronic $\chi^{(3)}$ (i.e., $n = n_0 + 12\pi^2 \chi^{(3)} I / (n_0^2 c)$, where n_0 is the refractive index in the absence of illumination, I is the light intensity, and c is the speed of light), and so forth.^{1,7} All of these local mechanisms lack the nonlocal aspect of the PR effect arising from the physical motion of charges in the material, usually over a distance on the order of micrometers. This charge transport leads to a spatial phase shift (displacement) between the incident light intensity pattern and the refractive index modulation. An important consequence of this phase shift is energy transfer between two light beams interfering in a PR medium, called asymmetric two-beam coupling (2BC, described in section 4.1.1). If the coupling is sufficiently strong, the 2BC gain may exceed the absorption and reflection losses of the sample, and optical amplification can occur. This cannot occur with a thick hologram in any local material (unless the light intensity pattern is translated at a particular rate,⁸ or the material is thin and has very large index modulation^{9,10}). Recently, the 2BC effect was claimed in thick films of non-PR materials.¹¹ However, later this observation was attributed to temporal instability of the laser system

which led to 2BC due to a moving grating effect.¹² Many of the applications that have been proposed rely on the 2BC gain, including coherent image amplification, novelty filtering, self-phase conjugation, beam fanning limiters, and simulations of neural networks and associative memories.^{5,13–16}

In 1990, the first observation of the PR effect in an organic material utilized a carefully grown nonlinear organic crystal COANP doped with TCNQ.^{17,18} The growth of high-quality doped organic crystals, however, is a difficult process because most dopants are expelled during the crystal preparation, but one additional crystalline material has been reported.¹⁹ Polymeric and/or glassy materials, on the other hand, can be doped with various molecules of quite different sizes with relative ease. Further, polymers and/or glasses may be formed into a variety of thin-film and waveguide configurations as required by the application (section 7). The second-order nonlinearity of polymers containing nonlinear chromophores can be produced by poling, whereas in crystals one may only consider the relatively rare subset of crystals with noncentrosymmetric crystal structures.

The first proven polymeric PR material²⁰ was made in 1990 and was composed of a NLO epoxy polymer bisA-NPDA which was made photoconductive by doping with 30 wt % of the hole transporting agent DEH. This material provided a key proof-of-principle that the simultaneous requirements of optical nonlinearity, charge generation, transport, trapping, and absence of interfering photochromic effects can be combined in one material to produce photorefractivity.

PR polymer composites are now numerous, and the performance of most new materials exceeds that for conventional inorganic crystals. Comprehensive reviews covered developments from the inception of the field up through late 1993²¹ and further until late 1996.²² Refs 21 and 22 should be consulted for basic background material; recent reviews of various classes of PR organic materials (general overview,²³ fully functionalized polymers,²⁵ liquid crystal (LC)-containing materials,²⁶ chromophores, and low-molecular-weight glasses^{24,27}) may also be consulted. The present review complements ref 22 by describing new models, physical studies, applications, novel optical effects, and materials with high diffraction efficiency and/or high beam coupling gain from 1997 up to March 2004. The goal of this review is to describe the current status of the field of PR organic materials. Therefore, there will be important recent articles that we neglect to cite, and we apologize for this in advance.

The structure of this paper is as follows. Section 2 reviews the fundamentals of the PR effect by describing the necessary elements for photorefractivity that must be considered in materials design. Section 3 describes models developed for PR organic materials that take into account differences in physical properties between organic and inorganic materials, in particular, differences in charge generation, transport and trapping mechanisms, and in the electric field-dependent nonlinearity which leads to the orientational enhancement (OE) effect. Section 4 reviews

various experimental techniques developed for characterization of PR materials. Section 5 describes recent studies of the influence of various physical parameters and constituents of the PR composite on overall PR performance and outlines the main strategies developed to understand the limitations of the materials and optimize their performance. Section 6 reviews the best up-to-date PR polymer composites, organic glasses, fully functionalized and liquid crystalline materials as well as outlines new materials classes under exploration. Abbreviated names of all the compounds are used throughout the paper; the full names of these compounds can be found in the list of abbreviations or in the primary references. Where necessary, the concentration of the constituents in composites is given in weight percents unless stated otherwise. Section 7 summarizes the applications and various space-charge field-related effects observed in high-performance PR organic materials, and section 8 concludes with an outlook for this field.

2. Necessary Elements for Photorefractivity: Materials Design

On a basic level, the mechanism for the PR effect in polymers is the same as in inorganic crystals; however, different constituents give rise to the required properties. The PR effect requires both photoconductivity and a dependence of the optical index of refraction on electric field. In organics, these properties necessary for producing a PR phase hologram are generally provided by a combination of functional components in the material that includes a photoinduced charge generator, a transporting medium, trapping sites, and molecules that provide optical nonlinearity. However, the simple presence of these elements in a material does not guarantee that any diffraction grating produced by optical illumination arises from the PR effect—in practice experiments must be performed to show that the PR effect is the dominant mechanism of grating formation.

Figure 1 illustrates the well-known microscopic processes required to produce a hologram by the PR mechanism.²⁸ Two intersecting coherent beams of light produce a standing-wave interference pattern. This time-independent but spatially modulated intensity has a spatial wavelength or periodicity Λ given by

$$\Lambda = \frac{\lambda}{2n \sin[(\theta_2 - \theta_1)/2]} \quad (1)$$

where n is the index of refraction of the material, λ is the optical wavelength in a vacuum, and θ_1 and θ_2 are the internal angles of incidence of the two writing beams relative to the sample normal. For normally accessible opening angles between the two light beams and visible optical wavelengths, Λ is in the range 0.3–20 μm . The direction normal to the light and dark planes defines the direction of the grating wavevector \mathbf{K} , the magnitude of which is given by $K = 2\pi/\Lambda$. If one denotes the x axis as the direction of the grating wavevector, the optical intensity follows the sinusoidal pattern shown in Figure 1a.

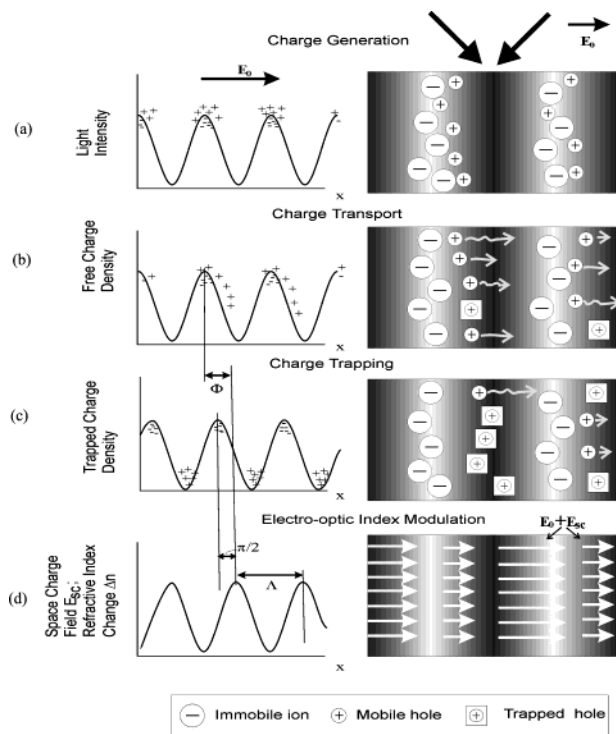


Figure 1. Photorefractive grating formation: (a) charge generation; (b) charge transport; (c) charge trapping; (d) space-charge field formation and refractive index modulation.

The first physical process required for the PR effect is the generation of mobile charge in response to the spatially varying illumination. This may be viewed as the separation of electrons and holes induced by the absorption of the optical radiation, denoted as plus and minus charges in the figure. In organic materials, photogeneration of charge is likely to be strongly field-dependent, and here we assume a constant electric field \mathbf{E}_0 is applied along the x -direction. Photoinduced charge generation is often provided by a molecule that absorbs light and then becomes reduced, injecting a hole into the material. (Electron generation and transport, although also possible, has not been widely utilized in organics (section 6.7.2), so we focus on holes here.) Because PR polymers are dynamic (erasable) hologram materials, it is generally desirable to later oxidize the charge generation site back to its original state, so reversible reduction/oxidation is important. Most widely used generators are donor–acceptor charge-transfer complexes formed between carbazole and TNF, TNFM, or fullerenes such as C_{60} (section 5.1.1). For example, the fullerene C_{60} was found to be an efficient charge generator due to its large triplet yield, broad absorption, solubility, and multiple stable reduced states.^{29,30}

The second element for the PR effect is transport of the generated charges, with one carrier being more mobile than the other. In Figure 1b, the holes are shown to be more mobile, which is the more common case for organics, although several electron and bipolar transporting PR organic materials have been reported^{31–34} (section 6.7.2). (If both carriers are equally mobile, the resulting space-charge distribution could have zero internal space-charge electric

field and hence no PR effect.) The physical processes giving rise to charge transport are either diffusion due to charge density gradients or drift in an externally applied electric field, and both generally proceed by hopping of the charge from transport site to transport site. Because in most organic materials the ability of generated charges to move by diffusion alone in zero electric field is quite limited, drift in the applied field is the dominant mechanism for charge transport. Another mechanism that may assist in charge separation is the photovoltaic effect. The field of organic photovoltaic materials has developed rapidly over the past several years.^{35–37} In particular, blends containing conjugated polymers and fullerene derivatives or quantum dots were found to be promising for organic solar cells.^{38,39} While systems based on similar materials were utilized in PR composites,^{40–43} no contribution of the photovoltaic effect (which would manifest itself by light-induced charge separation in the built-in internal electric field that exists in photovoltaic materials in the absence of applied electric field or prepoling) in the PR performance has been reported thus far.

The charge (hole) transporting function is generally provided by a network of oxidizable molecules (charge transport agents, CTA) which are close enough together in space to provide for hopping motion. Examples of transporting molecules are carbazoles, hydrazones such as DEH, and arylamines such as TTA or TPD, which are electron-rich and consequently have low oxidation potential. The field of electrophotography has identified many such molecules,⁴⁴ which may be added as dopants to an inert binder polymer in relatively high concentration (>25 wt % usually), or may be attached to the binder polymer backbone, as in PVK. In addition, conjugated polymers, characterized by improved charge carrier mobility due to an extended π -electron network along the polymer backbone,⁴⁵ were also explored as charge transporters.^{40–43} In all systems, energetics require that the highest occupied energy level of the photo-generator be lower than that for the transporting molecules.

The third element for the PR effect, especially when long grating lifetimes are desired, is the presence of trapping sites which hold the mobile charge. In general terms, a trapping site is a local region of the material where the mobile charge is prevented from participating in transport for some period of time. For example, in a hopping picture, a site with lower total energy for the hole may act as a trap, and the lifetime of the carrier in the trap will be determined by the trap depth compared to thermal energies. Since 1997, many studies were carried out to understand the nature of traps in PR materials,^{46–50} and the key relevant results will be discussed in sections 3.1 and 5.1.

After separation of charge carriers occurs, the resulting space-charge density is shown in Figure 1c. (More precisely, only the lowest-order sinusoidal component at the grating spatial frequency is shown; higher spatial frequencies lead to more complicated optical effects.) Poisson's equation of electrostatics dictates that such a charge distribution produces a

sinusoidal space-charge electric field as shown in Figure 1d, with the resulting internal electric field shifted in space by 90° relative to the trapped charge, or one-quarter of the grating wavelength.

The final requirement for photorefractivity is that the optical index of refraction of the material must change in response to the local electric field. Because of the sinusoidally varying space-charge electric field, a spatial modulation of the index of refraction results as shown in Figure 1d. For example, if the material exhibits a linear electro-optic effect, the magnitude of the index modulation Δn is related to the magnitude of the space-charge field modulation E_{sc} as follows

$$\Delta n = -(1/2)n^3 r_e E_{sc} \quad (2)$$

where r_e is an effective electro-optic coefficient. A field-dependent refractive index can also occur by a quadratic or Kerr orientational effect. Detailed discussion of the mechanisms producing electric field-induced birefringence in PR organic materials can be found in refs 22, 51, and 52, summarized in section 3.2. To provide an electric field-dependent refractive index in organics, molecular functionalities that possess high ground-state dipole moment and large linear polarizability anisotropy (birefringent molecules) or first hyperpolarizability (NLO chromophores) are added to the material in high concentration. Because the majority of such functionalities utilized in PR composites exhibit both birefringent and NLO properties, it is conventional to refer to these molecules as to NLO chromophores, a term we will use throughout this review.

According to eq 2, the sinusoidally varying space-charge field E_{sc} leads to a sinusoidally varying index modulation, which is a grating or hologram that can diffract light. If the sample is much thicker than the grating wavelength, the grating is actually a volume hologram,⁵³ and readout of the grating occurs only when the Bragg condition is satisfied for the readout beam angle and optical wavelength.

The total spatial phase shift between the peaks of the optical intensity pattern in Figure 1a and the peaks of the index of refraction modulation in Figure 1d is denoted Φ . When the phase shift is nonzero, the index grating is a *nonlocal* grating, and this property (which arises fundamentally from charge transport over a macroscopic distance) is one of the most important special properties of PR materials, which leads to the 2BC effect and many fascinating applications.

3. Theoretical Description of the Photorefractive Effect in Organic Materials

In this section, we summarize the development of a theoretical model describing PR properties of organic materials, beginning with the critical foundations provided by the prior models for PR effects in inorganic crystals. Two main considerations created a need to modify previous theoretical descriptions of the PR effect in inorganics to capture the essential physical differences in organic materials. First of all, a simple band theory developed for inorganic crystals,

often referred to as the Kukhtarev model,⁵⁴ did not take into account several important aspects of charge generation, transport, trapping, and recombination that are intrinsic to organic materials. Furthermore, discovery of the OE effect (which does not exist in PR inorganic materials) in 1994 by Moerner and co-workers⁵¹ altered the picture of the electro-optical nonlinearity and led to an even more complicated description of the PR effect in organics. Overall, the process of PR grating formation in most organic materials can be viewed as a space-charge field formation followed by noninstantaneous reorientation of birefringent chromophores in response to the total local field arising from the space-charge field and the applied dc field. In section 3.1, we discuss the evolution of a phenomenological model describing the space-charge field formation in PR polymers, and in section 3.2 we will summarize the main points of the OE theory.

3.1. Space-Charge Field Formation

The starting point for the theoretical description of the PR effect was the system of nonlinear differential equations known as the standard band transport model developed for inorganic crystals.⁵⁴ Briefly, these rate equations for the density of charges contain terms for generation, diffusion, drift, recombination, and so on described above. Twarowski⁵⁵ modified the model to take into account the electric field dependence of the charge photogeneration efficiency. Schildkraut and Buettner⁵⁶ included the rate equation for trap density in the system of PR dynamical equations and took into account the field dependence of both photogeneration efficiency and carrier mobility. By considering several limiting cases, Schildkraut and Buettner have generated numerical solutions to the full set of equations by employing several simplifying assumptions about the trapping dynamics.⁵⁶ In a subsequent study of the rate equation model,⁵⁷ linearization was used to develop analytical solutions for the zero-order and first-order Fourier components of the charge density and space-charge field. The authors considered two limiting cases: (a) once a charge is trapped, it cannot be released (deep traps), and (b) no hole traps are present. For both cases, a steady-state analytical expression for the first-order Fourier component of the space-charge field (E_{sc}) was derived.⁵⁷ Using this expression, E_{sc} was calculated and shown to be in good agreement with the values obtained from numerical simulations using two kinds of boundary conditions that describe ohmic and Schottky types of electrical contacts, respectively. Cui et al.⁵⁸ took this study a step further and obtained an analytical solution for the space-charge field time evolution during the PR grating erasure, assuming that the zero-order parameters change instantaneously. Several cases were considered: (a) no traps, (b) deep inactive traps (trapped charge cannot be released), (c) deep optically active traps (charge can be released under illumination), and (d) shallow traps (charge can be released both optically and thermally). For each case, the zero-order free charge density, which affects the rate of PR grating erasure, was derived

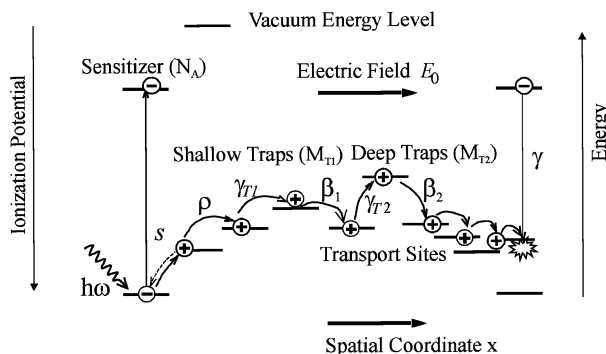


Figure 2. Schematic representation of the PR model. Symbols are described in the text. Reproduced with permission from ref 48. Copyright 2002 American Institute of Physics.

as a function of erasing beam intensity. By comparing the dependence of the speed of grating erasure on the erasing beam intensity, experimentally measured in a PVK/DEANST/TCP/C₆₀ composite, with analytical solutions, the authors concluded that the case of shallow traps provided the best description of their material.

Yuan et al.⁵⁹ followed the Fourier decomposition formalism and numerically modeled the kinetics of space-charge field as a function of light intensity and grating vector in the case of no traps. Further, the same group expanded their numerical simulations to the cases of arbitrary density of deep traps or high density of traps with arbitrary depth (in both cases, the detrapping is neglected) and simulated the electric-field dependence of the steady-state and temporal behavior of the space-charge field⁶⁰ as well as moving gratings driven with a periodic force of an arbitrary frequency ω .⁶¹ One of the results produced by this group was that the dependence of the space-charge field on total intensity of writing beams varied for different kinds of traps available in the material.⁶¹ For example, in the case of no traps, the space-charge field increased as a function of total incident intensity, while in the case of deep traps or low trap densities of arbitrary depth it decreased. In the case of high trap densities (on the order of acceptor density and higher), the space-charge field was independent of total incident intensity, the result predicted by Kukhtarev's model for inorganic crystals.⁵⁴ Experimental studies on materials with reliable control over trapping properties are needed to assess the validity of the described numerical predictions.

The PR model was further developed by Ostroverkhova and Singer⁴⁸ who introduced in the model two kinds of traps: shallow and deep. In this study, the term "deep" meant that the rate of thermal detrapping for these traps was at least an order of magnitude smaller than that of the shallow traps, but still having a nonzero probability for detrapping. The main focus of this study was to develop an understanding of trapping and recombination processes as well as to determine various photoelectric rates from the photocurrent dynamics to predict the time evolution of the space-charge field. The processes taken into account are depicted in Figure 2. A sensitizer (electron acceptor to generate a hole) with density N_A is excited and subsequently photo-

reduced by light of frequency ω with cross-section s . A free hole is injected into the transport manifold and hops between transport sites until it either becomes trapped or recombines with ionized acceptors with rate γ . Two kinds of traps with well-defined energy levels (set by ionization potential I_p), shallow traps (M_{T1}) and deep traps (M_{T2}), are considered. It is assumed that the trapping rate does not depend on the trap depth, so that shallow and deep traps are filled with the same trapping rate $\gamma_T = \gamma_{T1} = \gamma_{T2}$. This is an approximation that assumes Miller-Abrahams hopping rates⁶² for the process of filling traps of similar nature (e.g., both shallow and deep traps are neutral when empty). Detrapping proceeds with a thermal excitation rate β_1 for shallow traps or β_2 for deep traps, and optical detrapping is not taken into account. The modified system of nonlinear equations describing the PR dynamics is given by:⁴⁸

$$\begin{aligned} \frac{\partial \rho}{\partial t} &= \frac{\partial N_A^i}{\partial t} - \frac{\partial M_1}{\partial t} - \frac{\partial M_2}{\partial t} - \frac{1}{e} \frac{\partial J}{\partial x} \\ \frac{\partial M_1}{\partial t} &= \gamma_{T1}(M_{T1} - M_1)\rho - \beta_1 M_1 \\ \frac{\partial M_2}{\partial t} &= \gamma_{T2}(M_{T2} - M_2)\rho - \beta_2 M_2 \\ \frac{\partial N_A^i}{\partial t} &= sI(N_A - N_A^i) - \gamma N_A^i \rho \\ \frac{\partial E}{\partial x} &= \frac{e}{\epsilon_0 \epsilon} (\rho + M_1 + M_2 - N_A^i) \\ J &= e\mu\rho E - e\mu\xi \frac{\partial \rho}{\partial x} \end{aligned} \quad (3)$$

Here ρ is the free charge (hole) density, N_A is the total density of acceptors, N_A^i is the density of ionized acceptors, M_1 , M_2 , M_{T1} , M_{T2} are the densities of filled shallow traps, filled deep traps, and total shallow and deep trapping sites, respectively, E is the electric field, and I is the incident light intensity. J is the current density, μ is the charge carrier drift mobility, ξ is the diffusion coefficient given by $\xi = k_B T/e$. The quantity s is the cross-section of photogeneration (in the case of low absorption $s = \alpha\phi/(\hbar\omega N_A)$, where α is absorption coefficient, \hbar is Planck's constant divided by 2π , and ϕ is photogeneration efficiency), γ_{T1} , γ_{T2} , β_1 , β_2 are the trapping rates and detrapping rates for shallow and deep traps, respectively, γ is the recombination rate, and ϵ is the dielectric constant. The authors followed a Fourier decomposition approach similar to one used by Schildkraut and Cui⁵⁷ and considered separately the spatially uniform (zero-order) parameters and spatially varying (first-order) parameters. In addition to introducing a second trap level, this study took into account the time evolution of zero-order parameters, which has been neglected in all earlier studies. By relating the numerically simulated data to the experimentally observed dc photoconductivity transients, the authors determined detrapping and recombination rates as well as prod-

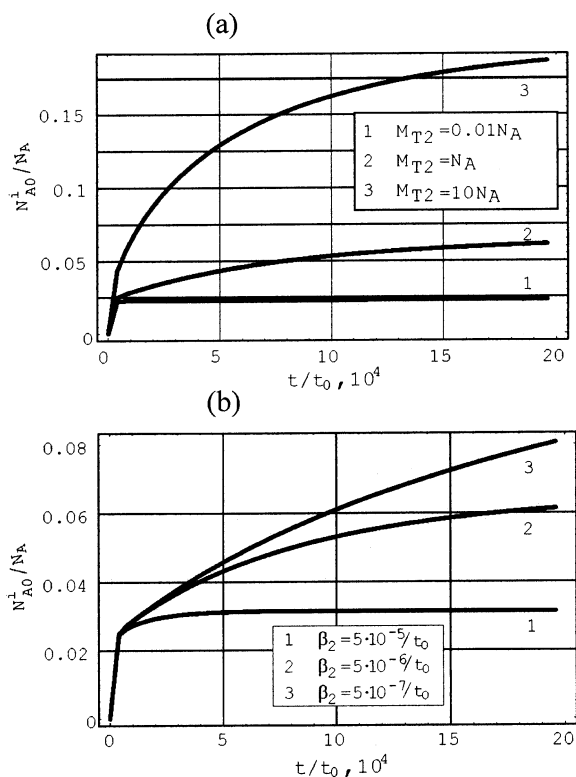


Figure 3. Time evolution of ionized acceptor density (N_{A0}^i) normalized by total acceptor density (N_A), simulated using eq 3 and photoelectric rates typical for PVK-based composites in the case of (a) various deep trap densities $M_{T2} = 0.01N_A$, N_A and $10N_A$ at fixed detrapping rate $\beta_2 = 5 \times 10^{-6}/t_0$, where $t_0 = 1/(\gamma_T M_{T1})$; (b) various detrapping rates $\beta_2 = 5 \times 10^{-5}/t_0$, $5 \times 10^{-6}/t_0$, $5 \times 10^{-7}/t_0$ at fixed deep trap density $M_{T2} = N_A$. Adapted from ref 48 with permission. Copyright 2002 American Institute of Physics.

ucts of trapping rates and trap densities. Combining these with charge carrier mobility and photogeneration efficiency obtained from the time-of-flight and xerographic discharge experiments, the authors were able to simulate numerically the space-charge field time evolution. The simulated growth of the space-charge field showed good agreement with the time evolution of the PR grating measured in the four-wave mixing (FWM) experiment for a number of PVK-based composites.⁴⁸

The main results from the numerical simulations for the zero-order variables were the following: (1) In agreement with previous experimental results by Grunnet-Jepsen et al.⁴⁶ (section 5.1.1), the growth of the ionized acceptor density (N_{A0}^i) upon uniform illumination was strongly affected by (compensating) trap densities available in the material as well as by trap depth. Figure 3 illustrates the growth of the ionized acceptor density (N_{A0}^i) normalized by total acceptor density (N_A), simulated using eq 3 with parameters typical for PVK-based materials' photoelectric rates, parametrized by the total deep trap density ($M_{T2} = 0.01N_A$, N_A , and $10N_A$ at fixed detrapping rate $\beta_2 = 5 \times 10^{-6}/t_0$, where $t_0 = 1/(\gamma_T M_{T1})$, Figure 3a) and by the deep trap depth ($\beta_2 = 5 \times 10^{-5}/t_0$, $5 \times 10^{-6}/t_0$, $5 \times 10^{-7}/t_0$ at fixed deep trap density $M_{T2} = N_A$, Figure 3b). (2) The steady-state density of ionized acceptors (N_{A0}^i) depended on the photogeneration cross-section (s) as $N_{A0}^i \sim s^{0.5}$. (3) The time

evolution of the free charge density upon uniform illumination strongly depended on trapping, detrapping, and recombination rates as well as trap densities.^{48,63}

Similarly, for the first-order properties, the key results were the following: (1) Out of all the parameters in eq 3, the photogeneration cross-section s followed by charge carrier mobility μ had the strongest impact on PR dynamics. For example, an order of magnitude increase in s led to an order of magnitude increase in PR speed. (2) Such effects as preillumination history dependence of the photoconductivity and space-charge field, experimentally observed in various systems,^{42,46,48,64,65} stemmed from deep trap filling (equivalent to an increase in M_2 of eq 3) accompanied by growth of ionized acceptor density (N_A^i) during the preillumination, which altered the initial conditions for both photoconductivity and PR experiments and therefore affected the observed photocurrent and space-charge field.

As a next step in assessing photoelectric parameters contributing to PR performance, Kulikovskiy et al.⁶⁶ further expanded the photocurrent dynamics study. Rise, decay, and steady-state values of the photocurrent during uniform illumination with a single pulse (with duration of 1–500 ms) were experimentally measured in the TPD-PPV/DMNPAA/MNPAA/DPP/PCBM composite. Various photoelectric rates were determined by fitting the experimental transients with eq 3 in the zero-order (spatial uniformity) approximation. In addition, the photocurrent transients from double pulse illumination were measured. By combining the experimental results from the single pulse experiments with measuring the photocurrent as a function of the time delay between the pulses in the double pulse experiments, the authors were able to separately determine trapping rates and trap densities—the parameters that could not be determined in previous studies.⁴⁸ Furthermore, using the photoelectric parameters measured, the effects of preillumination and time-gating on the space-charge field were numerically simulated and found to be in a good agreement with the experimental results previously obtained from the PR measurements carried out in the same TPD-PPV/DMNPAA/MNPAA/DPP/PCBM composite.^{42,66} We note that Marc et al. previously reported several studies of charge transport⁶⁷ and trapping properties⁶⁸ of PVK-based materials, in which charge carrier mobility, trap densities, carrier lifetimes, etc. were determined from the analysis of photocurrent dynamics. However, these studies did not take into account recombination of free charges with ionized acceptors, the process that plays an important role in PR organic materials.

Although understanding of the photoconductivity in PR organic materials has significantly improved over the past years, there are still issues that need to be resolved to facilitate the comparison between the theory and experiment. First of all, the zero- and first-order equations obtained from Fourier decomposition of eq 3 assume an infinite bulk material and do not take into account the possible effects of electrodes. As mentioned above, Schildkraut and

Cui⁵⁷ found good agreement between steady-state values for the free carrier density, amplitude, and phase of the space-charge field calculated analytically from the zero- and first-order dynamic equations (infinite bulk) and simulated using eq 3 (with a single trap level) with ohmic ("infinite" supply of charge from the electrodes) boundary conditions as well as with blocking (Schottky barrier) boundary conditions. However, a careful experimental study of both steady-state and dynamics of the photocurrent and space-charge field, with various electrode materials, is needed to probe the contribution of electrodes into experimental data. Second, the current PR model for organics does not take into account either electronic or ionic dark current. Because most PR materials perform the best at temperatures around or slightly above T_g (section 5.2.1), the dark current can become a concern when trying to optimize the material.⁶⁹ Third, the effects of nonuniform illumination due to absorption in the sample are not taken into account, yet may contribute to the experimental data.⁷⁰ Finally, effects of nonsinusoidal gratings due to fanning,⁷¹ grating bending,⁷² and grating competition^{73,74} are not taken into account, and therefore the results are limited to low applied electric fields. Therefore, further studies, especially those that combine theory and experiment, are required to elucidate the factors contributing to the overall PR performance.

As discussed in section 2, the primary mechanisms that lead to the PR effect in polymers are photoconductivity (steps 1–3, discussed above) and electric field-induced birefringence arising from NLO chromophore orientation (step 4). We now discuss the role of orientational effects in the PR effect in polymer composites.

3.2. Orientational Enhancement Effect

The last step in PR grating formation is concerned with the refractive index change in response to the space-charge field produced during steps 1–3 (eq 2). Initially, by analogy to inorganic crystals, this step was attributed to a linear electro-optic ($\chi^{(2)}$) effect exhibited by poled polymers containing NLO chromophores with high first hyperpolarizabilities (β_{ijk}). However, it turned out that experimentally observed 2BC gains and diffraction efficiencies in polymers were much higher than those expected due to a simple linear electro-optic effect. A study by Moerner and co-workers⁵¹ revealed an additional mechanism participating in the PR grating formation in organic materials. The essence of this mechanism called "orientational enhancement" (OE) is that in a material with T_g near the operating temperature, the NLO chromophores, which are necessary constituents of a PR polymer composite or glass, can be aligned not only by the externally applied electric field \mathbf{E}_0 but also in situ by the sinusoidally varying space-charge field \mathbf{E}_{sc} during grating formation. There are many manifestations of the OE effect such as appearance of a grating at twice the grating wave vector \mathbf{K} , dependence of the 2BC energy transfer direction on the polarization of the writing beams, etc.⁵¹ On a molecular level, the OE effect in organic materials occurs because the refractive index change relies not

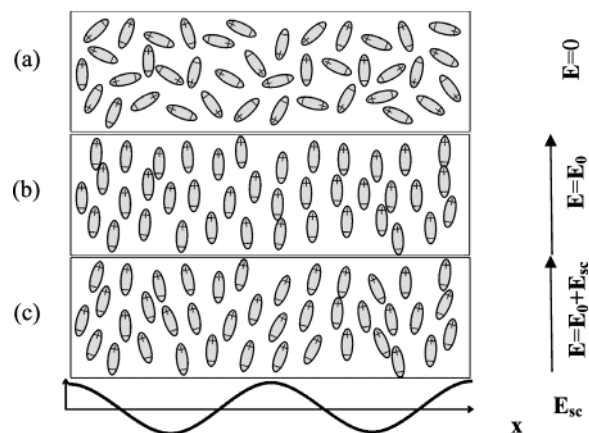


Figure 4. Chromophore orientation in the electric field: (a) no electric field; (b) electric field \mathbf{E}_0 is applied; (c) spatially modulated space-charge field \mathbf{E}_{sc} is added to the applied field. The order parameter is exaggerated for the illustration purposes.

only on the chromophore hyperpolarizability β_{ijk} that leads to an electric field-induced change in second-order susceptibility $\chi^{(2)}$, but also on the polarizability anisotropy $\Delta\alpha$ of the chromophore that leads to an electric field-induced change in the first-order susceptibility $\chi^{(1)}$. A comprehensive treatment of the OE effect can be found in refs 22 and 51; here, we briefly summarize the main points.

Many types of NLO chromophores can be synthesized, with an emphasis on various polarizabilities leading to linear electro-optic effects, second harmonic generation, third harmonic, two-photon fluorescence, etc.⁷⁵ The chromophores utilized in PR materials rely on two particular molecular properties: large hyperpolarizability β_{ijk} and/or large polarizability anisotropy $\Delta\alpha = \alpha_{\parallel} - \alpha_{\perp}$, where parallel and perpendicular refer to the molecular axis. In either case, the entire sample must be made noncentrosymmetric by using an applied electric field (also called the poling field or bias field) to achieve net macroscopic orientation of the chromophores by the interaction between their ground-state dipole moments (μ_g) and the applied field (\mathbf{E}_0). Thus, the value of μ_g should also be large. The poling may occur at temperatures around or above the glass transition temperature T_g , in which case the orientation is quasi-permanent or temporary, depending mostly upon how far the operational temperature is below T_g . For example, when T_g is near the operating temperature, the molecules remain aligned only as long as the orienting field is applied to the material. In most PR polymers, T_g is sufficiently near room temperature (by addition of plasticizers or by chance) so that the external field must be continuously applied to the sample.

Figure 4 illustrates the OE effect schematically. When no electric field is applied to the sample, the molecules are randomly oriented (Figure 4a). As an external field \mathbf{E}_0 is applied, the molecules reorient and align along the electric field (Figure 4b). A theoretical description of the molecular orientation via biased rotational diffusion in response to a step-function electric field can be found in ref 76. In the PR experiment, the interfering light beams 1 and 2

produce a sinusoidally varying space-charge field \mathbf{E}_{sc} by the mechanisms described in section 2. We note that a simplified configuration of electric fields is used in Figure 4 for clarity; the exact experimental geometry employed in PR measurements will be considered in section 4. The uniform external field \mathbf{E}_0 will vectorially add to \mathbf{E}_{sc} to produce a total local field \mathbf{E} . Because the NLO chromophores have orientational mobility due to the low T_g or to their molecular size, a spatially periodic orientational pattern is produced as the electric field orients the molecules by virtue of their ground-state dipole moment (μ_g). Figure 4c illustrates the local order parameter for the total field consisting of $\mathbf{E}_{\text{sc}} + \mathbf{E}_0$ (for illustration purposes, the order parameter shown is exaggerated). The result is a complex spatial pattern of dipolar order, the effect of which on different polarizations is treated in detail in ref 51. The full tensorial description of the local response of the PR medium to the spatially modulated electric field can be found in ref 52. Here, we briefly summarize that in PR materials exhibiting the OE effect, the refractive index change (Δn) in response to the total electric field ($\mathbf{E} = \mathbf{E}_{\text{sc}} + \mathbf{E}_0$) is a sum of the birefringent (Δn_{BR}) and electro-optic (Δn_{EO}) contributions ($\Delta n = \Delta n_{\text{BR}} + \Delta n_{\text{EO}}$) given by

$$\begin{aligned}\Delta n_{\text{BR}} &\sim (1/2n)\Delta\chi^{(1)} \sim (1/2n)C_{\text{BR}}E^2, \\ \Delta n_{\text{EO}} &\sim (1/2n)\Delta\chi^{(2)}E \sim (1/2n)C_{\text{EO}}E^2, \\ C_{\text{BR}} &= \frac{2Nf_\infty\Delta\alpha}{45}\left(\frac{\mu_g}{k_B T}\right)^2, \quad C_{\text{EO}} = \frac{Nf_0 f_\infty^2}{5} \frac{\mu_g\beta}{k_B T}\end{aligned}$$

where N is the dipole concentration, f_0 , f_∞ are the local field factors, k_B is the Boltzmann constant, T is the temperature, $\Delta\alpha$ is the polarizability anisotropy, and β is the only nonvanishing component of the hyperpolarizability tensor β_{ijk} (in the case of one-dimensional molecule). An extension of the OE effect to the case of alternating external electric fields is numerically treated in ref 77.

As a result of the OE effect, the design of chromophores for photorefractivity has diverged from the strategy of the early 1990s in which only hyperpolarizability was emphasized. Thus, rather than seeking chromophores that possess large first hyperpolarizability, it is often more important to select chromophores with a large linear polarizability anisotropy. For both effects, a large ground state dipole moment is required, and the polarizability anisotropy contribution benefits more than the hyperpolarizability contribution, as described more fully in section 5.1.3.

In overall PR performance, the OE effect leads to enhanced steady-state properties (larger gain and diffraction efficiencies than expected due to the simple electro-optic effect) as well as more complicated dynamics determined not only by the rate of space-charge field formation (section 3.1), but also by the ability of the NLO chromophores to dynamically orient during grating formation. Therefore, an additional factor that could limit the speed of hologram growth—rotational mobility of the chromophores in the polymer composite—is introduced. Molecular

orientation times can range from picoseconds (observed in liquids⁷⁸) to extremely long times of years or more observed in permanently poled polymers,⁷⁹ depending upon the viscosity of the material, the size of the chromophore, the presence of plasticizing agents, temperature relative to T_g , and other factors.^{69,80–83}

To summarize, space-charge field formation in the PR organic materials is a complicated process that requires further theoretical modeling supported by experimental results. The OE effect brings an advantage of higher diffraction efficiencies and gain coefficients. However, because chromophore orientation does not proceed instantaneously, the analysis of the PR dynamics is challenging, especially when the rate of space-charge field formation is of the same order of magnitude as the reorientational speed. To assess the factors that limit PR speed in every material, it may be helpful to separately measure the orientational mobility. In section 4.2, we will briefly outline the experimental techniques utilized to probe various processes including the orientational properties of PR materials. In addition, several methods helpful in assigning the observed PR dynamics to a certain physical effect will be covered in section 5.3.

4. Experimental Techniques

In this section, we first consider the techniques that assess the PR optical performance of the material—a brief description of standard 2BC and FWM methods will be given, and several proposed modified techniques will be mentioned (sections 4.1.1–4.1.3). Then, an experiment utilizing two-photon absorption for PR grating recording in polymers will be described (section 4.1.4). As discussed in section 2, the PR grating forms via several mechanisms, and much information about the potential behavior of a material may be gathered by measuring separately the properties of the individual contributors to photorefractivity, i.e., charge generation quantum efficiency, carrier mobility, and electro-optic response. While measuring the presence of all these necessary elements is no guarantee for photorefractivity and is therefore no substitute for the direct optical characterization of a material, it is important to study the contribution of each mechanism to the overall PR performance to determine limiting factors and optimize the behavior. In section 4.2, we summarize the experimental methods developed and currently used for assessing charge photogeneration, transport, and trapping properties as well as ability of the chromophores to reorient in the electric field.

4.1. Photorefractive Measurements

4.1.1. Two-Beam Coupling

As mentioned before, the two-beam coupling (2BC) experiment is one crucial experiment to perform when a new material is tested for PR performance.⁸⁴ The geometry of the 2BC experiment is shown in Figure 5a. A typical PR polymer sample consists of two conductive but transparent indium tin oxide (ITO)-coated glass slides with a PR polymer film of

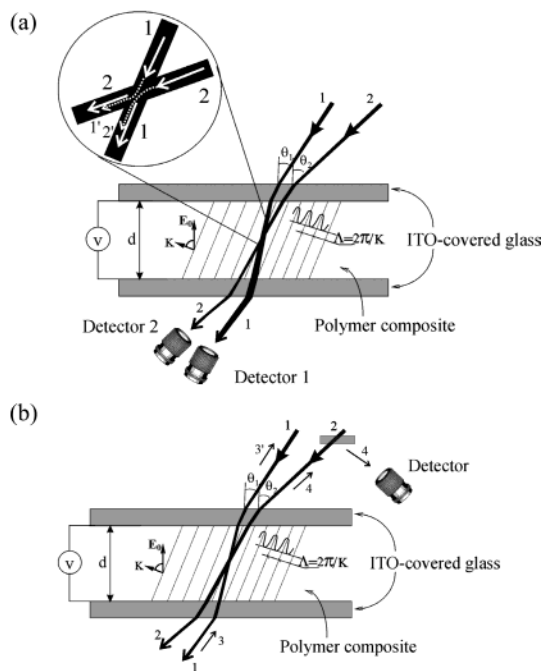


Figure 5. Experimental configuration used in (a) two-beam coupling; (b) four-wave mixing geometry.

30–100 μm thickness in between. Optical beams 1 (“probe” or “signal”) and 2 (“pump”) are incident at angles θ_1 and θ_2 respectively, and interfere in the PR material, creating a nonlocal ($\Phi \neq 0$) diffraction grating. Then, the same beams 1 and 2 partially diffract from the grating they have just created (beams 1' and 2' in the inset of Figure 5a). Because of nonlocality of the grating, one diffracted beam (for example, 1') interferes destructively with its companion beam 2, while the other diffracted beam 2' interferes constructively with beam 1. As a result, the beam 1 is amplified (energy gain) while the beam 2 is attenuated (energy loss). It should be emphasized that it is important that the energy transfer persists in *steady-state* because *transient* asymmetric energy exchange is known to occur in materials with local response (photochemistry, $\chi^{(3)}$, absorption and thermal gratings). In inorganic crystals, the direction of energy transfer depends on the sign of the electro-optic coefficient (which is fixed, so that the refractive index change is linear in electric field) and the sign of the charge carrier. In low T_g organic materials, because the materials are poled in situ and the refractive index change is quadratic in local electric field (section 3.2), the energy transfer direction is determined by the direction of majority carrier drift in the electric field and therefore can be reversed by changing the polarity of electric field. As a result of the OE effect, there is another way of reversing the energy transfer, which is to change the polarization of writing beams 1 and 2. For more explanation of the meaning of asymmetric energy exchange, see ref 21.

The 2BC experiment involves measurement of the transmitted beam intensities as a function of time, \mathbf{E}_0 , K , angles, and so forth; for details see ref 85. A modification of the standard 2BC technique, which was shown to be useful for 2BC measurements in a highly scattering medium with a strong diffraction

to higher orders, such as LCs, was proposed.⁸⁶ The standard geometry (Figure 5a) was used, but one of the writing beams (the pump beam) was chopped with a frequency higher than the inverse grating decay time, and lock-in detection of the probe beam intensity was utilized. In a standard 2BC measurement conducted in a highly scattering material, instead of amplification of one beam and attenuation of the other, the attenuation of both beams was observed due to scattering and diffraction to higher orders. In contrast, when the pump beam was chopped, the demodulated probe beam intensity reflected the amplitude of the 2BC.

As shown Figure 5a, the beams 1 and 2 are incident at angles (θ_1 and θ_2) on the same side of the sample surface normal. This choice of experimental geometry is governed by several factors. First, all the processes in polymers that are responsible for space-charge field build-up are strongly electric field-dependent. Therefore, to assist in charge transport along the grating vector \mathbf{K} , a large component of external electric field \mathbf{E}_0 in the direction of the vector \mathbf{K} is needed. Second, because the NLO chromophores that are part of the PR polymer composite are aligned in the direction of applied field, it is necessary to provide a nonzero component of electro-optic response along the grating vector \mathbf{K} . Recently, several groups reported a 2BC effect in organic materials with no electric field applied.^{11,87,88} However, unless this occurs in prepoled high T_g polymers^{43,89} or sol-gels⁹⁰ that may retain high internal electric fields for a long time after poling, care should be taken to elucidate the mechanism of the observed behavior and eliminate artifacts. Other explanations for a 2BC effect in polymer composites, organic glasses, and polymer-dispersed LCs, observed without electric field applied, included coupling between the space-charge field and light-induced orientational gratings in azo dye-containing materials,⁸⁷ longitudinal intensity gradients leading to charge displacement and local electric field formation,^{88,91} etc. However, none of the explanations presented thus far was unambiguously substantiated by theoretical and experimental evidence. In particular, if the experimental geometry is completely symmetric for the two beams, it is hard to produce an asymmetry in the direction of beam coupling.

Ideally, the beams 1 and 2 would be incident symmetrically from opposite sides of the sample, so that the directions of applied electric field \mathbf{E}_0 and grating vector \mathbf{K} coincide. However, due to refraction at the air-glass-film interfaces, the smallest internal angle of incidence is equal to $\sim 54^\circ$, and for a material with a typical polymer composite refractive index $n = 1.7$, the largest grating spacing Λ calculated using eq 1 for a light beam of wavelength $\lambda = 633$ nm is approximately equal to $0.26 \mu\text{m}$. This is far below the preferable range of grating spacings of $1\text{--}5 \mu\text{m}$.^{50,85} One way around the refraction at the air-glass interfaces is to optically contact glass hemispheres on both sides of the sample.⁸⁵ Nevertheless, recently several PVK/C₆₀ and PPT-Cz/C₆₀-based PR polymer composites were characterized without glass hemispheres using the opposite-side geometry

($\lambda = 633$ nm, $\Lambda = 0.205$ μm , $d = 100$ μm).⁹² The best PR performance was achieved in a PPT-Cz/PDCST/ C_{60} composite, in which 2BC gain coefficient Γ (defined below) of 104 cm^{-1} (net gain coefficient $\Gamma - \alpha = 51$ cm^{-1} , where α is the absorption coefficient) was obtained at 60 $\text{V}/\mu\text{m}$. In all other composites studied, gain coefficients (Γ) of only 15 – 20 cm^{-1} (no net gain) were measured in this geometry, although the same composites exhibited high gain coefficients $\Gamma \sim 200$ – 250 cm^{-1} under similar experimental conditions (section 6.1, Table 2) in the conventional geometry (Figure 5).^{72,93–95} Another experimental geometry, recently explored in 2BC measurements, utilized coplanar electrodes and two beams incident symmetrically with respect to the sample normal.⁹⁶ PVK/TNF-containing films with a thickness up to 600 μm were prepared and characterized. The gain factor (γ_0 ; defined below) increased as a function of sample thickness, reaching 1.47 for a 600 - μm -thick sample at 50 $\text{V}/\mu\text{m}$ at 633 nm, while the Γ decreased with sample thickness, so that the highest value $\Gamma = 32.5$ cm^{-1} was achieved in a 100 - μm film. The advantages of such a geometry include the possibility to operate at lower voltages (since $\mathbf{E}_0 \parallel \mathbf{K}$) and to make thicker devices while maintaining reasonable ranges of applied voltage. Disadvantages include dealing with nonuniform electric field distribution throughout the sample thickness, small operating area, etc. For this reason, the oblique geometry such as shown in Figure 5, with external angles $\theta_1 = 30^\circ$ – 45° and $\theta_2 = 60^\circ$ – 75° , is still the usual choice for PR experiments.

The theoretical description of the 2BC effect involves solving coupled-wave equations which govern the interaction of two beams of light in an NLO material. The details of this description can be found in refs 5, 97, and 98. Here, we only cite the solution, which is used for extracting material parameters from experimentally measured quantities. Denoting beam 2 as the “pump”, the intensities of the “signal” beam (beam 1) ($I_1(\text{out})$) and of the “pump” beam ($I_2(\text{out})$) may be written as follows:⁵

$$I_1(\text{out}) = \frac{I_0}{1 + \beta_p \exp(-\Gamma L)}; \quad I_2(\text{out}) = \frac{\beta_p I_0}{\beta_p + \exp(\Gamma L)} \quad (4)$$

where the initial beam ratio (in the absence of coupling) is $\beta_p = I_2(\text{in})/I_1(\text{in})$, the total intensity $I_0 = I_1 + I_2$, the interaction length $L = d/\cos \theta_1$, where d is a sample thickness, and the 2BC gain coefficient is

$$\Gamma = \frac{4\pi}{\lambda} \frac{\Delta n}{m} \sin \Phi \quad (5)$$

where λ is the wavelength, Δn is refractive index modulation, and m is the modulation depth of the interference pattern defined as $m = 2\sqrt{\beta_p}/(1 + \beta_p)$. Using eqs 4 and 5, the gain coefficient can be determined from experimentally measured intensities as follows: $\Gamma = \ln(\beta_p I_1(\text{out})/I_2(\text{out}))/L$. Note that in the undepleted pump regime ($\beta_p \gg 1$), the gain factor γ_0 defined as $\gamma_0 = I_1(\text{out})/I_1(\text{in})$ simplifies to $\gamma_0 = \exp(\Gamma L)$, i.e., the intensity of the signal beam grows exponentially.

From eq 5, it is clear that a phase shift of $\Phi = 90^\circ$ leads to the optimum energy transfer, whereas no energy coupling occurs for an in-phase grating, $\Phi = 0^\circ$. This is the importance of the existence of a nonzero phase shift for the PR grating, as has already been stressed. To measure the phase shift Φ , a simple experimental technique based on translating the grating with respect to the interference pattern at a rate much faster than the response rate of the material has been developed.^{84,99,100} The required fast displacement of the grating with respect to the intensity pattern can be accomplished either by the direct movement of sample or by changing the relative phase of the two writing beams (which translates the interference pattern). The sensitivity of the measurement can be further improved by ac phase modulation and lock-in detection.¹⁰¹ The 2BC technique in conjunction with phase shift measurements has been widely utilized to assess material parameters such as the PR trap density and electro-optic nonlinearity.^{46,49,50,85,102,103}

4.1.2. Four-Wave Mixing

The experimental geometry for the FWM experiment is quite similar to that of 2BC—two writing beams are obliquely incident on the PR sample (Figure 5b). The difference is that in the FWM experiment, in addition to the writing beams 1 and 2, there is also a probe (reading) beam (beam 3 in Figure 5b) that is being partially diffracted from the grating created by the writing beams to create the fourth beam (beam 4). In the degenerate FWM geometry, which is common in PR measurements, beam 3 has the same wavelength as the writing beams and is usually chosen to be counter-propagating to one of the writing beams as this allows for the phase-matched readout and background-free detection of very weak diffraction signals (beam 4). The diffracted beam intensity (i.e., that of beam 4) is typically measured as a function of time, applied electric field (\mathbf{E}_0), writing beam intensities, etc. Then, the diffraction efficiency (η), defined as the ratio $\eta^{\text{ext}} = I_4/I_3$ (external diffraction efficiency) or $\eta^{\text{int}} = I_4/(I_4 + I_3)$ (internal diffraction efficiency) is determined. In probing the grating, it is important that beam 3 not affect the grating or interact with the writing beams. This can be assured by making the probe beam much weaker than the pump beams and/or by having the probe beam polarized orthogonal to the writing beams. Because p -polarized beams experience a larger diffraction efficiency due to the polarization dependence of the OE response of the material,²² beam 3 is typically p -polarized, while beams 1 and 2 are s -polarized in most FWM experiments. Another advantage of this choice of the polarizations is that the energy transfer between the s -polarized writing beams is typically weaker than that between p -polarized writing beams, which reduces undesirable grating distortion, beam fanning, etc.

From the measured diffraction efficiency, the modulation amplitude of the refractive index (Δn) is typically obtained by using the following simple expression:⁵³

$$\eta^{\text{ext}} = \exp(-\alpha L) \sin^2\left(\frac{\pi \Delta n L}{\lambda} \hat{e}_1 \cdot \hat{e}_2\right) \quad (6)$$

Here α is the absorption coefficient, the effective interaction length $L = d/\sqrt{\cos\theta_1 \cos\theta_2}$, and \hat{e}_1 and \hat{e}_2 are unit vectors along the electric field of the incident and diffracted beams, respectively. For the configuration with p -polarized readout, $\hat{e}_1 \cdot \hat{e}_2 = \cos(\theta_2 - \theta_1)$, while for s -polarized readout the dot product is unity. Equation 6 should only be regarded as an approximate solution as it assumes a straight uniform grating, which is not necessarily true in all PR materials.²²

In addition to measurements of steady-state diffraction efficiency which is an important parameter for applications, the FWM experiment is widely used for temporal studies (e.g., formation and erasure) of the PR grating. Electric field and intensity dependence of the PR dynamics can yield much information about the material parameters (section 5.3.1).^{48,49,58,69,93,104} Furthermore, the FWM experiment is ideally suited to measure the dark decay of gratings, i.e., the decay after both writing beams are turned off.^{69,104,105} This parameter is especially of interest for data-storage applications for which long dark-lifetimes are desirable. Moreover, at small dark currents, the dark decay time constant can provide information about detrapping rates (e.g., $\beta_{1,2}$ of eq 3)^{58,105} (section 5.3.2). To ensure that the probe beam does not itself erase the grating, the illumination of the grating can be made negligibly small by only probing the grating intermittently.

4.1.3. Photoelectromotive Force

An alternative PR characterization technique that takes advantage of the nonsteady photoelectromotive force (photo-EMF) was originally developed for inorganic crystals¹⁰⁶ and recently applied to PR polymers.¹⁰⁷ In this technique, the PR hologram is recorded under nonstationary conditions, e.g., by a vibrating interference pattern. The interaction between the quasi-stationary space-charge field grating and the oscillating distribution of the mobile carriers leads to a periodic electric current with the frequency of the oscillation (Ω) of the interference pattern (j^Ω). In the presence of an external dc field, a second-harmonic photo-EMF current ($j^{2\Omega}$) appears. Both currents j^Ω and $j^{2\Omega}$ are measured as a function of modulation amplitude of the interference pattern, frequency, etc., from which the information about the space-charge field formed in the film can be extracted.¹⁰⁷ The advantage of the photo-EMF experiment is that it can be performed in any photoconductor or PR material at low electric fields at which standard PR techniques might not provide sufficient sensitivity. The disadvantage of the experiment is a complicated data interpretation due to competing multiple grating effects,⁷⁴ which could be the reason for the limited use of this technique in PR organic materials thus far.

4.1.4. Photorefractive Gratings Written via Two-Photon Excitation

In the process of developing highly efficient materials for holographic data storage, the issue of nonde-

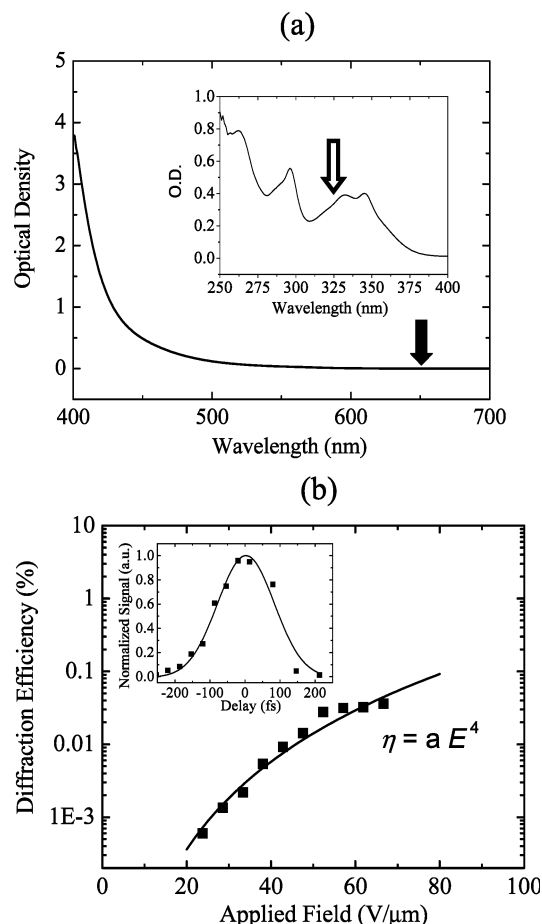


Figure 6. (a) Linear absorption spectrum of the 105- μm -thick film of the PVK/FTCN/ECZ/BBP composite used for holographic recording via two-photon absorption. The filled arrow indicates the laser wavelength used in the PR experiment. Inset shows linear absorption spectrum of the thin film of the same composite. The open arrow indicates the spectral position of the two-photon excitation. Reprinted from ref 110 with permission. Copyright 2002 Optical Society of America. (b) Diffraction efficiency, obtained from a grating written via two-photon absorption, as a function of applied electric field. Inset shows diffraction efficiency as a function of delay between femtosecond writing beams. Reprinted from ref 111 with permission. Copyright 2002 Wiley VCH.

structive readout arises. In standard techniques such as degenerate FWM, the readout is performed using the beam of the same wavelength as that of the writing beams, and therefore it is bound to partially erase the hologram while retrieving the information. Nondestructive readout using two-photon absorption was previously utilized in inorganic PR crystals^{108,109} and recently demonstrated in PVK-based materials.^{110,111} In ref 111, PVK was used as a photoconductor, ECZ and BBP as plasticizers, and FTCN (25 wt %) both as a NLO chromophore and a sensitizer exhibiting two-photon absorption. A FWM experimental geometry similar to one shown in Figure 5b was utilized in this experiment. The grating was written with femtosecond pulses of the wavelength of either 650 or 700 nm. In this wavelength region, the composite exhibited no linear absorption (Figure 6a), and the sample was excited only by two-photon absorption (inset of Figure 6a) of the FTCN. The readout of the grating could be obtained with both

pulsed and cw beam of the same wavelength. Utilizing a cw beam as a probe beam represented a nondestructive readout because (i) the intensity of the cw probe beam was too low to induce a two-photon absorption in the material, and (ii) the probe beam could not perturb the grating via linear absorption, because the composite did not exhibit any sensitivity in the red wavelength region (Figure 6a). The diffraction efficiency measured at total writing beam intensity of 5 GW/cm^2 as a function of applied electric field is shown in Figure 6b (squares), along with a fit of the diffraction efficiency to the electric field dependence ($\eta \sim E^4$) derived from the standard Kukhtarev model (line). The inset of Figure 6b illustrates the normalized diffracted signal measured at an electric field of $50 \text{ V}/\mu\text{m}$ and total writing beam intensity of 5.3 GW/cm^2 as a function of time delay between writing beams. Clearly, the maximal diffracted signal was obtained when the writing beams were temporally overlapped. While low diffraction efficiencies ($\sim 0.04\%$ at best) and slow PR response speed (on the order of seconds) were obtained in this composite, this study was the first proof-of-principle demonstration of the PR grating written via two-photon excitation in a polymer composite. Dopants with high two-photon absorption cross-section utilized in PR composites (e.g., ref 112) can potentially improve both steady-state and dynamical performance of the two-photon absorption-induced PR grating.

4.2. Experimental Techniques for Probing Various Processes Relevant to Photorefractivity

4.2.1. Photoconductive Properties

As discussed in section 2, the first stage of the PR grating formation—the buildup of the space-charge field—relies on the photoconductive properties of a material such as charge photogeneration efficiency, carrier mobility, trapping, and recombination. All these mechanisms can be separately probed using various standard methods from the electrophotographic community, the detailed descriptions of which can be found in refs 62 and 113. Here, we list the techniques that can be employed for characterization of PR organic materials.

(i) Photogeneration efficiency is commonly measured using a xerographic discharge technique^{47,48,114,115} or estimated from the dc photoconductivity.^{64,116,117}

(ii) Charge carrier mobility can be measured by time-of-flight (TOF),^{48,50,118,119} holographic time-of-flight (HTOF),^{120–122} and extraction current transients,^{123–125} as well as estimated from the dc photoconductivity.^{66,67} A recent overview of the experimental techniques used for charge transport studies in organic materials can be found in ref 126.

(iii) Trapping and recombination properties of PR composites have been extensively studied over the past few years. In particular, infrared optical spectroscopy was employed to probe the PR trap density,^{46,64} while various modifications of a dc photoconductivity experiment proved to be effective in studies of trapping, detrapping, and recombination parameters as described in section 3.1.^{48,66,127}

4.2.2. Orientational Properties

The last step of the PR grating formation is the refractive index change via electro-optic nonlinearity. In low T_g PR organic materials, a major mechanism responsible for this step is NLO chromophore reorientation in the space-charge field (OE effect).⁵¹ Therefore, the ability of the chromophores to reorient in the electric field is an important property that contributes to the overall PR performance. Several experimental techniques are available to evaluate chromophore reorientational properties.¹²⁸ Both the orientational order parameter and orientational mobility are of interest for studies of PR materials: the order parameter allows estimation of the electro-optic nonlinearity achievable in the material, while orientational dynamics studies help to clarify limiting factors in PR temporal performance. Orientational properties of the materials can be measured either in time or in the frequency domain. Measurements in the time domain involve applying a step-function electric field and monitoring the response of the system. Depending on the technique, the time evolution of different observables, such as electric field-induced birefringence in a transmission ellipsometry experiment^{69,104,129–132} or electric field-induced second harmonic generation (EFISHG) in EFISHG experiment,^{133,134} etc., is studied. In the frequency domain, electro-optic relaxation and dielectric spectroscopy can be utilized to measure frequency-dependent refractive index modulation and dielectric constant in low T_g polymer composites and glasses in response to an ac electric field.^{69,83,135–138}

To summarize, 2BC and FWM are the most widely used geometries for evaluation of PR properties and demonstration of applications. A modification of the PR experiment that allows writing PR gratings via two-photon absorption and then reading out nondestructively could potentially lead to improved stability of gratings required for applications. In addition, a variety of techniques are available for complementary characterization of photoconductive and orientational properties of PR materials.

5. Physical Studies

In this section, we describe a number of physical studies that have been performed on various materials with an aim to elucidate mechanisms, understand limiting factors, and improve performance of the PR material. First, we discuss the impact of various components of PR polymer composites on the physical properties relevant for photorefractivity. In particular, the role of sensitizers, photoconductors, chromophores, plasticizers, etc. will be considered (section 5.1). Then, we analyze the influence of experimental conditions such as temperature, preillumination, etc. on the PR properties (section 5.2). Finally, we review several tests that can be performed on a PR material to clarify the contribution of various mechanisms in the observed PR performance (section 5.3).

5.1. Materials Study of Key Components

5.1.1. Sensitizers

The primary role of a sensitizer added to the PR material is to assist in charge photogeneration. The

multistep process of charge photogeneration in many solids including PR organics includes photoexcitation (step 1), followed by creation of an electron–hole pair bound by Coulomb interaction (step 2), and finally, separation (dissociation) of the electron–hole pair, thus overcoming the Coulomb barrier (step 3). Charge photogeneration efficiency is governed by a competition between recombination of a charge carrier with its parent countercharge, termed geminate recombination, and electron–hole pair dissociation.⁶² The most common quantitative treatment of this process is a field-dependent charge separation theory by Onsager,¹³⁹ despite its recognized deficiencies,^{140,141} among which is the prediction of electron transfer distances on the order of nanometers inconsistent with spectroscopic estimates of several tenths of nanometers. The inadequacy of the Onsager theory originates from the assumption of infinitely fast annihilation of electron–hole pair when the distance between them reaches zero, and several models were developed to take into account finite recombination rates.^{140,141} Recently, the Marcus theory of electron transfer¹⁴² has been applied to provide a theoretical basis for the origin of slow recombination rates in photoconductive polymers.¹⁴³ Typical values for electron-transfer rates are $\sim 10^9$ – 10^{11} s⁻¹,¹⁴⁴ and information about time scales of the photogeneration process in sensitized polymers can be obtained by performing ultrafast transient absorption, transient photoconductivity, and time-resolved fluorescence experiments.^{145–150} The photogeneration efficiency in PR polymers and organic glasses strongly depends on electric field,^{47,115,117,151,152} mostly due to the field-dependent dissociation of the electron–hole pair (step 3), although attempts have been made to include the contribution of external electric field into Marcus electron-transfer rates describing step 2.¹⁴³ Generally, the electric field dependence of photogeneration efficiency (ϕ) has a complicated form.^{62,113} However, in most polymers in the range of applied electric fields of ~ 10 – 100 V/ μm , it can be approximated reasonably well with a power law ($\phi \sim E^p$), where the power law exponent (p) ranges between 1.5 and 3.5 (e.g., in PVK-based composites $p \approx 2$).^{47,48}

The choice of a sensitizer depends on the desired wavelength sensitivity and is often dictated by the transport molecule as well. The best performance is obtained by optimizing the charge-transfer (CT) properties between a given sensitizer and its parent transport molecule. Several classes of organic molecules and pigments have been utilized as sensitizers in organic photoconductors, including phthalocyanines, squaraines, perylene dyes, and thiapyrylium salts. One recent approach involved incorporating sensitizing agents, e.g., various transition metal complexes, including phthalocyanines and porphyrins, into fully functionalized polymers and glasses.^{89,153–155} The region of wavelength sensitivity depended on the transition metal complex utilized and could be varied by synthetic modifications.⁸⁹ Another approach was to explore semiconductor quantum dots such as CdS and CdSe as sensitizers in hybrid organic–inorganic composites.^{43,116,156–159} In this case, the wavelength sensitivity was determined

by the composition and size of the quantum dots.¹¹⁶ Despite these new approaches, the most successful class of sensitizers to date remains the CT complexes formed between a donor-like and an acceptor-like molecule or moiety. The intermolecular interaction (partial charge transfer) between the donor D and the acceptor A leads to a new absorption band that does not appear in the spectrum of either component alone. Hence, spectral sensitivity in the visible and the near-infrared (IR) part of the spectrum can be achieved with CT complexes. Thus far, the most commonly used sensitizers that readily form CT complexes with donor-like molecules and polymers are C₆₀, TNF, and TNFM.

A recent detailed study of photogeneration in CT complexes in PR materials was carried out by Hendrickx et al.¹¹⁷ In this work, C₆₀ was used as a sensitizer, and various arylamine derivatives were introduced into the PS matrix to serve as hole transporters. The photogeneration efficiency of these composites was measured in a dc photoconductivity experiment as a function of arylamine moiety concentration and its ionization potential (I_p). The absorption spectra of the composites exhibited clear evidence of CT bands formed between the arylamine and C₆₀. The main results of the study were (i) The photogeneration efficiency increased as the difference between the I_p of the donor (arylamine molecule) and acceptor (C₆₀) increased; and (ii) the photogeneration efficiency increased as the distance between the donor (arylamine) molecules decreased. These results were explained in a framework of Marcus theory for the electron-transfer process, which is characterized by an electron-transfer rate k_{ET} :¹¹⁷

$$k_{\text{ET}} = k_0 \exp(-b\Delta R) \exp\left[-\frac{(\Delta H_C - \lambda)^2}{4\lambda k_B T}\right] \quad (7)$$

where k_0 and b are prefactors, λ is a reorganization energy, ΔR is the distance between the reaction centers, and ΔH_C is the enthalpy of complexation. (i) For a given acceptor, ΔH_C scales with a donor strength, increasing for stronger donors, i.e., for molecules with lower I_p . According to eq 7, in the noninverted regime ($\Delta H_C < \lambda$), this would lead to an increase in k_{ET} as I_p decreases (or, equivalently, the difference between I_p of donor and acceptor increases), as observed by the authors. (ii) The exponential term containing ΔR in eq 7 as well as the intermolecular distance-dependent probability of electron–hole dissociation were claimed to be responsible for the experimentally observed decrease in photogeneration efficiency as the distance between the donor molecules increased.

Photogeneration efficiency is a crucial parameter for both the PR dynamics and steady-state performance. As discussed in section 3.1, numerical simulations of eq 3 predicted a strong dependence of PR speed on the photogeneration efficiency. Therefore, optimization of the sensitizer is important for the best dynamical performance. Moreover, the sensitizer is a major player in the steady-state properties of a PR material as it is also linked to charge trapping, one of the crucial processes in PR grating formation

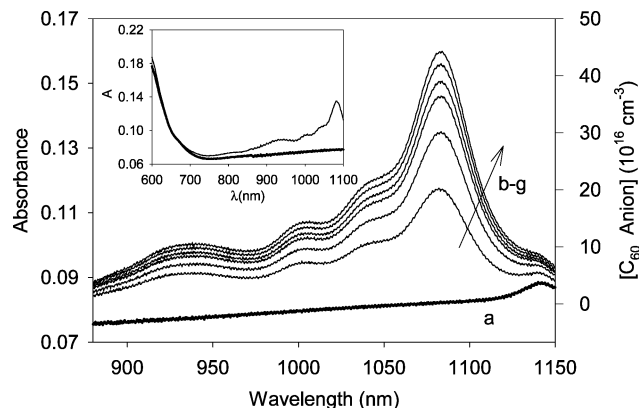


Figure 7. Absorption spectrum of PR polymer composite PVK/AODCST/BBP/C₆₀, showing light-induced growth of the absorption peak at ~1080 nm due to an increase in C₆₀⁻ concentration (right-hand axis). Initial trace a was obtained prior to exposure to light. Traces b–g were taken at 5, 10, 25, 35, 45, 65 min after the start of irradiation with 10 mW/cm² light at 647 nm at applied electric field of 20 V/μm. Inset shows spectra over wider wavelength range taken before (thick trace) and after 65 min irradiation (thin trace). Reprinted from ref 46 with permission. Copyright 1998 Elsevier.

(section 2). The first experimental demonstration of the link between the sensitizer and PR traps was performed by Grunnet-Jepsen et al.⁴⁶ in several PVK-based composites sensitized with C₆₀. In this study, the authors uniformly illuminated PR samples containing chromophores with different I_p values, with 647 nm light under electric field and measured the growth of ionized sensitizer (i.e., C₆₀ anion) density by monitoring the spectral changes. Figure 7 shows the change in absorption spectrum measured in a PR sample with composition PVK/AODCST/BBP/C₆₀ at an electric field of 20 V/μm upon illumination with 10 mW/cm². An absorption peak at a wavelength of ~1080 nm, characteristic for C₆₀ anions, grows in time as their concentration in the sample increases (the inset of Figure 7 shows the wider spectral range). Both the steady-state concentration of C₆₀ anion and the dynamics of its growth and decay were linked to the I_p of the NLO chromophores used in the samples. Furthermore, the PR trap density deduced from a 2BC experiment was found to strongly correlate with the ionized acceptor density, which unambiguously proved the link between the two and emphasized the role of chromophores as compensating traps. This work initiated a number of detailed studies on the role of chromophore and sensitizer in the trapping process. Hendrickx et al.⁶⁴ measured number density of C₆₀ anions in PVK/C1–C9/ECZ/C₆₀ composites, where C1–C9 were fluorinated styrene chromophores (whose core structure was similar to that shown in the inset of Figure 11) with I_p values ranging between 5.8 and 6.3 eV, upon illumination with 633 nm light with intensity of 30 mW/cm² at electric field of 80 V/μm. The authors found that the steady-state number density of C₆₀ anions monotonically decreased as the I_p of the chromophore increased (Figure 8). This result can be qualitatively explained in a framework of the PR model described in section 3.1. Numerical simulations of eq 3 showed that the ionized acceptor density N_A^{\dagger} (if the sensitizer is C₆₀, then it would be

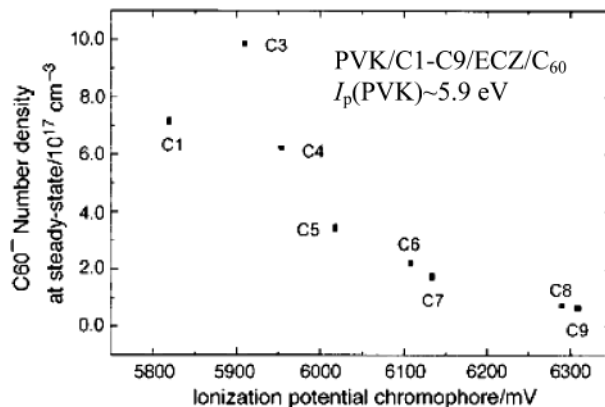


Figure 8. Correlation between number density of C₆₀⁻, obtained after illumination at 633 nm with 30 mW/cm² at an applied electric field of 80 V/μm, and I_p of the fluorinated styrene chromophores (C1–C9) observed in the PVK/C1–C9/ECZ/C₆₀ composites. Reproduced from ref 64 by permission. Copyright 1999 The Royal Society of Chemistry.

the density of C₆₀ anion) that grows under uniform illumination is affected by compensating trap densities available in the material as well as trap depths (see Figure 3).⁴⁸ Because chromophores could serve as compensating traps in the composite,⁴⁶ the trapping properties (e.g., trap depths) would depend on the I_p of the chromophores compared to that of the transport molecule. One of the other results of the study by Hendrickx et al.,⁶⁴ confirmed in a separate examination of a similar system by Herlocker et al.,⁶⁵ was that in the samples with I_p close to or lower than that of carbazole the authors observed degradation of photoconductivity and PR speed after continuous illumination prior to the experiments (see section 5.2.2 for discussion of preillumination effects).

To further investigate the role of sensitizer in the PR performance, several experimental studies were performed in which a sensitizer was varied while the other components of the PR material remained the same. Hendrickx et al.⁶⁴ found that at 633 nm, the photogeneration efficiency of PVK-based composites sensitized with C₆₀ was much higher than in analogous composites sensitized with TNFM. Ostroverkhova et al.¹⁰⁴ studied PR properties of low molecular weight DCDHF glasses sensitized with C₆₀ or TNFM and found that the 2BC gain coefficient measured at a wavelength of 676 nm in C₆₀-sensitized glasses was several times higher than that obtained at 830 nm in the same glasses sensitized with TNFM at similar absorption coefficients of the samples and similar experimental geometry.^{104,160} The observed difference in gain coefficient at the two wavelengths was too large to be explained only by the dependence of the gain coefficient on grating period that changed with wavelength (eq 1). Because only the sensitizer molecules were different, while all other components were unchanged, the total density of available compensating traps in the material was the same in C₆₀ and TNFM-sensitized composites. However, the 2BC gain depends on the density of *filled* traps, rather than total trap density, and *filled* trap density is linked to the ionized sensitizer density by charge neutrality.⁴⁸ The ionized sensitizer density depends on various parameters (section 3.1), including photo-

generation efficiency, which is different for the composites sensitized with TNFM and C₆₀. In several studies exploring the contribution of a sensitizer to the PR performance, various characteristics (e.g., photoconductivity, 2BC gain, phase shift, diffraction efficiency, etc.) were measured as a function of the sensitizer concentration.^{29,49,161,162} In all studies, addition of up to 1% of a sensitizer led to a significant improvement of both PR dynamics and steady-state properties. For example, in ref 162, an organic glass containing a mixture of DCDHF derivatives (TH-DCDHF-6V(50%)/DCDHF-8(50%)) was doped with 0, 0.1, and 1% TNFM. While significant 2BC gain coefficients of $\sim 120 \text{ cm}^{-1}$ at an electric field of 50 V/ μm and a wavelength of 830 nm were observed in an unsensitized mixture (0% TNFM), the sensitization with 1% TNFM led to an approximately 5-fold increase in 2BC gain coefficient, reaching $\sim 400 \text{ cm}^{-1}$ at 40 V/ μm (section 6.6), as well as a 3-fold increase in PR response speed. However, an increase in a sensitizer concentration beyond several percent may lead to adverse effects. For example, in a PVK-based material, it was observed⁴⁹ that as the concentration of the sensitizer (in this case TNFM) increased above 1.5%, the refractive index modulation decreased and the build-up time increased due to an excessively high trap density. In addition, an increased concentration of the sensitizer leads to an undesirable increase in absorption; thus, there is an optimal concentration of sensitizer, which for commonly used sensitizers is below or around $\sim 1\%$.

5.1.2. Photoconductors

As discussed in section 2, the ability of the material to conduct charges is crucial for the PR effect. Several types of photoconductors have been utilized in PR materials including photoconductive polymers (e.g., PVK, PSX, PPV),^{42,43,93,163–165} inert polymer hosts (e.g., PS, PC, polysiloxane) doped or synthetically conjugated with charge transporting molecules,^{155,166–169} photoconductive low molecular weight glasses,^{104,151,170–172} etc. Most photoconductors currently used in PR composites are unipolar (hole) conductors, although recently several electron-transporting and bipolar organic materials have been explored (section 6.7.2).

It is conventional to describe charge transport in organic amorphous materials with a disorder formalism developed by Bässler and co-workers.¹⁷³ The model is based on the argument that charge transport occurs by activated hopping with asymmetric Miller-Abrahams probability through a manifold of localized states that are distributed in energy and space. In molecularly doped systems, organic glasses, or polymers with charge transport moieties (e.g., PVK), hopping occurs between charge transporting molecule sites, and disorder is due to impurities, differences in conformation, site energy distribution, etc. of the charge transporting molecules. In conjugated polymers, hopping proceeds through the conjugated parts of the polymer chain, and the disorder is due to impurities, kinks, and cross-links in the conjugated path.¹⁷⁴ In the disorder formalism, the

charge carrier mobility (μ) at moderate electric fields is described by the following relation:

$$\mu = \mu_0 \exp[C[(\sigma/k_B T)^2 - \Sigma^2]\sqrt{E} - (2\sigma/3k_B T)^2] \quad (8)$$

where μ_0 is a prefactor, C is a constant, E is the electric field, k_B is the Boltzmann constant, and T is temperature. The key parameters of the formalism are the diagonal (energy) disorder parameter (σ) and the off-diagonal (positional) disorder parameter (Σ) that are influenced by the concentration of additives, their dipole moment, I_p , etc.^{113,119,175,176} In addition, as seen from eq 8, the mobility is electric field- and temperature-dependent and typically is an increasing function of electric field and temperature. Under experimental conditions normally utilized in PR experiments, the disorder formalism seems to approximate reasonably well a majority of the photoconductors used in current PR materials. However, recent experimental observations of a decrease in mobility as electric field increases prompted a reexamination of the assumptions of the disorder formalism and, in particular, the treatment of hopping using Marcus electron-transfer rates instead of Miller-Abrahams rates,^{177,178} the treatment of charge transport as three-dimensional,¹⁷⁹ etc.

A number of experimental studies were conducted to understand factors that affect charge carrier mobility in various materials. In polymer composites, the general trends of charge carrier mobility are that (i) mobility decreases as the dipole moment of a host or a dopant increases due to dipole–dipole interactions affecting energetic disorder,^{119,175} and (ii) mobility increases as a function of concentration of charge transport moiety.¹⁷⁶ There are also specific properties that may vary from composite to composite. For example, a dopant (which could be an additional charge transport molecule or a chromophore) added in high concentrations can form an additional transport manifold that would transport charges in addition to a main manifold formed by a host conducting polymer.^{180,181} Alternatively, if the I_p of the dopant is close to that of the main transport molecule, the dopants can participate in transport and either increase or decrease mobility depending on dopant concentration and I_p .^{48,181,182}

In the context of PR properties, the essential question is how the charge carrier mobility affects the PR dynamics. Numerical simulations of eq 3 showed that the PR speed is highly mobility-dependent.⁴⁸ In addition to charge transport properties, the disorder that exists in a polymer composite influences trapping and recombination dynamics which are important for both steady-state and dynamical PR response.^{47,48,50,66,180,183,184}

Over the past years, the host polymer PVK, characterized by carrier mobilities $\mu \sim 10^{-6}–10^{-8} \text{ cm}^2/(\text{Vs})$ depending on electric field,¹¹³ was the photoconductor most widely utilized in PR polymer composites. Although a recent study showed that the mobility of PVK can be slightly improved by adding small concentrations of CdS quantum dots,¹⁸⁵ better photoconductors are needed to dramatically improve mobility and PR speed. In PVK/C₆₀-based composites,

the best PR response times achieved to date were on the order of several milliseconds at external electric fields of ~ 100 V/ μm and incident intensities of $\sim 0.5\text{--}1$ W/ cm^2 .^{93,129} There have been several attempts to replace PVK with another photoconductive polymer with higher mobility to improve PR response speed of the PR composite.^{41,164,165,169,186,187} Unfortunately, other contributing processes such as charge photogeneration, chromophore orientation, etc. prevented sub-millisecond PR speed in these materials. The choice of photoconductor is not limited to a polymer, and other photoconductors with high charge carrier mobilities such as smectic and discotic LCs,^{188–192} nematic LCs doped with small concentrations of a conjugated polymer,¹⁹³ conjugated organometallic polymers,¹⁹⁴ etc. could potentially serve as photoconductive hosts in PR composites. An alternative approach involves developing multifunctional (including photoconductive) molecular glasses.^{16,32,104,151,195,196} For recent reviews of charge transport properties of various organic materials, see refs 196 (organic glasses), 174, 197 (conjugated polymers and oligomers), and 187 (triarylamines).

5.1.3. Chromophores

The primary role of the NLO chromophore in PR polymer composites is to provide a functionality leading to a refractive index change in response to the electric field. As discussed in section 3.2, several molecular parameters such as ground-state dipole moment (μ_g), polarizability anisotropy ($\Delta\alpha$), and first hyperpolarizability (β) are of importance for the electric field-induced refractive index change. It was shown that a certain combination of these parameters, or chromophore figure-of-merit (FOM), adequately describes the electro-optic nonlinearity important for the PR performance.^{52,198,199} The FOM is defined as⁵²

$$\text{FOM} = \frac{1}{M} \left[9\mu_g\beta + \frac{2\mu_g^2\Delta\alpha}{k_B T} \right] \quad (9)$$

where M is the molar mass, k_B is the Boltzmann constant, and T is the temperature. (This expression is equivalent to the C parameter of ref 51 and applies to the most common geometry. In refs 198 and 200, the FOM was defined as that of eq 9 multiplied by $M/9$.) A series of studies was devoted to the optimization of the chromophores to maximize the FOM given by eq 9.^{170,200–203} Strategies of chromophore design related to the optimization of FOM can be found in a recent review in ref 27.

Considering the overall PR performance, various additional properties of the NLO chromophore need to be taken into account. For example, a high concentration of NLO chromophores is desirable to maximize electric field-induced birefringence. However, addition of high concentrations of small-molecule NLO chromophores can cause PR composites to undergo phase separation which affects optical clarity and reduces the shelf life of the PR device.^{204–206} Furthermore, in PR composites with high chromophore content, there are spectroscopic evidences of dimer and aggregate formation,^{207,208} which may

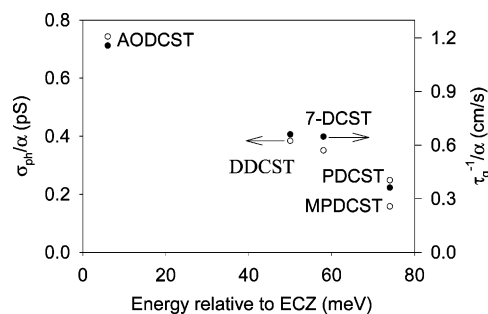


Figure 9. Normalized PR response speed (right axis, filled circles) and photoconductivity (left axis, open circles) obtained in PVK/DCST/BBP/ C_{60} composites as a function of HOMO energy of the DCST chromophore relative to that of the carbazole. Reprinted from ref 209 with permission. Copyright 1999 American Chemical Society.

influence the electro-optic response. Moreover, highly polar chromophores that possess high FOM (eq 9) may reduce the charge carrier mobility in the composite.¹¹⁹ Finally, as we discussed above (sections 5.1.1 and 5.1.2), the chromophore I_p needs to be optimized with respect to that of the sensitizer and charge transport molecule because chromophores can participate in photogeneration, transport, and trapping processes.^{48,117,209,210} As a result, the PR performance is highly influenced by relative I_p values of all constituents of the composite. Diaz-Garcia et al.²⁰⁹ studied PVK(49.5%)/DCST(35%)/BBP(15%)/ C_{60} (0.5%) composites, in which different DCST derivatives with various I_p (but all below that of PVK) were utilized as NLO chromophores. Figure 9 shows PR response speed (τ_g^{-1}/α , right axis, filled circles) and photoconductivity (σ_{ph}/α , left axis, open circles) normalized by the absorption coefficient α (in the case of low absorption) as a function of HOMO energy of the chromophore relative to that of PVK. The highest PR response speed as well as photoconductivity was obtained in the composite containing AODCST chromophores, in which the HOMO energy level is closest to that of PVK. This was attributed to most favorable charge transport and trapping dynamics obtained in this case of almost matching energy levels. In similar composites, Ostroverkhova and Singer⁴⁸ varied the concentration of a chromophore (NLO) complementary to that of a plasticizer (BBP) (molar PVK(49%)/NLO($x\%$)/BBP($50 - x\%$)/ C_{60} (1%)). Two chromophores, with I_p values higher and lower than that of PVK (5CB and AODCST, respectively), were studied. The PR speed increased with chromophore concentration in the case of AODCST and remained almost constant in the case of 5CB. The difference was attributed to the participation of the AODCST in photogeneration and charge transport—a conclusion that was supported by photoconductivity experiments and numerical simulations.⁴⁸ Furthermore, in PVK-based composites it was confirmed that chromophores with I_p lower than that of the transport molecule can create deep traps in the PR material, while shallow traps form due to impurities and defects in the PVK itself.^{47,48} While the presence of traps is necessary for achieving high space-charge field in the material, excessive amounts of deep traps could be detrimental for PR dynamics and consistency of the PR performance (section 5.2.2), which complicates the material

design. For example, in PVK/NLO/ECZ/TNFM composites,²¹⁰ in which NLO chromophores with various I_p lower than that of PVK were utilized, the fastest PR dynamics were achieved in the composite containing the chromophore with I_p closest to that of PVK, while the highest 2BC gain coefficient and diffraction efficiency were observed in the composite containing the chromophore with the lowest I_p . This emphasizes the need to optimize a material for a particular application, because the trade-off between steady-state and dynamical properties could be unavoidable.

5.1.4. Plasticizers

Plasticizers are commonly added to a PR composite to lower the T_g to enhance the OE effect, i.e., chromophore reorientation in the space-charge field.⁵¹ Bolink et al.²¹¹ completed a study of a PVK/EPNA-(30%)/ECZ/C₆₀(0.1%) composite in which the concentration of ECZ used as a plasticizer was varied from 0 to 17.5% to replace PVK. The steady-state PR performance was enhanced as the concentration of ECZ increased due to improved orientational properties and therefore higher electro-optic response. Because the plasticizer itself does not typically have a direct functionality contributing to the PR performance, several studies were concerned with “functionalizing” a plasticizer (e.g., using a charge transporting molecule as a plasticizer)^{103,184} or eliminating the need for a plasticizer.^{102,212–215} For example, Van Steenwinckel et al.¹⁰³ doped their fully functionalized polymethacrylates with various concentrations of inert plasticizer (LC) as well as charge-transporting plasticizer (in this case ECZ). While the inert plasticizer was more effective in lowering the T_g , it also diluted the charge transporting moieties and at concentrations above 10% lowered mobility and reduced the PR phase shift. With ECZ as a plasticizer, although larger amounts were needed to lower the T_g to the desired value, charge transport properties did not deteriorate. The same group explored an alternative approach to plasticization²¹⁶ and synthesized functionalized polymethacrylates that among functional moieties (charge transporting, NLO, etc.) contained a plasticizer moiety (“internal plasticizer”) and thus did not require external plasticization. However, similar to polymer composites, at same relative-to- T_g temperatures, functionalized polymethacrylates that did not contain plasticizing moieties exhibited better PR properties than those with an “internal plasticizer” due to a higher concentration of “functional” moieties.²¹⁷ In one of the studies, directed toward increasing the functionality of the plasticizer, Zhang and Singer¹⁰² showed that the commercially available LC 5CB can efficiently plasticize a composite, while also serving as a NLO chromophore. 5CB was added to the PVK/C₆₀ mixture in concentrations of 0–65%, which lowered the T_g from ~230 °C (0%) to ~25 °C (65%). PR properties of the composite PVK(59.8%)/5CB(40%)/C₆₀(0.2%) (T_g ~ 40 °C) at room temperature were reported, for example, 2BC net gain coefficients of ~100 cm⁻¹ and external diffraction efficiencies of ~61% at a wavelength of 633 nm and an electric field of 150 V/μm. Another study that among other results demon-

strated that NLO chromophores can perform the role of a plasticizer was carried out by Bittner et al.^{130,218} who varied the concentration of the chromophore DMNPAA substituting either the molecules of ECZ or PVK in PVK/DMNPAA/ECZ/TNF composites. At fixed a concentration of ECZ (e.g., 10%), the T_g 's of the composites containing 30, 40, and 50% DMNPAA were ~62, 25, and 14 °C, respectively, which led to different PR dynamics (PR response times of 129, 62.8, and 5 s, respectively) in these composites at room temperature.¹³⁰ This work was one of the numerous studies that emphasized the role of T_g in PR performance. A detailed description of the influence of T_g on PR properties is given in section 5.2.1.

5.1.5. Other Dopants

Recently, several studies reported manipulation of the PR properties by using small concentrations of various dopants. In particular, gold nanoparticles added in low (below 1%) concentrations to a PVK-(70%)/DCVDEA(28.6%)/TNF(1.4%) composite led to an increase in 2BC gain coefficient and diffraction efficiency (section 6.7.1).²¹⁹ In a different study, addition of 0.82% hole-transporting molecules TPD to the PVK(39%)/DMNPAA(25%)/MNPA(25%)/ECZ-(10%)/TNF(1%) composite led to a change in the rate of grating dark decay.¹⁰⁵ Both results were explained by dopants affecting trapping properties of the material.

You et al. introduced a small amount (0–0.5%) of a dopant (M1) that served as an electron trap into a monolithic PR material (M0) that exhibited bipolar charge transport.³⁴ Both the 2BC gain coefficient and diffraction efficiency measured at 780 nm increased as the concentration of M1 increased from 0% (Γ ~ 140 cm⁻¹ at 35 V/μm, η_{\max} ~ 67% at 26 V/μm) to 0.05% (Γ ~ 235 cm⁻¹ at 35 V/μm, η_{\max} ~ 78% at 23 V/μm), which was attributed to increased trap density. However, further increases in concentration of M1 worsened PR steady-state properties (Γ ~ 80 cm⁻¹ at 35 V/μm, η_{\max} ~ 35% at 31 V/μm at 0.5% of M1) due to participation of M1 in electron transport that effectively reduced the trapping density.

5.2. Improving the Photorefractive Performance by Tuning the Experimental Conditions

The previous section discussed a number of physical studies directed toward optimizing polymer composites for the best performance. Next, we consider several ways to enhance the performance of the materials by varying the physical conditions. In particular, fine-tuning of T_g or the temperature at which the measurements are conducted with respect to T_g proved to be an effective way to improve PR properties.^{47,69,130,212,220–222} In section 5.2.1, we consider some pros and cons of the temperature tuning approach. Another topic that we address is the effect of preillumination. Several groups have reported the effects of preillumination, both positive and negative, on the photoconductive and PR performance of various materials.^{42,46,48,64–66,223,224} In section 5.2.2, we summarize the results of some of these studies.

5.2.1. Fine-Tuning the Temperature

Temperature is a key parameter in the PR performance because it affects all the processes participating in the PR effect—photogeneration, charge transport, trapping, and chromophore orientation in the electric field. Several groups have reported the effect of temperature on various material parameters such as photogeneration efficiency,⁴⁷ charge carrier mobility,^{119,151} PR phase shift,¹⁰³ orientational mobility,^{69,132,218,225} etc. Generally, at temperatures below T_g , an increase in temperature leads to improved dynamic and steady-state PR properties due to an enhanced orientational response and an increase in photoconductivity.^{130,218,221,222} However, at temperatures above T_g , while the PR dynamics can still improve, thermal disruption of the chromophore alignment, reduced trap densities, and increased dark conductivity lead to a deteriorated steady-state performance.^{47,69,130} Among the material classes whose properties are highly sensitive to the temperature with respect to T_g are organic glasses.^{69,226} In many organic glasses, the PR dynamics at temperatures around T_g are limited by the chromophore orientational speed.^{16,69,104,226} It is well-known from the vast literature on poled polymers and nonlinear optical organic glasses that chromophore orientational speed can be dramatically enhanced by increasing the temperature. As an illustration, Figure 10a shows birefringence rise (Δn_{BR}) due to chromophore orientation in response to a step-function electric field of 25 V/ μm , measured in a transmission ellipsometry experiment carried out at a wavelength of 976 nm in an organic glass DCDHF-6(50%)/DCDHF-6-C7M(50%) with $T_g = 23^\circ\text{C}$ at various temperatures ranging between 20 and 49 $^\circ\text{C}$.⁶⁹ Fine-tuning the temperature to the value $\sim 1^\circ\text{C}$ above T_g improved the orientational mobility by more than an order of magnitude compared with the orientational mobility at temperatures several degrees below T_g . Similar to other organic glasses, at temperatures around T_g , the PR speed in this mixture of DCDHF derivatives is limited by chromophore orientational mobility and, therefore, improved orientational speed should improve the PR speed. Figure 10b shows the PR speed (κ_r) obtained by fitting diffraction efficiency (η , $\eta \sim (1 - \exp[-\kappa_r t])^2$) transients at a wavelength of 676 nm at an electric field of 20 V/ μm in the same DCDHF glass sensitized with 0.5% C₆₀ as a function of light intensity at various temperatures. Indeed, the PR speed exhibited more than an order of magnitude increase as the temperature increased from several degrees below T_g to $\sim 10^\circ\text{C}$ above T_g , although as seen from the increase in exponent b of power law fits ($\kappa_r \sim I^b$) with temperature (inset of Figure 10b), the PR speed at higher temperatures becomes limited by photoconductivity rather than chromophore orientational mobility (section 5.3.1) and therefore is not expected to increase at higher temperatures as fast as in the temperature region around T_g . Moreover, an increase in temperature beyond $\sim T_g + (5-10)^\circ\text{C}$ leads to detrimental effects in the steady-state performance. In particular, the 2BC gain coefficient starts to dramatically decrease even at just a couple of degrees above T_g .⁶⁹ All DCDHF glass-forming

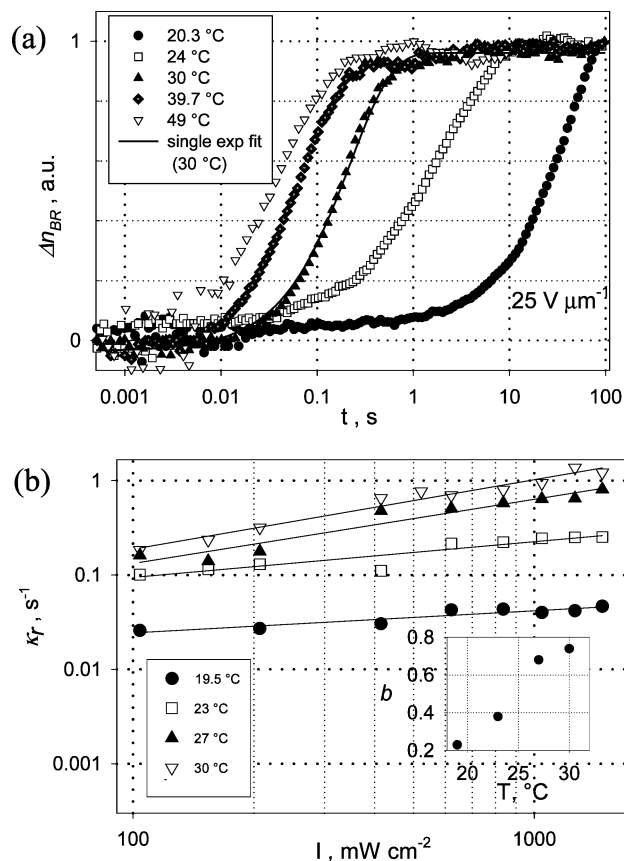


Figure 10. (a) Birefringence rise in response to step-function electric field of 25 V/ μm obtained in DCDHF-6/DCDHF-6-C7M organic glass ($T_g = 23^\circ\text{C}$) as a function of temperature. Single-exponential fit to the transient measured at 30 $^\circ\text{C}$ is also shown. (b) PR speed of grating formation measured in the FWM experiment at 20 V/ μm at 676 nm in the DCDHF-6/DCDHF-6-C7M/C₆₀ glass as a function of total intensity of the writing beams at various temperatures. Lines correspond to fit with a power law ($\kappa_r \sim I^b$). Inset shows the power law exponent (b) as a function of temperature. Reprinted from ref 69 with permission. Copyright 2003 Wiley-VCH.

derivatives studied¹⁰⁴ exhibited similar properties, and the optimal temperature at which the PR dynamics are improved, while the 2BC gain coefficient and diffraction efficiency are still high, was determined to be around $T_g + (2-3)^\circ\text{C}$. Many parameters such as conductivity, grating dark decay speed, etc. may change dramatically at temperatures above T_g and have to be taken into account when trying to optimize the experimental temperature or the T_g of the material.

5.2.2. Preillumination Effects

One aspect to be considered when designing PR organic materials for applications is that the PR performance of the material could depend on the experimental sequence of events. For example, grating formation transients recorded by simultaneously applying electric field and both writing beams can be noticeably different from those obtained after the poling field and one of the beams are applied for a long time prior to grating recording.²²⁷ Both prepoling effects related to the chromophore alignment in the uniform electric field and preillumination effects related to the creation of the ionized acceptor and

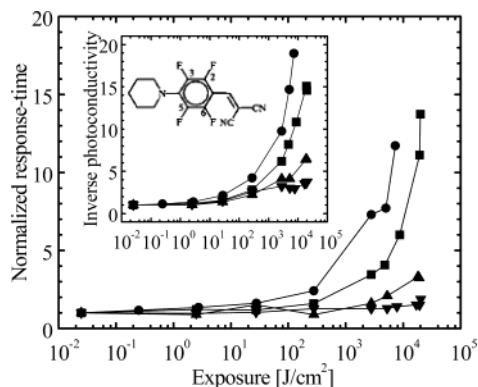


Figure 11. Normalized PR response time as a function of exposure of the PVK/NLO/ECZ/C₆₀ samples to 633 nm light at an electric field of 76 V/μm. Symbols correspond to the samples containing: F0 (circles), F1 (squares), F2 (triangles up), F4 (triangles down). Inset shows inverse photoconductivity as a function of exposure measured in the same samples and the chemical structure of the molecules. Reprinted from ref 65 with permission. Copyright 2000 American Institute of Physics.

filled trap densities prior to the PR grating recording have to be considered to optimize the grating recording scheme. In most PR studies, a scheme in which the samples are prepoled (i.e., electric field is applied for a long time before the PR measurements) is utilized, because it was shown to yield higher PR speed.²²⁷ The effect of preillumination, though, is not straightforward and varies depending on a material. The first observation of preillumination effects on PR steady-state and dynamic performance of polymers was reported in 1994 and attributed to optical trap activation.²²⁸ After the first report of the growth of ionized acceptors (C₆₀⁻) due to preillumination,⁴⁶ several studies were conducted to understand how the illumination of the PR sample prior to the photoconductivity or PR experiments affected the measured quantities. In several PVK-based polymer composites, the photoconductivity and PR response speed were found to decrease with preillumination.^{64,65} For example, Herlocker et al.⁶⁵ studied PVK/NLO/ECZ/C₆₀ composites, in which various fluorinated styrene derivatives F0, F1, F2, and F4 (in the inset of Figure 11, F0 is a nonfluorinated derivative, F1 contains fluorine at the position 2, F2 at the positions 2, 5, and F4 at the positions 2, 3, 5, and 6) with *I_p* values of 5.9, 6.0, 6.1, and 6.3 eV, respectively, served as NLO chromophores (*I_p* of carbazole is ~5.9 eV). Prior to the dc photoconductivity and FWM experiments, the samples were illuminated with various exposures of 633 nm light at an applied electric field of 76 V/μm. Figure 11 shows the PR response time (main figure) and inverse photoconductivity (inset) normalized at their values at minimal exposure of 10⁻² J/cm² as a function of exposure measured in the samples containing chromophores F0 (circles), F1 (squares), F2 (triangles up), and F4 (triangles down). As seen from Figure 11, the preillumination effect depended on the *I_p* of the chromophores and was stronger in the composites containing the chromophores with lower *I_p*. Ostroverkhova and Singer⁴⁸ studied the effect of preillumination on the time evolution of the diffraction efficiency in PVK/NLO(*x*%)/BBP(50 - *x*%)/C₆₀ composites contain-

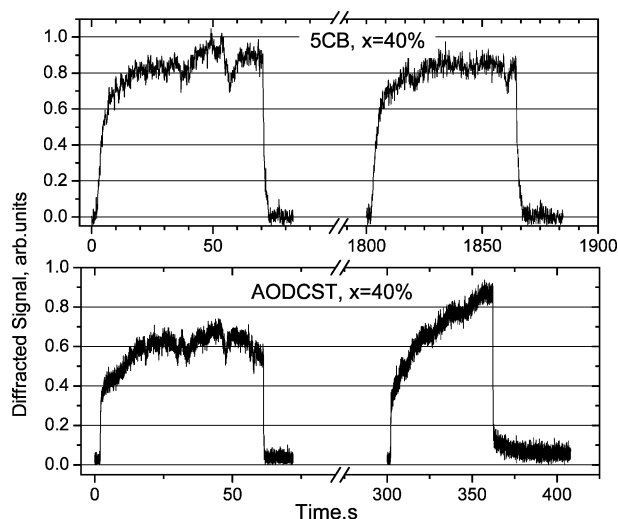


Figure 12. Diffracted signal as a function of time for "fresh" and preilluminated with 150 mW/cm² at 633 nm and 10 V/μm samples of the PVK/NLO(*x*%)/BBP/C₆₀ composites containing *x* = 40% of either (a) 5CB or (b) AODCST. Reprinted from ref 48 with permission. Copyright 2002 American Institute of Physics.

ing either 5CB (*I_p* higher than that of the carbazole⁴⁶) or AODCST (*I_p* lower than that of the carbazole⁴⁶) as NLO chromophores. FWM experiments were first performed in "fresh" samples and then after preillumination with 633 nm light with an intensity of 150 mW/cm² during 5–300 min at an applied electric field of 10 V/μm. Figure 12 shows diffraction transients obtained in "fresh" samples compared to those after 30 min of preillumination in the case of the 5CB-containing composite and 5 min in the case of the AODCST-containing composite. While the preillumination had no effect on a 5CB-containing composite even after 30 min of preillumination, in the AODCST-containing composite both the rise and decay in the diffraction efficiency transient completely changed after 5 min of preillumination (Figure 12). Both the photoconductivity and PR speed degradation observed in PVK-based composites were attributed to deep trap filling during the preillumination, which is consistent with the PR model described in section 3.1. The key mechanism is that during the preillumination, the ionized acceptor density as well as filled compensating trap density increase. If the PR experiment is performed shortly after preillumination, so that the traps with long detrapping times did not empty, then there is a certain concentration of ionized acceptors and filled traps in the materials at the starting time of the PR experiment. Therefore, the initial conditions for an illuminated sample are different from those for the "fresh" sample in which there are no ionized acceptors and filled traps in the beginning of the PR experiment. However, the effect of different initial conditions due to deep trap filling on the PR performance has to be determined for each material individually because it is controlled by the relative values of all the rates (e.g., trapping, recombination, etc.) introduced in section 3.1, and in principle the same physical mechanism can lead to different results, e.g., PR speed enhancement^{42,223} rather than degradation.^{64,65} Mecher et al. analyzed the effect of preillumination on PR performance in a

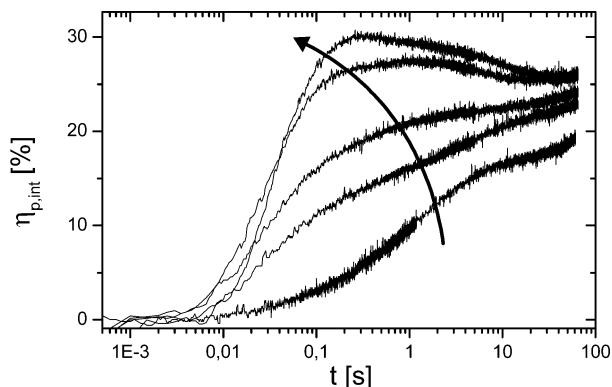


Figure 13. Time evolution of diffraction efficiency measured in the TPD-PPV/DMNPAA/MNPAA/DPP/PCBM composite at 830 nm in a pristine sample (the lowest trace) as well as after preillumination with 633 nm pulses of 955 ms duration and light intensity of 0.29, 0.58, 2.9 and 5.2 W/cm². Reprinted with permission from Nature (<http://www.nature.com>), ref 42. Copyright 2002 Nature Publishing Group.

variety of PVK- and TPD-PPV-based composites, including those containing permanent charges produced by adding a small amount of oxidizing agent TBPAH to a TPD-PPV-based composite.²²⁴ The authors concluded that the materials, in which the PR speed was limited by inefficient charge photogeneration in the absence of preillumination, exhibited improved PR dynamics after preillumination. In contrast, preillumination led to deteriorated PR dynamics in materials in which the PR speed was limited by charge carrier mobility.

To illustrate one case in which preillumination yielded speed enhancement, we discuss FWM experiments in the TPD-PPV/DMNPAA/MNPAA/DPP/PCBM composite at an electric field of 60 V/μm and total writing beam intensity of 3.27 W/cm² at a wavelength of 830 nm after various exposures to 633 nm light at 60 V/μm.⁴² Figure 13 shows the time evolution of the diffraction efficiency measured in a pristine sample and after pulsed preillumination (with pulse duration of 955 ms) with 0.29, 0.58, 2.9, and 5.2 W/cm² at 633 nm. As seen from the figure, in this material the preillumination improved PR dynamics, and thus with a proper choice of the preillumination duration and intensity, a considerable increase in PR speed can be achieved.⁴² Experimental diffraction efficiency transients for various intensities of the preillumination (Figure 13) showed qualitative agreement with those calculated using the PR model described in section 3.1 and photoelectric parameters obtained from the photoconductivity measurements.⁶⁶

5.3. Characterization Issues and Caveats

5.3.1. Photorefractive Response Speed: Photoconductivity or Orientationally Limited?

Characterization of the temporal dynamics in PR organic materials is not an easy task. First of all, the growth of the space-charge field is a complicated function of various photoelectric rates that in most cases cannot be described with a single exponential.^{48,57,58,60} Second, the convolution of the space-

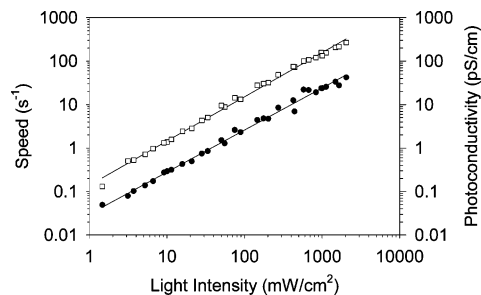


Figure 14. PR speed (filled circles) and photoconductivity (open squares) measured in the PVK/AODCST/BBP/C₆₀ composite as functions of light intensity at 50 V/μm at 647 nm. Solid lines represent power law fits. Reprinted from ref 93, with permission. Copyright 1998 American Institute of Physics.

charge field dynamics with noninstantaneous chromophore orientational response to yield the overall PR response speed further complicates the matter. Over the past years, there have been many suggestions regarding characterization of the PR dynamics. Among the functions employed to fit the refractive index change or 2BC gain measured in the PR experiments are single exponentials,^{69,162,226} biexponentials,^{48,129,218,229} stretched exponentials,^{93,104,230} power laws,¹⁵⁹ etc. Also, inverse Laplace transform analysis has been applied to the PR dynamics in order to reveal various components of the dispersive behavior and to assign them to certain processes.^{186,231} In addition to PR measurements, separate studies of chromophore orientational dynamics by independent techniques (section 4.2.2) are often performed and followed by the comparison between orientational and PR dynamics. Typically, if the orientational dynamics are much faster than the PR dynamics, then the PR speed is limited by space-charge field dynamics and is often referred to as a photoconductivity-limited response.^{129,134} If the chromophore orientation and PR grating formation occur on the same time scale, the PR dynamics could be orientationally limited.^{104,226} However, further tests are needed to confirm this conclusion. One such test relies on the comparison between intensity dependencies of photoconductivity and PR speed.⁹³ This approach is based on the fact that the orientational speed does not depend on light intensity, and therefore, all the writing or erasing beam intensity dependence of the PR speed should come from the space-charge field, or photoconductivity-related processes, in which case the intensity dependencies of the photoconductivity and PR (photoconductivity-limited) speed would be similar.⁹³ An example of photoconductivity-limited PR speed (τ_g^{-1} , from fitting $\Delta n \sim (1 - \exp[-t/\tau_g])$), measured in a low T_g PVK/AODCST/BBP/C₆₀ composite in a 2BC experiment at an electric field of 50 V/μm at 647 nm, is presented in Figure 14 as a function of total writing beam intensity (filled circles). Dc photoconductivity (σ_{ph}) measured in the same material as a function of light intensity is also shown (open squares). As seen from Figure 14, both photoconductivity and PR speed follow the same slightly sublinear ($\sigma_{ph}, \tau_g^{-1} \sim I^b, b \sim 0.8-0.9$) dependence on light intensity.⁹³ Similar results were obtained in other PVK-based as well as PSX-based composites.^{49,169} In contrast, for the case of orientationally

limited PR speed, the intensity dependence of the PR grating formation or erasure speed is much weaker than that of photoconductivity. For example, in DCDHF glasses at temperatures several degrees below T_g , the photoconductivity is a linear function of light intensity, while both PR grating formation and erasure speed ($\kappa_{r,e}$) determined from FWM experiments are power law functions of light intensity $\kappa_{r,e} \sim I^b$ with $b \sim 0.2\text{--}0.4$ (Figure 10b). Further confirmation of the orientationally limited PR speed below T_g in DCDHF glasses comes from the similarity of orientational speed $k_{BR} \sim 0.02 \text{ s}^{-1}$ measured in the transmission ellipsometry experiment and the PR speed $\kappa_r \sim 0.025\text{--}0.045 \text{ s}^{-1}$.⁶⁹

5.3.2. Traps and Grating Dark Decay

According to the analytical description of grating erasure derived by Cui et al.⁵⁸ from the Schildkraut/Buettner model,⁵⁶ the PR grating dark decay could provide some information about the trap depth, because the speed of dark decay is directly connected to the detrapping rates (i.e., $\beta_{1,2}$ in eq 3). Zilker and Hofmann²³² studied grating dark decay in a DRDCTA/EHMPA/TNFM organic glass ($T_g = 21 \text{ }^\circ\text{C}$) as a function of applied electric field. At every value of electric field, the measured decay of the diffraction efficiency was fit with a stretched exponential ($\eta^{1/2} \sim \exp[-t/\tau_d]^\eta$). It was found that the time constant of the decay (τ_d) decreased by a factor of ~ 3 as the electric field increased from 40 to 80 V/ μm , while the dispersion parameter (β) remained the same ($\beta \sim 0.9$). The dispersion was attributed to the distribution of the release times from the traps, and the electric field dependence of the time constant was explained by electric-field-assisted release of charges from trapping sites with broad energy distribution.²³²

In general, care should be taken with interpreting the results of the grating dark decay measurements because several processes can contribute. First of all, because the Schildkraut/Buettner model describes only space-charge field formation, but does not take into account the OE effect,⁵¹ a contribution of chromophore relaxation to PR grating decay has to be ruled out. Moreover, even if the grating dark decay is dominated by a space-charge field decay rather than chromophore relaxation, surprising results can occur. For example, in the PVK/DMNPAA/MNPAA/ECZ/TNF composite, the dark decay speed was found to depend on the intensity of the writing beams and recording time.¹⁰⁵ Finally, the PR model used by Cui et al.⁵⁸ for derivation of the grating decay dynamics does not take into account dark conductivity, which undoubtedly will strongly affect the grating dark decay.⁶⁹

5.3.3. Other Concerns

5.3.3.1. Influence of Beam Attenuation and Gaussian Profile. While in most high-performance PR materials the absorption at the wavelength of the PR experiments is kept low (usually below $\sim 30 \text{ cm}^{-1}$ or $\alpha L \sim 0.3$), some promising materials have higher absorption coefficients.^{49,162,170} In this case, the effects of beam attenuation in the sample should be taken into account when performing material characteriza-

tion.⁷⁰ For example, absorption should be properly accounted for to determine the *intrinsic* values of photoconductivity and PR response speed from the corresponding experimentally measured values.^{49,70,162} In addition to the beam attenuation due to absorption, standard Gaussian beam profiles (as opposed to uniform intensity distribution) could affect the PR dynamics as was demonstrated in the analysis of the PR grating erasure in BisA-NAS/DEH PR polymer.⁷⁰

5.3.3.2. Beam Fanning and Multiwave Coupling Effects. Beam fanning is an amplified scattering effect that occurs in high-gain PR organic materials (just as in inorganic crystals). Fanning manifests itself through an intensity loss as a single beam is transmitted through a sample with an electric field applied. The physical mechanism of beam fanning relies on the energy transfer characteristic of a 2BC experiment. A part of the pump beam scattered in the sample is amplified when the scattered light propagates in a direction that experiences high gain, i.e., the direction along which the interaction length between the pump and scattered light is maximized. For the sample geometry shown in Figure 5 at a sample thickness much smaller than the diameter of the pump beam, maximal interaction occurs between the pump beam and scattered beams propagating parallel to the electrodes.⁷¹ For PR characterization, beam fanning can be detrimental because it limits the PR gain and affects the results. The magnitude of the beam fanning effect depends on the direction of the applied field.^{71,233} It was found that to minimize the beam fanning, a negative high voltage has to be applied to the sample electrode at which the writing beams are incident. Therefore, this geometry is a preferable choice for the measurements of 2BC gain. Also, reducing the beam diameter helps to minimize beam fanning.²³⁴ However, at higher electric fields, even these measures are not sufficient to suppress the fanning, which prevents extraction of useful parameters.^{104,131,162,170} Improving optical quality and thermal stability of the films may help to reduce the scattering and therefore the beam fanning effect even in high gain materials.¹⁰⁴ Although beam fanning can be detrimental for measurements of 2BC gain, it can be advantageous for some applications such as optical limiting. For example, in the high-performance PR organic glass DCDHF-6(89.5%)/PVK(10%)/C₆₀(0.5%), the transmission of a beam with incident intensity of 1 W/cm² at 647 nm was studied as a function of electric field in the experimental configuration maximizing beam fanning.¹⁶ At 60 V/ μm , only $\sim 25\%$ of the incident beam was transmitted through the 100- μm -thick film.

In addition to beam fanning, there are other effects that can complicate PR experiments designed to determine the 2BC gain coefficient and diffraction efficiency including electroabsorption,^{235,236} grating bending,^{72,237} grating competition,^{51,73,74,107,238} etc. These effects can play an important role depending on the experimental geometry and electric field. For example, in the PVK/BDMNPAB/TNF composite it was found²³⁶ that at low electric fields and small incident angles, electroabsorption was relatively small, while

the competition between transmission and reflection gratings could affect the observed 2BC gain. In contrast, at high electric fields and high incident angles, electroabsorption dominated over other effects in obstructing the PR measurements.

To summarize section 5, through careful measurement and selection of improved components, much progress has been made in the quest for the "ideal" PR material. The material parameters and experimental conditions that affect PR steady-state and dynamic properties were identified and thoroughly studied. However, as one might expect, it appears that a "perfect" material may not exist because the structure–function relationships for the various components are often mismatched. Instead, every PR material has to be optimized for a particular application due to trade-offs between high gain coefficients and/or diffraction efficiencies and PR speed, long grating storage times, and undesirable illumination history dependence, etc. Nevertheless, the tremendous pool of physical studies is of great help in taking into account all the parameters and predicting the performance of a material considered for a certain application.

6. New Photorefractive Materials

Over the past several years, tremendous progress in improving PR organic amorphous materials has been accomplished. Because of the wide scope of PR materials research, it is impossible to describe all the new materials in one review, and thus we refer to several recent reviews for detailed description of the material design strategies developed for various subclasses of organic materials.^{24–27,239–241} Here, we limit our discussion to the best performing materials, which we arbitrarily define as those exhibiting gain coefficients above 150 cm^{-1} and/or diffraction efficiencies above 50%, reported since late 1996 up to March 2004. For the high-performance materials developed before 1996, the reader may consult Table 1 and the related discussion in ref 22. The following materials categories will be considered: polymer composites (section 6.1), organic amorphous glasses (section 6.2), fully functionalized materials (section 6.3), polymer dispersed liquid crystals (PDLCs) (section 6.4), and other LC-containing materials (section 6.5). Then, special attention will be devoted to novel materials exhibiting high sensitivity in the near-IR wavelength region (section 6.6). Finally, other directions of material research such as PR hybrid organic–inorganic composites, sol–gels, etc. will be outlined in section 6.7.

6.1. Polymer Composites

The most common composition of the best PR polymer composites explored to date is $\sim 40\text{--}60\text{ wt }%$ of a photoconductive polymer (e.g., PVK, PSX, PPV derivatives, etc.) to provide sufficient density of transport sites, $\sim 25\text{--}35\text{ wt }%$ of a NLO chromophore (e.g., dyes, LCs, etc.) to ensure a sufficient electro-optic response, $\sim 15\text{--}30\text{ wt }%$ of a plasticizer (e.g., ECZ, BBP, DOP, etc.) to facilitate chromophore orientation by lowering T_g of the material, and

finally, a small amount (usually below 1 wt %) of sensitizer (e.g., C_{60} , TNF, TNFM) to assist in charge photogeneration. A common alternative approach involved introducing $\sim 1\text{ wt }%$ of external sensitizer and $\sim 40\text{--}60\text{ wt }%$ of multifunctional molecules that serve both as charge transporting agents and NLO chromophores in an inert polymer matrixes such as PS, PIBM, PTCB^{155,166} to minimize inert volume and improve thermal stability of the composite.

In section 5.1, we reviewed the main strategies that allow for optimization of the various components of the composite to improve the overall PR performance. In this section, we list the constituents (Table 1) and summarize the properties of the best-performing PR polymer composites reported thus far in the red wavelength region (Table 2).

Among the sensitizers, C_{60} ,^{93,131} its more soluble derivative PCBM,⁴¹ and TNF¹⁶³ were utilized in the best performing composites in the red. In the near-IR, TNFM^{163,170} was the most common choice (section 6.6), although PCBM was also utilized.⁴²

The most widely used photoconductive polymers were PVK,^{93,131,163} various modifications of PSX,^{164,165,169} and several derivatives of PPV.^{41–43,242} As discussed in section 5.1.2, charge mobility is an important factor in PR dynamics, and thus the choice of photoconductor is an important issue to consider. PSX exhibits a mobility comparable to PVK,²⁴³ with a lower T_g , which leads to a reduced concentration of required plasticizer in a PR polymer composite and therefore a possible improvement of the PR properties due to reduced inert volume. PPV derivatives exhibit mobilities several orders of magnitude higher than PVK,⁴⁵ which could potentially lead to a faster PR speed (section 5.1.2). Other high-mobility polymers such as TFB,¹⁸⁶ PBPEs,²⁴⁴ PMPS,²⁴⁵ TDPANA-FA,²⁴⁶ were also considered as photoconductive hosts in polymer composites. Unfortunately, no considerable improvement of PR dynamics was achieved in these materials compared to the best performing PVK-based composites due to other factors such as photogeneration efficiency and orientational dynamics. Furthermore, many of the composites with fast PR dynamics exhibited low 2BC gain and diffraction efficiencies, in part due to reduced trap densities.^{186,246}

Among the most successful NLO chromophores utilized in PR polymer composites (see ref 27, for a recent review) are azo dyes (e.g., DMNPAA), oxopyridone derivatives (e.g., ATOP-3), dicyanostyrene derivatives (e.g., AODCST), dicyanomethylenedihydrofuran derivatives (e.g., DCDHF-6), pyridone derivatives (e.g., 2BNCM), rigidized polyene derivatives (e.g., DHADC-MPN), etc. In addition to the NLO properties, many chromophores such as DHADC-MPN, ATOP-4, DCDHF-6, etc. exhibited charge-transporting properties. Such multifunctional chromophores allowed minimizing inert volume and stabilization of the composite. For example, a high-performance PVK-based composite containing DHADC-MPN as a chromophore had poor thermal properties due to phase separation between the highly polar chromophore and relatively nonpolar PVK.¹⁶³ When the inert polar polymer PTCB was

Table 1. Chemical Structures of Sensitizers, Photoconductors, Plasticizers, and NLO Chromophores Utilized in High Performance PR Polymer Composites

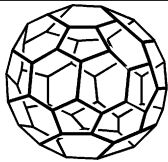
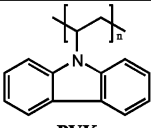
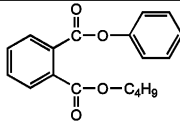
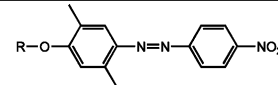
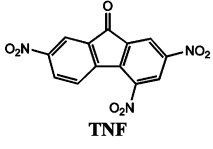
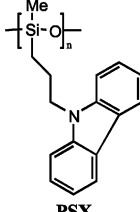
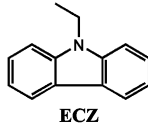
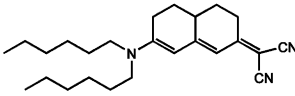
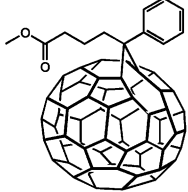
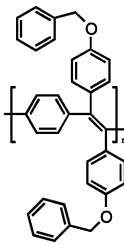
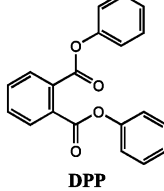
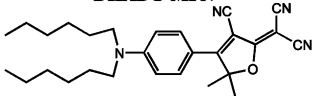
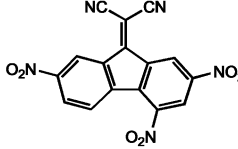
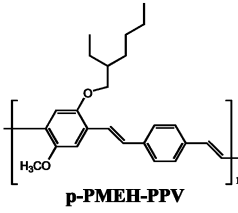
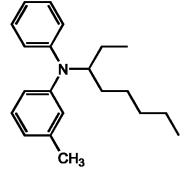
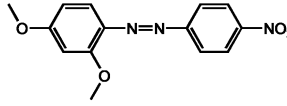
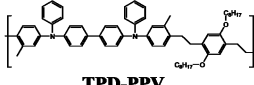
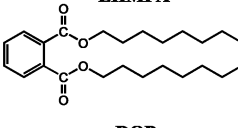
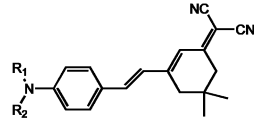
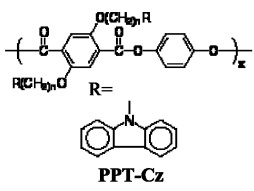
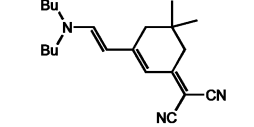
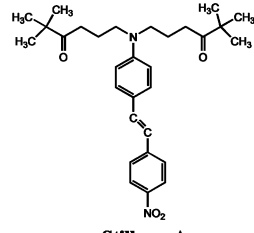
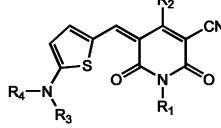
Sensitizers	Polymers	Plasticizers	NLO chromophores
 C₆₀	 PVK	 BBP	 DMNPAA: R=CH₃, BDMNPAB: R=n-C₄H₉, DMHNAB: R=CH₂CH₂OH
 TNF	 PSX	 ECZ	 DHADC-MPN
 [6,6]PCBM	 DBOP-PPV	 DPP	 DCDHF-6
 TNFM	 p-PMEH-PPV	 EHMPA	 MNPA
	 TPD-PPV	 DOP	 Lemke-E: R₁=R₂=CH₃ Ch C: R₁=CH₃, R₂=2-hydroxyethyl
	 PPT-Cz		 DB-IP-DC
			 Stilbene A
			 ATOP-3 R ₁ =2-Ethylhexyl R ₂ =Me R ₃ =R ₄ =Et

Table 2. PR Properties of High Performance Organic Materials in the Visible Part of the Spectrum^a

composite (conc of constituents, wt %)	T_g , °C	α , cm ⁻¹	d , μm	λ , nm	Γ , cm ⁻¹ (E , V/ μm)	τ_g^{-1} , s ⁻¹ (I , W/cm ²)	η_{max} , % (E , V/ μm)	τ_{FWM}^{-1} , s ⁻¹ (I , W/cm ²)	Δn , 10 ⁻³ (E , V/ μm)	ref
Polymer Composites										
PVK/AODCST/BBP/C ₆₀ (49.5/35/15/0.5)		9	80	647	235 (100)	200 (1) 6 (0.1)				93, 131
PVK/DCDHF-6/BBP/C ₆₀ (49.5/30/20/0.5)		15	80	647	400 (100)	4 (0.1)				131
PVK/BDMNPAB/TNF (55/44/1)	43		100	633	195 (85)	~1 (0.004)	40 ^{int} (70)		4.2 (92)	215
PVK/6OCB/C ₆₀ (49.8/50/0.2)	47.1		70		210 (65)					214
PSX/DB-IP-DC/TNF (69/30/1)	27.5	60	100	633	390 (100)	30 (0.04)	92 ^{int} (30)		3 (30)	165, 247
PSX/DMNPAA/TNF (53/46/1)	25			670	221 (80)			0.2 (1.2)	5.8 (80)	164
PSX/stilbene A/TNF (51/48/1)	25		40	670	53 (100)		100 ^{int} , 60 ^{ext} (70)	0.017 (1.2)	10.5 (100)	164
DBOP-PPV/DMNPAA/ MNPA/DPP/PCBM (52/20/20/5/3)	14.4	34	105	633			90 ^{int} (62)	1.7 (0.305)	2.6 (62)	41
<i>p</i> -PMEH-PPV/DO3/ DPP/C ₆₀ (74/5/20/1)	45			633	403 (0 ^b)	0.003 (0.28)				242
PPT-Cz/DDCST/C ₆₀ (64.5/35/0.5)	-7	36.6	100	633	250 (60)		93 ^{int} (100)	0.37 (0.034)	1 (50)	94
PTCB/DHADC-MPN/ DIP/TNFM (49.7/37.6/12.5/0.18)		22.6	105	633	225 (50)		71 ^{ext} (28)	0.07 (0.78)	8.5 (50)	166
Amorphous Glasses										
2BNCM/PMMA/TNF (90/9.7/0.3)	22	4	150	676	69 (40)		80 (40)	0.012 (1)	10 (40)	249
DCDHF-6/C ₆₀ (99.5/0.5)	19	12.7	70	676	240 (30)	0.6 (0.1)		0.41 (0.8)		104
DCDHF-6-CF3/C ₆₀ (99.5/0.5)	17	19.9	70	676	255 (40)	0.116 (0.1)		0.21 (0.8)		104
EHCN/TNF (99/1)	25	41	100	633	84 (40)		90 ^{int} (30)	0.67 (0.121)	1.3 (30)	251
Cz-C6-THDC/ECZ/TNF (89/10/1) ^c	33		50				65 (70)		4.5 (70)	252
methine A	6	1.64	130	633	118 (89)		74 ^{int} (53)		5.6 (53)	171
Fully Functionalized Polymers										
Ru-FFP	130	102		690	380 (0 ^b)	0.0014				89
Polymer-Dispersed Liquid Crystals and Liquid Crystals										
PMMA/TL202/ECZ/TNFM (42/40/17/1)		99 ^d	105 53	633	136 (10)		100 ^{int} (8) 56 ^{ext} (22)		3.2 (22)	265
PMMA/TL202/ECZ/CdS (42/40/16/2)		7.5	129	514.5	30 (31)		72 ^{ext} , 90 ^{int} (50)	~0.1 (3)		158
SCLP/E7/C ₆₀ (50/49.95/0.05)		<20	50	633	640 (0.7)	0.29 (8)				310
E7 on PVK/TNF (83/17) ^e		20	10	514.5	3700 ^e (0.9)		44 ^{ext.f} (0.9)	~100		293
Hybrid Organic-Inorganic Composites, Glasses, and Sol-Gels										
PiBM/AZPON (40/60)		113	55	633	350 (35)		80 ^{int} (13)		9 (25)	155
BEAPON	24	49	40	633	750 (100)		40 ^{int} (28) ^c		11 (33)	155
PVK/DCVDEA/TNF/Au (70/28.6/1.4/<1)	40		70	633	240 (130)		43 (90)			219
Sol-gel DMHNAB- urethane-SiO _{1.5} / SiO _{1.5} OH/ECZ/TNF (1:1.1:0.2:0.002) ^g		29	30	633	444 (0 ^b)		25.6 ^{int.h} (0 ^b)	0.0056	3.5 ^h (0 ^b)	87
Sol-gel SG-Cz/ SG-MN/PEG/TNF (45/45/9/1)	2		75	633	55 (94)		82.4 ^{ext} (94)	0.59 (0.14)		323

^a Columns represent: (1) composition (concentration of the constituents in wt %, unless stated otherwise); (2) glass transition temperature T_g ; (3) absorption coefficient α ; (4) sample thickness d ; (5) wavelength of the PR experiments λ ; (6) 2BC gain coefficient, measured with p-polarized writing beams, Γ (electric field E , at which the indicated Γ was obtained); (7) PR response time τ_g^{-1} obtained from fits to 2BC dynamics (total light intensity of writing beams, at which the indicated value of τ_g^{-1} was obtained); (8) maximal diffraction efficiency η_{max} , measured with p-polarized probe and s-polarized writing beams. External (η^{ext}) or internal (η^{int}) diffraction efficiency is indicated, where applicable (electric field E , at which the indicated η was obtained); (9) PR speed τ_{FWM}^{-1} obtained from fits to either formation or erasure of the PR grating measured in the FWM experiment (total light intensity of either writing beams or erasing beam); (10) refractive index modulation Δn , calculated from the diffraction efficiency (electric field E , at which the indicated refractive index modulation was obtained); (11) reference to work from which the data was taken. All data reported were obtained in Bragg regime (volume grating) at room temperature, unless stated otherwise. ^b Prepoled material. ^c Temperature of the measurements $T_m = 30$ °C. ^d Includes scattering losses. ^e All the measurements were done in the Raman-Nath regime. See discussion about the relevance of the gain coefficient in the text. ^f Maximal diffraction efficiency possible in the Raman-Nath regime is ~34%. The authors attributed their high diffraction efficiency by nonsinusoidal space-charge field. ^g Molar concentrations. ^h This value was obtained with p-polarized writing beams and p-polarized readout.

utilized instead of PVK, so that DHADC-MPN molecules served both as charge transport agents and NLO chromophores, high PR performance was pre-

served, while the thermal stability of the composite was considerably improved.¹⁶⁶ In addition to a number of functionalities that can be performed by single

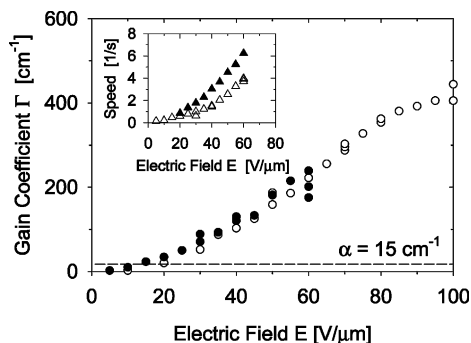


Figure 15. Electric field dependence of 2BC gain coefficient obtained in the composite PVK/DCDHF-6/BBP/C₆₀ at 647 nm at high beam ratio (open circles) and beam ratio of unity (closed circles). Inset shows PR response speed as a function of electric field measured at total writing beam intensity of 100 mW/cm² in PVK/DCDHF-6/BBP/C₆₀ (open triangles) and PVK/AODCST/BBP/C₆₀ (closed triangles). Reprinted from ref 131 with permission. Copyright 2001 American Institute of Physics.

moieties, some of the molecules (e.g., ATOP-4, DCDHF-6, 2BNCM) exhibited glass-forming properties and were utilized in low molecular weight monolithic PR organic glasses (section 6.2).

Among the small-molecule plasticizers, various types of molecules such as inert nonpolar molecules (e.g., BBP), LCs, and charge transporting molecules (e.g., ECZ) were used (Table 1). As usual, however, the addition of relatively small NLO chromophores as molecular dopants can also achieve a certain degree of plasticization.

Table 2 summarizes the PR properties of several high performance PR organic materials including polymer composites in the red wavelength region. Importantly, very large 2BC gain coefficients up to 400 cm⁻¹ were achieved in several polymer composites. As an illustration, Figure 15 shows the 2BC gain coefficient as a function of electric field obtained in the composite PVK/DCDHF-6/BBP/C₆₀ at 647 nm in the case of high writing beam ratio (open circles) and beam ratio of unity (closed circles).¹³¹ While at a beam ratio of unity, strong beam fanning effects prevented the experiments at electric fields above ~60 V/μm, the experiments with a high beam ratio allowed assessing the PR performance of the composite at higher fields. Gain coefficients of ~400 cm⁻¹ were obtained at electric fields of ~100 V/μm and were accompanied by a low absorption coefficient of ~15 cm⁻¹ at the wavelength of the 2BC experiment (647 nm), which led to high net gain coefficients of ~385 cm⁻¹.

Comparison of diffraction efficiencies is made complicated because some researchers report internal diffraction efficiencies, while others report external diffraction efficiencies. In the PSX/stilbene A/TNF composite, an internal diffraction efficiency of 100% which corresponded to external diffraction efficiency of 60% was obtained in 40-μm-thick films at 70 V/μm at 670 nm.¹⁶⁴ In several other composites, internal diffraction efficiencies of over ~90% were obtained (Table 2).^{41,94,247} In the PTCB(50.3%)/DHADC-MPN-(37.4%)/DIP(12.3%) composite, which did not contain any sensitizer, an external diffraction efficiency of 78% was obtained in a 105-μm-thick sample at only

36 V/μm at 633 nm.¹⁶⁶ However, the PR response time was slow, on the order of ~47 s. Addition of 0.18% TNFM led to severalfold improvement in the response time, while maintaining a high external diffraction efficiency of 71% at 28 V/μm and net gain coefficient of ~202 cm⁻¹ at 50 V/μm (Table 2).

As discussed in section 5, it is challenging to create a material with both excellent steady-state and dynamic performance. Most PR polymer composites which exhibit high gain coefficients >200 cm⁻¹ (Table 2) exhibit PR response speed ranging between 0.1 and 10 s⁻¹ at light intensities below 1 W/cm². In the red wavelength region, the best PR response time of ~5 ms while maintaining high 2BC net gain coefficient of ~225 cm⁻¹ at an electric field of 100 V/μm and light intensity of 1 W/cm² at a wavelength of 647 nm was achieved in PVK/AODCST/BBP/C₆₀.⁹³ In addition, in several composites, the PR speed was reported at lower light intensities, and therefore a faster response could be expected at higher intensities. For example, the PR response time measured in high performance polymer composite PVK/DCDHF-6/BBP/C₆₀ (Figure 15) was ~250 ms at 100 mW/cm² at 647 nm.¹³¹ The inset of Figure 15 shows the dependence of PR response speed on the electric field measured in the composite PVK/DCDHF-6/BBP/C₆₀ (open triangles) as well as in the above-mentioned composite PVK/AODCST/BBP/C₆₀ (closed triangles). Under similar conditions of total writing beam intensity of ~100 mW/cm², the PR dynamics in a DCDHF-6-containing composite is not significantly slower, and thus, similar to the PVK/AODCST/BBP/C₆₀ material, response times on the order of several milliseconds would be expected in the PVK/DCDHF-6/BBP/C₆₀ composite at light intensity of ~1 W/cm², accompanied with high 2BC gain (Table 2). As another example, the composite PSX/DB-IP-DC/TNF (Table 2) exhibited a net gain coefficient of 330 cm⁻¹ and a PR response time of 33 ms at 100 V/μm at light intensity of only 40 mW/cm² at 633 nm.²⁴⁸ Increasing the intensity could potentially reduce the response time of this material down to several milliseconds. However, it should be kept in mind that large intensities are not always desirable due to increased probability of photodamage, undesirable absorption grating formation, etc.

Overall, the advantage of polymer composites is the ability to tune their properties by varying the concentration and type of constituents. The disadvantages include the potential phase separation and crystallization that can occur when highly polar chromophores are added in large concentrations to the nonpolar matrixes.²⁰⁴ Also, as discussed above, an addition of a plasticizer which lowers T_g and therefore enhances chromophore orientation in the meantime increases the inert volume, which worsens photoconductive and NLO properties.

6.2. Organic Amorphous Glasses

Organic glasses refer to materials containing no amorphous polymer, and typically the one primary molecular component serves the functions of photoconductor as well as NLO molecule. The advantage of organic glasses is that the inert volume is mini-

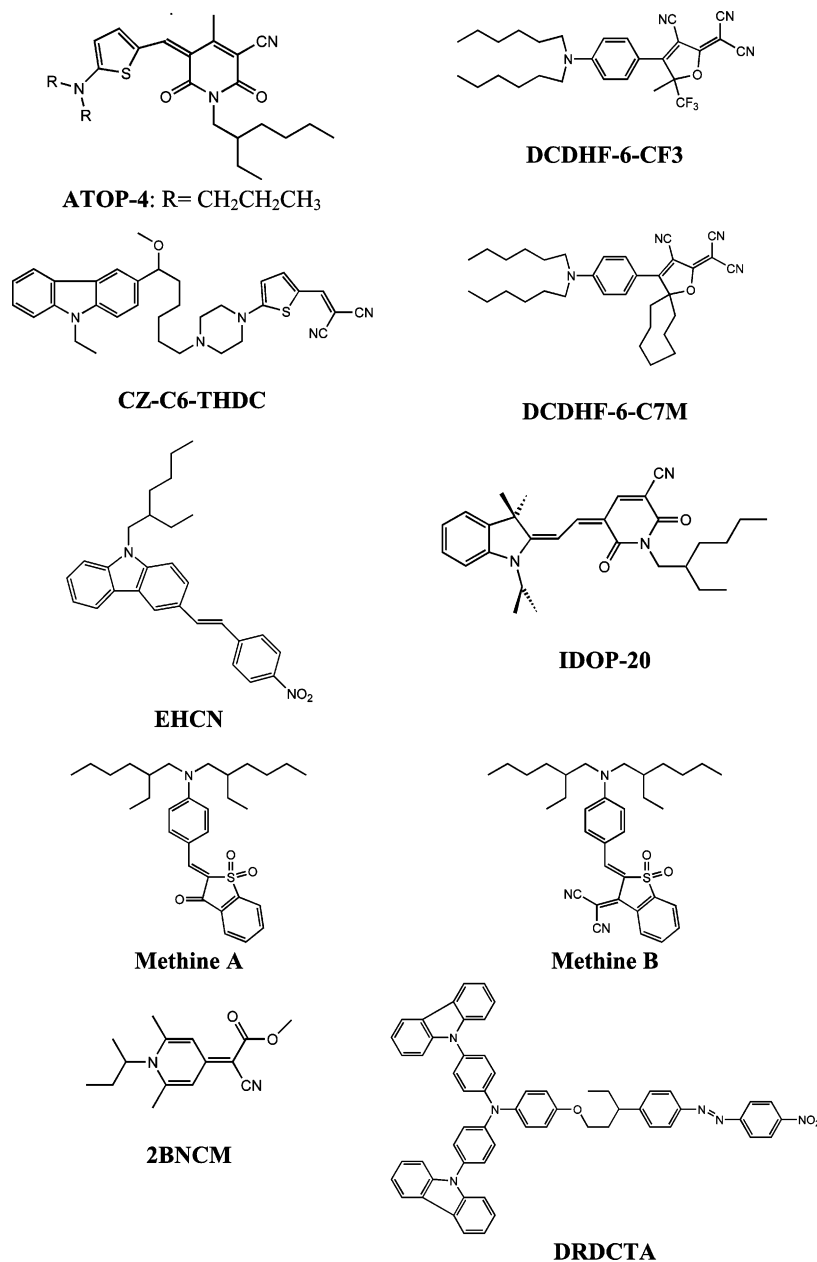


Figure 16. High performance glass forming molecules.

mized, i.e., the density of NLO moieties and charge transporting sites is the maximal achievable due to tight packing of the molecules in the glass, yet there is no phase separation problem that occurs in the polymer composites with high concentration of chromophores. The disadvantage is that the easy tunability of the properties that is the case for polymer composites is reduced to synthetic modifications of the glass-forming molecule. In addition, the molecule must be designed to prevent self-crystallization to maintain optical clarity. Nevertheless, by synthetic efforts, sets of molecules with the same core moieties but with various covalently attached substituents have been created to tune the thermal and optical properties.^{170,208,249,250}

The first PR organic amorphous glass was reported in 1996²⁴⁹ and was based on the 2BNCM multifunctional chromophore (Figure 16). A net gain coefficient of 65 cm⁻¹ and diffraction efficiency of ~80% were obtained in a 2BNCM(90%)/PMMA(9.7%)/TNF(0.3%)

mixture at 40 V/μm at 676 nm (Table 2). (The addition of the small amount of PMMA to the 2BNCM glass did not significantly affect the *T_g* and steady-state PR performance but improved the PR dynamics).²⁴⁹ Since then, a variety of PR glass-forming molecules have been synthesized and characterized.^{16,27,151,170–172,208,222,250–252}

Several representative molecules that form the highest-performing PR glasses reported to date are shown in Figure 16. Some of these molecules (e.g., methine B, ATOP-4, IDOP-20, etc.) exhibited extraordinary PR properties in the near-IR wavelength region and will be discussed separately in section 6.6. As a result of high density of functional groups in organic glasses, many materials exhibit high gain coefficients and diffraction efficiencies at low electric fields, which is important for applications. For example, at 676 nm, several glasses containing DCDHF derivatives (e.g., DCDHF-6, DCDHF-6-CF₃, a mixture of DCDHF-6 and DCDHF-6-C7M, etc.) sensi-

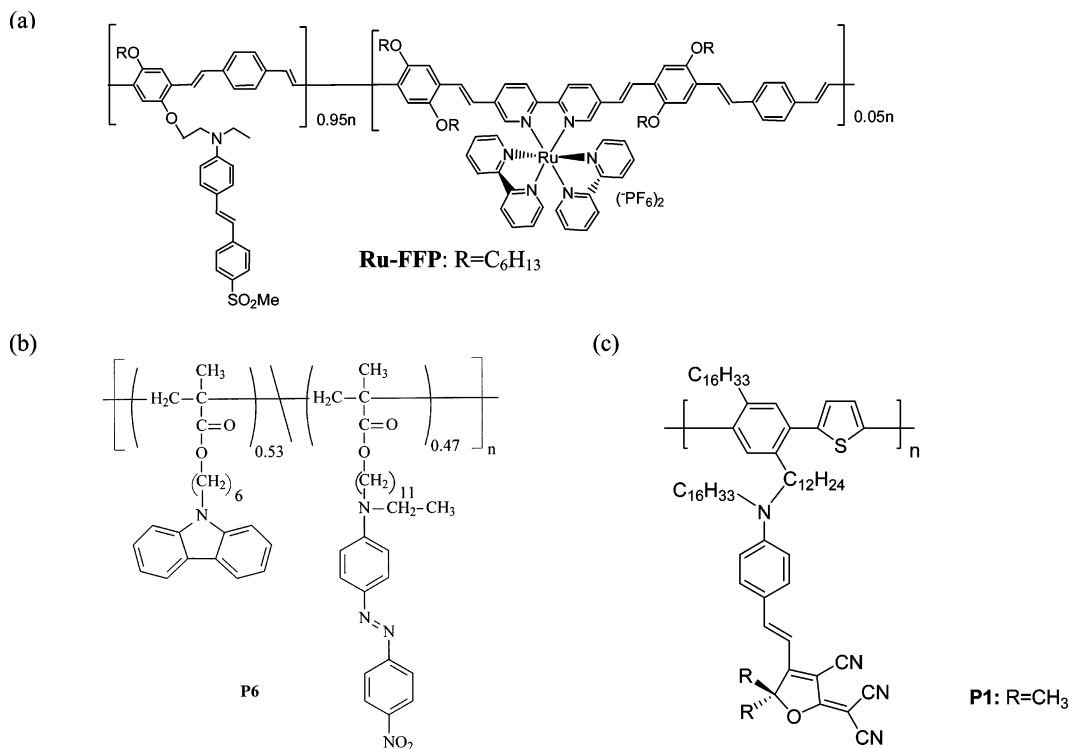


Figure 17. (a) Fully functionalized PR polymer containing ruthenium complex (Ru-FFP). (b) Fully functionalized PR polymethacrylate (P6). (c) Fully functionalized PR polymer containing DCDHF chromophore (P1).

tized with C_{60} exhibited net gain coefficients of $\sim 230 \text{ cm}^{-1}$ at electric fields of only $\sim 30\text{--}40 \text{ V}/\mu\text{m}$ (Table 2).¹⁰⁴ At 633 nm, a diffraction efficiency $\eta \sim 90\%$ was measured at $30 \text{ V}/\mu\text{m}$ in a $100\text{-}\mu\text{m}$ -thick film of EHCN glass sensitized with 1% TNF,²⁵¹ and $\eta \sim 74.3\%$ was observed at $53 \text{ V}/\mu\text{m}$ in $130\text{-}\mu\text{m}$ -thick film of a low-molecular-weight glass based on the unsensitized methine dye A.¹⁷¹ Many organic glasses that exhibited excellent steady-state performance had slow PR dynamics, with response times at best on the order of tens of seconds at temperatures around T_g ,^{104,170,226} although glasses with response times on the order of several tens of milliseconds (e.g., DRDCTA/DOP/ C_{60} ,¹⁵¹ methine dyes,¹⁷¹ etc.) were also reported. In many cases, slow PR dynamics are related to slow chromophore reorientation in the electric field due to intermolecular dipole-dipole interactions and low free volume. As described in section 5.2.1, the performance of PR glasses is strongly dependent on the temperature relative to T_g ,^{69,222,226} and the PR speed can be dramatically improved by increasing the temperature above T_g . However, at the same time the steady-state performance may worsen,⁶⁹ and therefore the temperature should be chosen to optimize both steady-state and dynamic performance.

6.3. Fully Functionalized Polymers

Fully functionalized PR polymers have attracted attention because they eliminate the problems of phase separation and crystallization and therefore could lead to a better thermal stability and longer shelf life for potential devices. The first fully functionalized PR polymer was reported in 1992 and

consisted of a multifunctional polyurethane upon which charge generator, charge transporter, and NLO moieties were incorporated as side chains.²⁵³ This material exhibited a 2BC gain coefficient of only 2.3 cm^{-1} . Since then, much progress has been made in the development of high-performance fully functionalized PR materials.^{25,153,154,168,216,217,254–257} A recent review of strategies of material design applied to the synthesis of fully functionalized polymers can be found in ref 25. Here we summarize the performance of the best fully functionalized polymers reported to date. Net gain coefficients of over $\sim 200 \text{ cm}^{-1}$ at zero external electric field at 690 nm were obtained in high T_g prepoled conjugated polymers containing Ru photogenerator complexes, introduced into the polymer backbone (Ru-FFP, Figure 17a, Table 2).⁸⁹ However, the PR response time in these materials was long, on the order of several hundreds of seconds. In oligothiophenes covalently attached to NLO chromophores, diffraction efficiencies of $\sim 40\%$ with PR response times of $\sim 40 \text{ ms}$ were obtained in $\sim 70\text{-}\mu\text{m}$ -thick films at electric fields of $\sim 70 \text{ V}/\mu\text{m}$ at the wavelength of 633 nm for the writing beams and of 780 nm for the probe beam.²⁵⁸ Polymethacrylates with attached charge transporting carbazole and NLO moieties (e.g., P6, Figure 17b), externally sensitized with 1% TNFM, exhibited 100% internal diffraction efficiencies in $125\text{-}\mu\text{m}$ -thick films at $\sim 58 \text{ V}/\mu\text{m}$ and gain coefficients of $\sim 150 \text{ cm}^{-1}$ at $65 \text{ V}/\mu\text{m}$ at 780 nm (Table 3).²¹⁷ In conjugated poly(*p*-phenylene-thiophene)s with attached tricyanodihydrofuran derivatives (P1, Figure 17c), external diffraction efficiencies of $\sim 68\%$ and gain coefficients of ~ 180

Table 3. PR Properties of High Performance Organic Materials in the Near-IR Wavelength Region^a

composite (conc of constituents, wt %)	T_g , °C	α , cm ⁻¹	d , μm	λ , nm	Γ , cm ⁻¹ (E, V/ μm)	τ_g^{-1} , s ⁻¹ (I, W/cm ²)	η_{max} , % (E, V/ μm)	τ_{FWHM}^{-1} , s ⁻¹ (I, W/cm ²)	Δn , 10 ⁻³ (E, V/ μm)	ref
Polymer Composites										
PVK/ATOP-3/ECZ/DPP/TNFM (31/40/14/14/1)	14	15	105	790	180 (30)		85 ^{int} (22)	1.3 (9.9)	7 (40)	170
PVK/DHADC-MPN/ECZ/TNFM (49/25/25/1)			105	830			74 ^{ext} (59)	~0.5 (1)	1.5 (40)	163
PVK/Lemke-E/ECZ/TNFM (43/28/28/1)			125	780	175 (72)	20 (4.5)				15
PVK/Ch C/ECZ/TNFM (42/28.2/28.5/1.3) ^b	21	~44	125	780	230 (68)		95 ^{int} (52)			210
Amorphous Glasses										
TH-DCDHF-6V/DCDHF-8/TNFM (49.5/49.5/1)	23	87.8	80	830	463 (45)	0.22 (0.1)				162
methine B	26	5.54	130	780	221.4 (89)		87.6 ^{int} (44)	60 (3)	10.4 (44)	171
IDOP-20/DPP/TNFM (69/30/1)	18	11	100	780	150 (50)	0.0068	83 ^{int} (40)	0.0075	9 (60)	226
ATOP-4/TNFM (99/1)	16	111	105	790	130 (28)		85 ^{int} , 32 ^{ext} (10.5)		10.7 (28)	170
M0/M1 (99.95/0.05)		2.5	125	780	237.5 (35)		77.5 ^{int} (23)			34
Fully Functionalized Polymers										
P6/TNFM (99/1) ^c	33	~65	125	780	150 (65)		100 ^{int} (58)	~0.05 (11)	2.8 (58)	217
P1	20	24	130	780	180 (50)		68 ^{ext} (46)	0.5 (1.9)		259

^a Structure of the table is described in the caption of Table 2. ^b The measurements were carried out at the temperature $T_m = 25$ °C. ^c The measurements were carried out at the temperature $T_m = 35$ °C.

cm⁻¹ were obtained in 130- μm -thick films at 50 V/ μm at 780 nm (Table 3),²⁵⁹ which approached the steady-state performance of many high performance PR composites and glasses at this wavelength.

6.4. Polymer-Dispersed Liquid Crystals

Polymer-dispersed liquid crystals (PDLCs), which contain high concentrations of both polymer and liquid crystalline molecules that phase separate into droplets, were initially of interest due to their electro-optic switching properties for potential applications ranging from optical shutters to displays.^{260,261} In PR PDLCs, the polymer typically provides the photoconductive properties needed for the space-charge field formation, while the LC droplets provide orientational nonlinearity needed for the refractive index modulation. The advantage of PDLCs compared with traditional polymer composites is that LC molecules in droplets can be reoriented with much lower electric fields than those used in polymer composites. PR in PDLCs was reported for the first time in 1997 by two groups.^{262,263} The two groups used similar polymer/LC mixtures (PMMA/E49²⁶² and PMMA/E44²⁶³), but with different sensitizers (1% TNF²⁶² and 0.05% C₆₀²⁶³). Additionally, Golemme et al.²⁶² used 21% ECZ as a charge transporter. The assessment of the hologram regime²⁶⁴ is commonly done using a parameter $Q_h = 2\pi d\lambda/(\Lambda^2 n)$, where d is the sample thickness, λ is the optical wavelength, Λ is the grating spatial wavelength, and n is the refractive index, and the cases of $Q_h > 10$ correspond to Bragg (volume, or thick) holograms, while $Q_h \leq 1$ represents the Raman-Nath (surface or thin) grating regime.⁵³ Interestingly, the experiments performed by Golemme et al.²⁶² were done in the Bragg regime (thick grating), while those by Ono and Kawatsuki²⁶³ operated in Raman-Nath regime (thin grating). In the Bragg regime,²⁶² an internal diffraction efficiency of ~40% (external ~8%) and refractive index modulation $\Delta n \sim 0.002$ at an electric field of 23 V/ μm as well as the 2BC gain coefficient of 41 cm⁻¹ at an electric

field of 6 V/ μm were obtained at 633 nm in a 53- μm -thick PDLC film. However, no net gain was observed in this material due to high scattering losses. In the Raman-Nath regime,²⁶³ similar values of refractive index modulation $\Delta n \sim 0.003$ were observed at an electric field of 40 V/ μm at 633 nm in a 25- μm -thick film.

Since 1997, the PR performance of PDLCs has considerably improved.^{158,265–268} For a recent review of LC-containing PR materials, including PDLCs, see ref 26. In the Bragg regime, one high-performance PR PDLC exhibited internal diffraction efficiencies of 100% in 105 μm films at an electric field of only 8 V/ μm and net gain coefficients of 37 cm⁻¹ at 22 V/ μm (composite PMMA(42%)/TL202(40%)/ECZ(17%)/TNFM(1%)²⁶⁵) at 633 nm. In another PDLC, external diffraction efficiencies of 72% (internal ~90%) in 129 μm film at 50 V/ μm (composite PMMA(42%)/TL202(40%)/ECZ(16%)/CdS(2%)¹⁵⁸) were observed at 514.5 nm. As a third example, internal diffraction efficiencies of 100% in 125 μm films at 25 V/ μm and refractive index modulations $\Delta n \sim 0.018$ at 50 V/ μm (composite containing 60% of functionalized polymethacrylate, 19% of LC, 20% of azo dye and 1% TNFM²⁶⁷) were obtained at 780 nm. The weak points of PDLCs include high losses due to scattering, which prevent high net gain, and slow, on the order of minutes, PR dynamics due to low mobility. Ono et al. compared scattering losses, photoconductive and PR properties in the Raman-Nath regime between PMMA-based phase-separated PDLC samples and miscible polymer-dissolved LC samples and concluded that the latter systems were superior to PDLCs in all parameters due to more favorable morphology.²⁶⁹ The potential to improve dynamics by substituting PMMA with a photoconductive polymer such as PVK was demonstrated in the composites PVK(48%)/TL202(51%)/TNF(1%) (PVK(56%)/E869(30%)/ECZ(13%)/TNF(1%)) in which PR response time reached ~100 ms (~25 ms) at ~400 mW/cm² (~1.2 W/cm²) at 633 nm.^{265,270} However, diffraction

efficiencies of only several percent and/or no net gain were obtained from these composites.

A number of physical studies were conducted in various PDLC systems to clarify the mechanism of PR in these materials.^{91,266,271–275,269} In particular, the orientational nature of PR in PDLCs was studied by scanning electron microscopy²⁶⁶ and by the analysis of the electric field dependence of diffraction efficiency measured in a FWM experiment.²⁷⁴ Recently, static and dynamic near-field scanning optical microscopy was applied to study photogeneration, ion migration, and electric field-induced LC reorientation in dye-doped PDLCs.²⁷⁶ In other studies, the importance of the direction of total electric field,²⁷⁴ droplet size²⁷⁵ and interfaces, local heating,²⁷³ residual internal polarization, etc. were investigated.

6.5. Other Liquid Crystal-Containing Materials

PR in LCs was first observed in 1994 in 5CB and several other nematic mixtures sensitized with a small amount of dye such as R6G, Methyl Red, etc.^{277–279} Here, the space-charge field was formed via nonuniform diffusion of photogenerated ions and depended on relative diffusion coefficients for the anions and cations as well as conductivity contrast.²⁷⁸ The resulting refractive index perturbation occurred due to reorientation of the highly anisotropic LC molecules in the space-charge field. The Raman-Nath (thin grating) regime was utilized, so that several diffraction orders were observed. At 514.5 nm, a 2BC gain coefficient of $\sim 25 \text{ cm}^{-1}$ and a diffraction efficiency of $\sim 1\%$ at an electric field of $0.01 \text{ V}/\mu\text{m}$ were reported in $100\text{-}\mu\text{m}$ -thick cells (the grating period was $\sim 278 \mu\text{m}$) filled with 5CB.²⁷⁹ A theoretical formalism for the PR effect in LCs was developed in refs 277 and 280–282.

Since 1994, much improvement was achieved in PR performance for these materials (see ref 26. for a recent review). For example, in the Raman-Nath regime, diffraction efficiencies of $\sim 20\%$ (the maximal diffraction efficiency for the Raman-Nath regime is $\sim 34\%$ ²⁸³) were reported at 514.5 nm in a $10\text{-}\mu\text{m}$ -thick cell coated with 63 nm of a photoconductive polymer and filled with an E7 nematic mixture.²⁸⁴ It is difficult to report 2BC gain coefficients extracted from measurements in the Raman-Nath regime, because the formulas for Bragg regime (eq 4) assume exponential growth of the gain with sample thickness, which is not necessarily true for a thin grating. Yet, some researchers report gain coefficients (Γ) calculated using eq 4, while others use values of gain factor defined as $\gamma_0 = I_1(\text{out})/I_1(\text{in})$, where $I_1(\text{in})$ ($I_1(\text{out})$) is the intensity of the probe beam in the absence (presence) of the pump beam. However, because gain γ_0 can depend on pump beam intensity (I_2) (or pump/probe intensity ratio $\beta_p = I_2(\text{in})/I_1(\text{in})$), it is difficult to compare the results reported by different groups, and therefore further in this section we will list the PR parameters together with relevant experimental conditions.

One of the strategies that led to an improvement of the PR performance of LCs was doping the LC with donor and acceptor molecules to increase photogeneration efficiency.²⁸⁵ In the eutectic LC mixture

8OCB/5CB doped with perylene as an electron donor and NI as an electron acceptor, a gain of $\gamma_0 = 1.88$ with PR response time of $\sim 40 \text{ ms}$ at $\beta_p = 1$, $I_2 = 50 \text{ mW}/\text{cm}^2$ and applied electric field of $\sim 0.07 \text{ V}/\mu\text{m}$ was obtained in a $37 \mu\text{m}$ cell at 514.5 nm.²⁸⁵ It was also demonstrated that similar to polymer composites, doping with fullerenes enhanced the PR properties of LCs. For example, in 5CB doped with 0.05% C_{60} , $\gamma_0 = 18$ with a PR response time of $\sim 300 \text{ ms}$ at $\beta_p = 245$, $I_2 = 400 \text{ mW}/\text{cm}^2$ and an electric field of $0.3 \text{ V}/\mu\text{m}$ ²⁸⁶ was observed in a $10 \mu\text{m}$ cell at 488 nm. In addition, recently it was shown that PR sensitivity of LCs can be improved by doping them with carbon nanotubes.^{287,288}

To increase the trap density and improve charge carrier mobility, it was proposed to stabilize the LC with low concentration of polymer.^{193,289} Moreover, it was found that PR in LCs can be promoted by surface activation, e.g., by using a photoconductive substrate such as a PR crystal²⁹⁰ or thin layers of photoconductive polymers on the ITO surfaces of the LC cell.^{291–297} In a $10 \mu\text{m}$ LC cell coated with 100-nm-thick layers of the PVK(83%)/TNF(17%) polymer composite, a 2BC gain factor of $\gamma_0 = 12$ with a PR response time below 10 ms was obtained at $\beta_p = 15$, pump beam power $P_2 = 15 \text{ mW}$ and an electric field of $\sim 0.9 \text{ V}/\mu\text{m}$ at 514.5 nm (Table 2).²⁹³ Other techniques such as prealigning the LC with a magnetic field²⁹⁸ and using various alignment layers^{299–301} also affected PR performance of the LC.

Recently, the PR effect in chiral smectic LC phases,²⁹⁵ including ferroelectric SmC^* phases,³⁰² was observed and launched extensive studies directed toward understanding the mechanisms and improving the materials.^{303–308} Ferroelectric SmC^* LCs exhibit a net polarization (\mathbf{P}_s) that leads to fast ($\sim \mu\text{s}$) and efficient molecular reorientation in the space-charge field (\mathbf{E}_{sc}) as a result of the coupling between \mathbf{P}_s and \mathbf{E}_{sc} and in principle can exhibit an electronic electro-optic effect (not possible in nematic phases).³⁰² However, the PR properties of ferroelectric LCs explored thus far are inferior to those of other LC materials, with typical 2BC gain factors $\gamma_0 \sim 1.02\text{--}1.04$, diffraction efficiencies of $\sim 1\text{--}3\%$, and PR response speed $\sim 20\text{--}100 \text{ ms}$ (at $\beta_p = 1$ and electric fields of $\sim 0.1\text{--}5 \text{ V}/\mu\text{m}$ in $4\text{--}10 \mu\text{m}$ cells); partly due to challenging sample preparation.

Although the majority of studies of PR LCs involved the Raman-Nath regime, Bragg gratings were also demonstrated.^{289,298} In the Bragg regime, diffraction efficiencies of over $\sim 65\%$ at $37 \text{ V}/\mu\text{m}$ were obtained in the $100\text{-}\mu\text{m}$ -thick films of polymeric LCs in the isotropic phase doped with 30% DEH and 1% TNF at 633 nm.³⁰⁹ Moreover, high gain coefficients and diffraction efficiencies at low electric fields were obtained in several polymer dissolved LCs. Ono and Kawatsuki³¹⁰ studied the 2BC at 633 nm in the E7/ C_{60} combination, to which a side-chain LC polymer (SCLP), whose chemical structure is illustrated in Figure 18a, was added in the concentration of 0–50%. The highest net gain coefficient of over 600 cm^{-1} at an electric field of $0.7 \text{ V}/\mu\text{m}$ was achieved in a SCLP-(50%)/E7(49.95%)/ C_{60} (0.05%) mesogenic composite, although the PR response time in this composite was

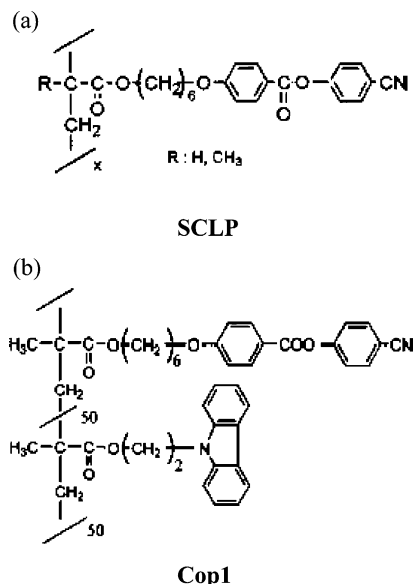


Figure 18. (a) Side-chain liquid crystalline (SLCP) polymer utilized in high performance PR mesogenic composites SLCP/E7/C₆₀. (b) Copolymer (Cop1) added to E7/TNF mixture to improve PR performance.

the slowest of all, on the order of ~ 3.5 s at 8 W/cm^2 (Table 2). As the concentration of SCLP decreased, the 2BC gain decreased, although the PR response time improved. For example, in the composite containing 30% of SCLP and 69.95% of E7, a net Γ of $\sim 400 \text{ cm}^{-1}$ with a PR response time of ~ 400 ms was obtained. In another study by the same group, 20% of the copolymer (Cop1), the chemical structure of which is shown in Figure 18b, was added to the mixture E7/TNF to improve photoconductivity, and the concentration of TNF was varied from 0.64 to 2%.³¹¹ At 532 nm, a diffraction efficiency of $\sim 39\%$ with PR response time of ~ 1 s was obtained at an electric field of $0.3 \text{ V}/\mu\text{m}$ and total writing beam intensity of $\sim 20 \text{ mW/cm}^2$ in the $50\text{-}\mu\text{m}$ -thick film of the composite containing 2% TNF.

6.6. Near-Infrared-Sensitive Materials

Near-infrared (IR) PR sensitivity is of interest due to several reasons, among which is the possibility to utilize PR materials in biological applications by taking advantage of the tissue transparency window in the 700–900 nm wavelength region. Another motivation comes from the ability to employ low-cost compact semiconductor laser diodes, available at numerous wavelengths in this part of the spectrum, as light sources in a variety of applications. Originally, the PR performance of the organic materials in this wavelength region was inferior to that in the red due to a lack of efficient sensitizers. However, recently considerable progress has been made in increasing the near-IR sensitivity. Table 3 lists the PR properties of the best-performing organic materials in the near-IR, and there are examples from the classes of polymer composites, glasses, and fully functionalized polymers. Almost all of the materials utilized TNFM as a sensitizer, and several approach the performance of the best materials in the red wavelength region. Among the best near-IR materials are PVK-based composites sensitized with TNFM

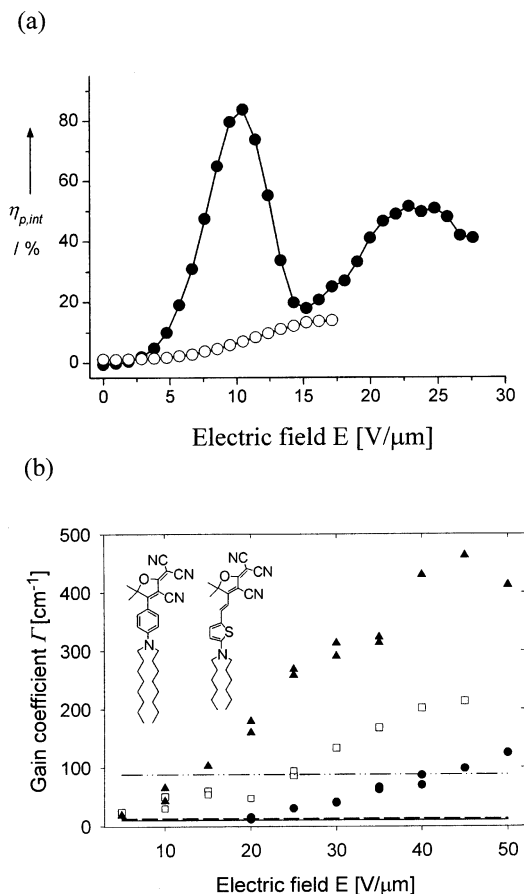


Figure 19. (a) Diffraction efficiency as a function of applied electric field measured at 790 nm in organic glass ATOP-4 (open circles) and in ATOP-4/TNFM (closed circles). Reprinted from ref 170, with permission. Copyright 2001 American Chemical Society. (b) Gain coefficient as a function of electric field obtained in 1:1 TH-DCDHF-6V/DCDHF-8 organic glass sensitized with 0, 0.1, and 1% TNFM (closed circles, open squares, and closed triangles, respectively). Double symbols correspond to different samples. Lines illustrate absorption coefficients (solid, dashed, and dash-dotted lines correspond to 0, 0.1, and 1% TNFM composites, respectively). Inset shows molecular structures of DCDHF-8 (left) and TH-DCDHF-6V (right). Adapted from ref 162 with permission. Copyright 2003 American Institute of Physics.

such as PVK/DHADC-MPN/ECZ/TNFM, which exhibited external diffraction efficiency of 74% at an electric field of $59 \text{ V}/\mu\text{m}$ at 830 nm,¹⁶³ PVK/ATOP-3/ECZ/DPP/TNFM with a 2BC gain coefficient of 180 cm^{-1} at only $30 \text{ V}/\mu\text{m}$ and internal diffraction efficiency of 85% at only $22 \text{ V}/\mu\text{m}$ at 790 nm,¹⁷⁰ PVK/Ch C/ECZ/TNFM with a gain coefficient of 230 cm^{-1} at $68 \text{ V}/\mu\text{m}$ and internal diffraction efficiency of 95% at $52 \text{ V}/\mu\text{m}$ at 780 nm,²¹⁰ etc. (see Table 3 for details and Table 1 for chemical structures). Moreover, several organic amorphous glasses outperformed polymer composites in the near-IR. Some of these multifunctional materials did not require a plasticizer and exhibited considerable 2BC gains and diffraction efficiencies even without external sensitization. For example, in the organic glass composed of 100% of merocyanine dye ATOP-4, an internal diffraction efficiency of $\sim 15\%$ was observed at $\sim 17 \text{ V}/\mu\text{m}$ at 790 nm (Figure 19a, open circles),¹⁷⁰ although the speed was not remarkable. Upon sensitization with 1%

TNFM, the diffraction efficiency overmodulated (Figure 19a, closed circles) reaching its maximum of 85% (which corresponds to the external diffraction efficiency of 32%) at the electric field of only 10.5 V/ μm .¹⁷⁰ Similarly, an unsensitized organic glass consisting of a 1:1 mixture of TH-DCDHF-6V and DCDHF-8 molecules (right and left, respectively, in the inset of Figure 19b) exhibited 2BC gain coefficients of $\sim 100\text{ cm}^{-1}$ at 45 V/ μm at 830 nm. Sensitization with TNFM led to an increase in PR response speed as well as in the gain coefficient, which in the composite containing 1% TNFM reached the value of $\sim 463\text{ cm}^{-1}$ at 45 V/ μm , as illustrated in Figure 19b.¹⁶²

Despite excellent steady-state performance, PR speed in the near-IR wavelength region remains low in many materials. In several organic glasses including those based upon DCDHF and IDOP derivatives, the PR speed at temperatures around T_g is orientationally limited and is on the order of several seconds at best. However, several glasses exhibited considerably faster PR response. In the glass-forming dye methine B (Figure 16), the increase in refractive index modulation (Δn) during the PR grating formation was characterized with a biexponential, yielding time constants of 16.6 ms (52% of the signal) and 1.2 s (48%) at an electric field of 84 V/ μm , total writing beam intensity of 3 W/ cm^2 and a wavelength of 780 nm.¹⁷¹ Moreover, at this wavelength, a pure methine B glass exhibited 2BC net gain coefficients of $\sim 216\text{ cm}^{-1}$ at 89 V/ μm and diffraction efficiencies of 87.6% at 44 V/ μm . Another glass that showed a millisecond response time in the near-IR wavelength region consisted of 69% of the bifunctional molecule DRDC-TA (Figure 16), 30% of the plasticizer EHMPA (Table 1), and 1% of TNFM.²³² At 790 nm, this glass exhibited diffraction efficiencies of $\sim 37\%$ ($\Delta n \sim 0.003$) at 80 V/ μm in a 25- μm -thick film and was characterized with biexponential PR dynamics, with the smaller time constant dropping to 4 ms at total writing beam intensity of 7.2 W/ cm^2 .

In section 5.2, we discussed the influence of the experimental conditions on PR performance. For example, it was found that the PR response time in the TPD-PPV/DMNPAA/MNPAA/DPP/PCBM composite could be dramatically improved by gated preillumination (section 5.2.2).⁴² In the "fresh" samples, the PR response times obtained in the FWM experiment were on the order of several seconds at an electric field of 60 V/ μm and total writing beam intensity of 1 W/ cm^2 at 830 nm. However, when the same experiment was performed after uniform preillumination of the sample for 955 ms with a light intensity of 5.2 W/ cm^2 at a wavelength of 633 nm, the PR response times decreased to several tens of milliseconds (Figure 13).

6.7. Other Materials Directions

6.7.1. Hybrid Organic–Inorganic Composites and Glasses

In addition to optimization in the standard classes of PR organic materials, several groups have pursued hybrid organic–inorganic composites as a new direction in the development of PR materials. For a recent

review of optical properties of hybrid organic–inorganic composites see ref 312. One class of such composites utilized semiconductor quantum dots such as CdS or CdSe, which were introduced in small concentration into standard PVK- and PPV-based composites^{43,116,157,159} as well as PDLCS.¹⁵⁸ Although the influence of quantum dots on photoconductivity of polymers was studied earlier at about the same time as fullerenes,^{156,313} until recently the polymers doped with quantum dots were not explored as PR media. Indeed, some early attempts to use quantum dots as sensitizers resulted in large photochromic effects. For PR materials, an attractive property of quantum dots as sensitizers is that their wavelength of maximum sensitivity is size-dependent, which allows for tunability of the PR response over a range of wavelengths.¹¹⁶ In addition, it was found that doping photoconductive polymers (e.g., PVK, PPV) with quantum dots improved photoconductive properties.^{314–316} In particular, in PVK doped with 1% of CdS, the photogeneration efficiency depended on the size of the nanoparticles and when optimized for a particular wavelength, considerably exceeded the photogeneration efficiency of PVK doped with 2% C₆₀ at this wavelength (in this case at 514.5 nm).¹¹⁶ In addition, doping PVK with $\sim 5\%$ of CdS led to a severalfold increase in mobility.¹⁸⁵ Thus far, the PR performance of the composites sensitized with quantum dots is inferior to that of similar composites sensitized with traditional C₆₀ or TNF.^{158,159} However, recently high external diffraction efficiencies of 72% (corresponding to internal of $\sim 90\%$) were obtained at an electric field of 50 V/ μm at a wavelength of 514.5 nm in 129- μm -thick films of the PMMA/TL202/ECZ/CdS composite (Table 2).¹⁵⁸

Inorganic dopants other than quantum dots were also explored as constituents in a polymer composite. One of the studies²¹⁹ found that less than 1% gold (Au) nanoparticles added to the otherwise standard PVK/DCVDEA/TNF composite led to an increase in the 2BC gain coefficient, reaching 206 cm^{-1} at 118 V/ μm at 633 nm, compared to 152 cm^{-1} in the undoped composite under the same conditions. The increase in PR gain was explained by an increased trap density confirmed by PR phase shift measurements.²¹⁹

Another approach involved the use of various transition metal complexes as sensitizers in fully functionalized polymers and glasses. PR properties of fully functionalized polymers containing Ru and Os complexes were explored in the red and near-IR wavelength regions, respectively.⁸⁹ High 2BC net gain coefficients of over 200 cm^{-1} were obtained in Ru-containing polymers (section 6.3). In Os-containing polymers, gain coefficients of $\sim 80\text{ cm}^{-1}$ were obtained at 780 nm. However, because of the high absorption coefficient of 186 cm^{-1} at this wavelength, net gain was not achieved in these materials. Among other PR hybrid materials are those based on cyclopalladated complexes which can be implemented into a polymer matrix, form a glass or a liquid crystalline phase, in which case they can be used without additives. Figure 20 shows the chemical structures of two high-performance cyclopalladated complexes

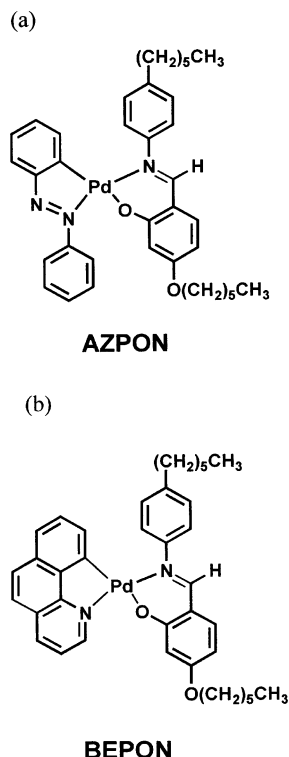


Figure 20. Cyclopalladated complexes exhibiting PR effect.

AZPON and BEPON.¹⁵⁵ The composite containing 60% of AZPON introduced in the inert polymer PIBM did not require external sensitization and showed high 2BC net gain coefficient of $\sim 240 \text{ cm}^{-1}$ at an electric field of $35 \text{ V}/\mu\text{m}$ at a wavelength of 633 nm (Table 2). At the same wavelength, pure BEPON, which formed glass with T_g of 24°C , exhibited a 2BC net gain coefficient of $\sim 700 \text{ cm}^{-1}$ at an electric field of $100 \text{ V}/\mu\text{m}$ and a refractive index modulation of 0.011 at an electric field of $33 \text{ V}/\mu\text{m}$.¹⁵⁵ In addition, a cyclopalladated complex that formed a ferroelectric SmC* phase was synthesized and without sensitization exhibited PR performance similar to that observed in dye-doped PR ferroelectric LCs.³⁰⁶

6.7.2. Electron-Transporting and Bipolar Organic Materials

PR properties of inorganic crystals with bipolar transport were extensively studied both theoretically and experimentally.^{3,317} A number of organic materials with bipolar transport have been developed and characterized for potential applications in OLEDs, solar cells, etc. Materials with high electron and hole mobilities (μ_e and μ_h , respectively) were reported (e.g., amorphous ter(9,9-diarylfuorene)s³¹⁸ with $\mu_{e,h} \sim 10^{-3} \text{ cm}^2/(\text{Vs})$). The majority of organic photoconductors currently used in PR composites are unipolar and most frequently hole transporters. However, recently several electron-transporting and bipolar photoconductors were implemented in PR organic materials.^{31–33} The best-performing electron transporting PR materials thus far are glass-forming dyes methine A and B (Figure 16) described in sections 6.2 and 6.6, respectively.¹⁷¹ The first PR bipolar organic glass based on a sexithiophene derivative (hole transporter) covalently linked to a methine dye (electron transporter) was reported in 2000.³² In this

glass, complementary gratings formed due to simultaneous electron–hole transport were observed. Because of different mobilities and trapping properties of electrons and holes, these gratings exhibited different PR dynamics. Other signatures of complementary gratings such as cancellation, revelation, and oscillatory behavior of the gratings³¹⁹ were also demonstrated. A 2BC net gain coefficient of $\sim 70.4 \text{ cm}^{-1}$ and diffraction efficiency of 19.8% were measured in a $130 \mu\text{m}$ film at an electric field of $77 \text{ V}/\mu\text{m}$ at a wavelength of 633 nm. The PR dynamics were described with a biexponential function, with a faster component reaching $\sim 10 \text{ s}^{-1}$ at a light intensity of $1 \text{ W}/\text{cm}^2$. In another study, a dopant that served as an electron trap was introduced in a bipolar PR glass, and the PR properties measured as a function of dopant concentration.³⁴ At the dopant concentration of 0.05%, high gain coefficients of $\sim 235 \text{ cm}^{-1}$ at $35 \text{ V}/\mu\text{m}$ and diffraction efficiencies of $\sim 78\%$ at $23 \text{ V}/\mu\text{m}$ were obtained at 780 nm (section 5.1.5, Table 3). Grating revelation effect was also observed and depended on the concentration of the dopant. Recently, fully functionalized PR polymers (poly(*p*-phenylene-thiophene)s with tricyanodihydrofurans attached) exhibiting bipolar charge transport were synthesized and characterized.²⁵⁹ One of the polymers (P1, Figure 17c, section 6.3) exhibited high gain coefficients of $\sim 180 \text{ cm}^{-1}$ at $50 \text{ V}/\mu\text{m}$ and diffraction efficiencies $\sim 68\%$ at $46 \text{ V}/\mu\text{m}$ at 780 nm (Table 3).

6.7.3. Sol-Gels

Sol–gel materials encompass a large variety of inorganic and hybrid organic–inorganic composites which are prepared by a certain technique, sol–gel processing. This technique involves the generation of colloidal suspensions (“sols”) which are subsequently converted to viscous gels.³²⁰ Transition-metal oxide and silica sol–gels have been utilized as catalysts, ceramics, coatings, fibers, etc.³²¹ The stages of the sol–gel process include hydrolysis, condensation, gelation, aging, drying, and densification. Advantages of the sol–gel preparation technique include low processing temperature, high purity, sample geometry flexibility (from fibers to thick films), good thermal, optical and mechanical quality, although sample preparation can involve slow drying in ambient humidity to prevent cracking. The benefits of PR sol–gel materials include the ability to utilize high concentrations of NLO chromophores without phase separation problems, long grating dark decay times in high T_g sol–gels for data storage applications, etc.³²² Recently, several PR materials with both high and low T_g were prepared by sol–gel route starting from hydrolysis of silicon alkoxides.^{87,90,323} In a corona-poled high T_g sol–gel containing the NLO chromophore DR1 and charge transporting carbazole moieties covalently attached to the silica-based backbone and doped with TNF,⁹⁰ 2BC net gain coefficients of $\sim 200 \text{ cm}^{-1}$ at zero applied field were obtained at 633 nm. However, in this case of a film thickness of only $3.5 \mu\text{m}$ (with a grating period of $0.81 \mu\text{m}$), equations 4 from which the gain coefficient was calculated have a limited applicability, and the grating may have had a strong photochromic component from the well-known cis–trans isomerization

of DR1. Also, the PR response time of this material was slow, on the order of several minutes. Similar PR response times were obtained in another high T_g sol-gel containing the azo dye DMHNAB covalently attached to the silica glass backbone, ECZ and TNF. In this glass, permanently poled at the temperature of 125 °C, net gain coefficients of $\sim 415 \text{ cm}^{-1}$ were observed at 633 nm.⁸⁷ In the absence of prepoling, the same material yielded a 2BC gain coefficient of $\sim 188 \text{ cm}^{-1}$, which was explained by the interaction between space-charge field and azo dye orientational gratings. However, these results require further studies, both theoretical and experimental, to explain the source of asymmetric 2BC effect in a centrosymmetric material.

In the attempt to improve the PR dynamics, low T_g sol-gels were explored. Sol-gels containing triethoxysilanes bearing charge transporting carbazole (SG-Cz) and NLO chromophore (SG-MN) units, doped with PEG as a plasticizer and TNF as a sensitizer, yielded glass transition temperatures ranging between 2 and 16 °C, depending on the relative concentration of SG-Cz and SG-MN units.³²³ These sol-gels exhibited PR net gain coefficients of $\sim 105 \text{ cm}^{-1}$ (SG-Cz(30.1%)/SG-MN(60.2%)/PEG(9%)/TNF-(0.7%)) and diffraction efficiencies of $\sim 82\%$ ((SG-Cz(45%)/SG-MN(45%)/PEG(9%)/TNF(1%))) in 75 μm films at an electric field of 94 V/ μm at 633 nm. The PR dynamics depended on the composite and were characterized with a biexponential, with a faster time constant of 1.7–9.9 s and a slower time constant on the order of several minutes at a light intensity of 140 mW/cm².³²³

To summarize section 6, much progress has occurred in the last seven years in the development of high performance PR materials in all materials classes. Almost complete energy transfer between two light beams as well as 100% diffraction efficiency are now possible over a wide wavelength spectrum, and millisecond response times have been demonstrated in a variety of materials. In addition, mechanistic issues such as phase separation, dye aggregation, etc. have been successfully treated, improving materials shelf life, durability, and ability to sustain a large number of duty cycles. However, further studies of stability against photochemical degradation are needed.

7. Applications and Novel Effects

One of the main driving forces for the development of PR organic amorphous materials is their ease of processing for technological applications. As a confirmation of this fact, it was recently demonstrated that large-scale PR polymer devices can be fabricated using one of the traditional plastic manufacturing technologies— injection molding—without compromising the PR performance.³²⁴ Many potential applications in data storage, image processing, optical computing, etc. were proposed for PR polymers, and the past several years have been productive in realizing these applications in real materials. In section 7.1, we review the applications demonstrated in PR organic materials to date. Space-charge fields in PR materials can lead to fascinating phenomena;

several space-charge field related effects that could potentially open new possibilities for PR organic materials will be discussed in section 7.2.

7.1. Applications

7.1.1. Data Storage

Reversible holographic high-density storage was one of the most important applications proposed for PR materials. For a recent highlight of the field of holographic data storage, see ref 325. A holographic material should possess high optical quality, reasonable thickness for low cross-talk, high dynamic range for high density, reliable retrieval of information, long-term stability, and nondestructive readout.³²⁶ In two-dimensional (2D) holographic storage, a reference beam and a signal beam containing the pattern to be stored intersect in a PR material to form a grating. The hologram is retrieved by shining the reference beam through the material at the recording angle. Using angle multiplexing, many pages of data can be stored by changing the angle of the reference beam for each recording. Specific pages can be accessed by selecting the corresponding angle for the reference beam. In addition, phase multiplexing and wavelength multiplexing have been proposed.³²⁷

High-efficiency PR polymers are attractive materials for holographic storage applications because they display high diffraction efficiencies, in addition to having reasonable optical quality and long dark lifetimes are available in some cases. In early studies, digital data storage with 64 kbit random single data pages was achieved with the long-dark-lifetime material PMMA/DTNBI/C₆₀, with an upper limit for the bit error rate of 1.5×10^{-5} .³²⁸ However, difficulties with optical quality and sample scattering prevented this material from being an optimal storage medium. In the same year, digital data recording experiments in high optical quality a PSX/FDEANST/TNF composite demonstrated significantly improved performance.³²⁹ Holograms of 64 kbit single data pages were continuously written (recording time of ~ 20 s at object and reference beam powers of 1 and 10 mW, respectively, at 676 nm) and retrieved in 100–150- μm -thick samples over an area of 0.12 cm² with errorless readout up to 5 min after recording.

For long data storage times, a material with slow dark grating decay is required. In terms of material parameters, this means low dark current, deeper traps, slow chromophore relaxation, etc. However, some of these properties can lead to an undesirable increase in recording times. To overcome this problem, a thermal fixing method was proposed in analogy to the thermal fixing processes in inorganics.³³⁰ In this technique, the hologram is written in a high- T_g material at elevated temperatures (near T_g) to take advantage of the OE effect (section 3.2) and faster recording due to enhanced photoconductivity and chromophore orientational mobility. Then, the material is quenched to room temperature, freezing the chromophore orientation, decreasing thermal detrapping and ionic dark current and therefore preventing the hologram decay. In the proof-of-principle demonstration, the polymer composite PVK/

DEANST/TCP/C₆₀ with T_g of 69 °C was used. The grating was written at a temperature of 72 °C. Then, the sample was cooled with the electric field and writing beams applied, and finally, the grating was read out at 20 °C.³³⁰ However, although this idea works in principle, in practice thermal expansion effects cause the grating recorded at high temperature to have a different grating wavevector at low temperature. While this effect can be compensated for at a single wavelength, a complex hologram with many grating wavevector components will be severely aberrated.

To combine the ability to write a dynamic grating with the possibility of long storage times, composites with both photochromic and PR properties were studied.^{331,332} In one of the studies, an image was recorded in the PVK/Lemke-E/BBP/C₆₀ composite via the photochromic effect with no electric field applied at 675 nm (recording time ~ several minutes). Then, a different image was recorded at the same location via the PR effect at an electric field of 100 V/μm at 730 nm (recording time ~1 s). Illumination with either 675 or 730 nm light restored both quasi-permanent photochromic (dark decay time ~several weeks) and erasable PR holograms. In addition, angular multiplexing allowed for simultaneous recovery of 10 photochromic and one PR hologram in the same volume.³³¹

For dynamic holograms written in PR inorganic crystals, it was proposed to characterize dynamic range of a hologram with a parameter $M/\#$ defined as follows:³³³

$$M/\# = \frac{A_0}{\tau_r} \tau_e \quad (10)$$

where A_0 is the saturation grating strength, τ_r is the recording time constant, and τ_e is the erasure time constant. Although eq 10 assumes single-exponential PR dynamics similar for all holograms, which is not the case in most PR organic materials, it reflects the general trends needed for optimization of the PR material for data storage. For holographic characterization of PR polymers with non-single-exponential dynamics, a more complicated formalism was developed that allows for an accurate estimate of the parameter $M/\#$.³³⁴ However, for clarity we limit our discussion to the simple expression of eq 10. It is clear that for the best recording efficiency, fast recording times (τ_r) are necessary. In addition, during hologram multiplexing, it is necessary to minimize erasing of previously recorded holograms during the recording of the new ones. This is why slow erasing times (τ_e) are desired. Because PR recording and erasure in organic materials are essentially governed by the same processes, a change in the recording time will be accompanied with a similar change in the erasure time—the effect opposite to the one needed to maximize $M/\#$.

Two-dimensional holographic data storage was demonstrated in a variety of PR organic materials.^{247,328,329,331,334–339} Although most materials exhibited recording times (τ_r) on the order of seconds, in the fully functionalized oligothiophenes recording times on the order of several tens of milliseconds were

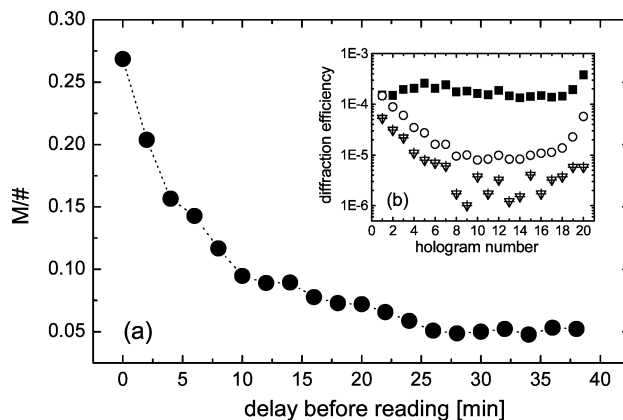


Figure 21. Dependence of the $M/\#$ on the delay t between recording and the beginning of the read-out in the TPD-doped PVK/DMNPAA/MNPAA/ECZ/TNF composite. Inset shows diffraction efficiencies of 20 multiplexed holograms after delays $t = 0$ (filled squares), $t = 10$ min (open circles), and $t = 20$ min (closed triangles). Reprinted from ref 334 with permission. Copyright 2000 Elsevier.

demonstrated.³⁴⁰ Furthermore, a near-IR-sensitive TPD-PPV/DMNPAA/MNPAA/DPP/PCBM composite, in which the PR speed could be significantly improved by preillumination, was utilized for holographic recording with writing pulses of frequencies up to ~120 Hz.⁴² Both the recording and erasure time constants as well as the grating strength (A_0) in organic materials can be affected by illumination history of the material, i.e., grating strength, recording intensity, and duration, etc. of the previously written holograms, which complicates achieving similar writing/erasure cycles for multiple holograms. Other factors such as grating dark decay may also contribute to the dynamic range. A recent detailed study of the contributing factors was carried out by Steckman et al.³³⁴ who studied the potential for hologram multiplexing in the PVK/DMNPAA/MNPAA/ECZ/TNF composite doped with a small amount (~0.82%) of TPD at a wavelength of 633 nm. It was found that for 20 holograms, the dynamic range $M/\#$ yielded a value of ~0.3, while for 30 holograms $M/\#$ reduced to 0.23. This was explained by the effect of grating dark decay over the longer period of time needed for a read-out of 30 holograms compared to 20. To gain more insight into the influence of the grating dark decay on the relative strength of the holograms, the authors recorded 20 holograms and then read them out after time t , which varied from 0 (immediate read-out) to ~37 min. Figure 21 shows the dependence of the dynamic range $M/\#$ on the time delay t between the recording and the beginning of the read-out. Because all holograms experienced dark decay, $M/\#$ decreased with increasing time delay. The inset shows the diffraction efficiency of each of 20 multiplexed holograms after the time delay $t = 0$ (filled squares), $t = 10$ min (open circles), and $t = 20$ min (closed triangles). During the immediate read-out, the diffraction efficiency of all the holograms was approximately equal. However, as the time delay increased, the diffraction efficiency experienced more hologram-to-hologram variation, reflecting different dynamics of the dark decay in the individual holograms,^{105,334} which complicates the optimization of

the recording schedule for hologram multiplexing. Clearly, additional materials with a two-photon recording mechanism (see section 4.1.4) will change the behavior in the storage application in a useful direction.

For a large number of holograms (M), the average diffraction efficiency (η) can be approximated as an inverse quadratic function of M :³³³

$$\eta = \left(\frac{M/\#}{M}\right)^2$$

which limits the candidates for data storage applications to materials with high diffraction efficiencies. While there are many PR polymers with nearly 100% diffraction efficiencies (section 6), there are certain limitations that hinder their storage capabilities. For example, the number of holograms that can be stored depends on the Bragg selectivity (angular reconstruction width) of the polymer, which varies inversely with sample thickness. Therefore, samples millimeters in thickness, hard to achieve by usual preparation techniques, are required for multiplexing of hundreds of holograms. Special geometries such as the stratified volume holographic optical element (SVHOE) configuration geometry³⁴¹ may be required to overcome this limitation.

The next logical step in the development of holographic optical storage in PR materials is true three-dimensional (3D) storage. In 1997, an erasable hologram of a 3D object was demonstrated in a Ce-doped strontium barium niobate (SBN:Ce) PR crystal.^{342,343} In PR polymers, 3D imaging has not been explicitly reported thus far, although the readout of multiple 2D holograms by angular multiplexing is a functionally equivalent experiment.

An alternative to holography as a way to achieve high-density storage is so-called 3D bit-oriented data storage that involves scanning single-photon or two-photon confocal microscopy. 3D bit data storage was initially demonstrated in photochromic and photopolymerizable polymers, PR crystals, and inorganic glasses and recently extended to PR polymers and PDLCS.^{344–346} The advantages of this type of data storage include high storage density and high signal-to-noise ratios. Reviews of various aspects of 3D bit-oriented optical data storage can be found in refs 347 and 348.

7.1.2. Image Processing

7.1.2.1. Optical Phase Conjugation. In a classical three-beam geometry, phase conjugation (PC) is produced when two counter-propagating pump beams (e.g., I_1 and I_2) intersect in an NLO material; then, a third beam incident (I_3) generates its PC replica (I_4). Popularly referred to as “time reversal”, a PC replica of an optical beam propagates through space with the complex conjugate phase of the original beam, which may be viewed as propagation backward in time.³⁴⁹ The potential applications include the transmission of undistorted images through optical fibers (or the atmosphere), lensless imaging down to sub-micrometer-size resolution, optical tracking of objects, phase locking of lasers, refreshing of holograms for long-term optical storage, optical in-

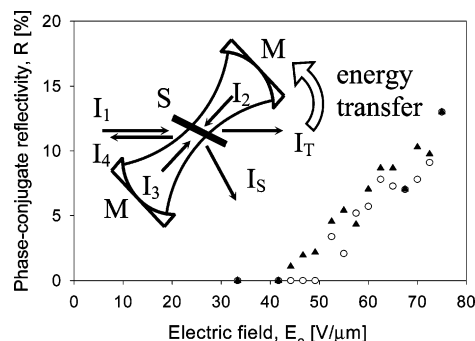


Figure 22. Self-pumped PC reflectivity as a function of applied electric field for a two-layer sample of the PVK/PDCST/BBP/C₆₀ composite measured at incident intensity of $I_1 = 180 \text{ mW/cm}^2$ (triangles) and 90 mW/cm^2 (circles). Inset shows experimental arrangement for the linear cavity oscillator. Reprinted with permission from Science (<http://www.aaas.org>), ref 13. Copyright 1997 American Association for the Advancement of Science.

terferometry, beam cleanup, and image processing.^{3,5,349} The early demonstrations of phase conjugation used a time-consuming process of holographic recording, development, and reading with carefully aligned counter-propagating plane reference waves. Subsequently, dynamic (real-time) phase conjugation was demonstrated with stimulated Brillouin scattering,³⁵⁰ FWM in an NLO material,³⁵¹ and PR inorganic crystals.^{352,353} Since the early days of PR organics, the readout of gratings in the FWM geometry as the grating is being recorded may be regarded as PC readout. Additional studies in the PC in the classical three-beam geometry were recently reported in several PR polymers and mesogenic composites,^{354,355} including a demonstration of image distortion compensation.²⁴⁷ In ref 354, the PC reflectivity (R) defined as $R = I_4/I_3$ was studied in the mesogenic composite containing copolymer Cop1 (Figure 18b), the nematic LC mixture E7, and TNF as a function of applied electric field, power of the probe (P_3) and pump (P_1, P_2) beams, wavelength, etc. At 532 nm, the PC reflectivity reached $\sim 70\%$ at an electric field of $0.3 \text{ V}/\mu\text{m}$, with probe beam power P_3 below 1 mW and pump beam powers of $P_1 = 6.5 \text{ mW}$ and $P_2 = 13.1 \text{ mW}$. In a separate study in the PVK/PNP/ECZ/TNF composite,²³⁸ PC was observed in a geometry different from the classical one, namely the forward geometry, in which only two beams are incident, and the PC replica of one of the beams propagates in the direction of higher diffraction order. This type of PC was attributed to a nonlinear interaction between space-charge field and refractive index change leading to the appearance of non-Bragg diffraction orders.^{356,357}

A major advance in the field of optical phase conjugation was the development of the self-pumped phase conjugator (SPPC),^{358,359} which required a PR material with high 2BC gain. Such SPPC was first realized with organics using the high-performance PR polymer composite PVK/PDCST/BBP/C₆₀ (Figure 22).¹³ The device operated as follows. A single beam (I_1) was incident on the sample (inset of Figure 22) and produced scattered light in various directions (because of impurities and material imperfections). Of all scattered beams, those that were scattered in the direction of large gain (here, into smaller angles

of incidence) were amplified due to 2BC. Then, of all the amplified scattered light beams, only the beam confined in the cavity formed between the two external mirrors underwent successive amplification due to the optical feedback. An increase in the gain achieved by increasing the applied electric field E_0 above a threshold of ~ 45 V/ μm led to the spontaneous formation of a cavity beam on a time scale on the order of seconds. As a result, a “phase-conjugate” beam, I_4 , appeared in the direction counter-propagating to the incoming pump (inset of Figure 22). Therefore, the PR polymer sample with its two external mirrors acted as a SPPC mirror. Figure 22 shows the PC reflectivity R , in this case defined by $R = I_4/I_1$, measured in a two-layer PR polymer stack at an incident intensity of $I_1 = 180$ mW/cm² (closed triangles) and 90 mW/cm² (open circles). As E_0 increased, the 2BC gain increased rapidly until it reached a threshold value for the onset of cavity oscillation and phase conjugation. Above the threshold, the 2BC gain exceeded the total optical losses of about 40% experienced by the cavity beam for one complete pass. As E_0 increased further, the PC reflectivity steadily increased, reaching a value of 13% at 75 V/ μm .

7.1.2.2. Optical Correlation. Image correlation is of importance for military, navigation, and security applications. The general idea is to compare the image of interest with various images stored in a database and find the identity of the object by correlation with known images. On the instrumental level, the correlation can be realized in PR materials in a FWM geometry with spatially modulated beams using joint-transform or matched-filter architectures. In the joint-transform architecture, the two spatially modulated beams form the grating, and a uniform (unmodulated) beam is used as a probe and diffracts from this grating. In the matched-filter architecture, one spatially modulated and one uniform (unmodulated) beam create a grating, and the other spatially modulated beam diffracts from this grating. The first PR polymer-based optical correlator, which utilized the PR polymer composite PVK/DMNPAA/ECZ/TNF, operated in a matched-filter geometry and was reported in 1995.³⁶⁰ In this demonstration, writing beams of femtosecond duration at a wavelength of 630 nm were employed, although only the average power of the writing beams formed the PR grating. In one of the writing beams, the “target” mask (“image of interest”) was inserted, while the reading beam passed through a mask with a “database”. At an electric field of 57 V/ μm , optical correlation was demonstrated with a signal-to-noise ratio of 10:1 and response time below 1 s. In subsequent work by the same group, a similar composite was utilized,³⁶¹ but this time a low-power cw HeNe laser was used as a laser source which permitted compact design required for military and space applications. Other studies of optical correlation using matched-filter geometry in PR polymers were reported in refs 362 and 363. In addition, correlators based on the joint-transform architecture were demonstrated using the PVK/PNP/ECZ/TNF³⁶⁴ and PSX/DB-IP-DC/TNF³⁶⁵ polymer composites as well as the nematic LC E7.³⁶⁶

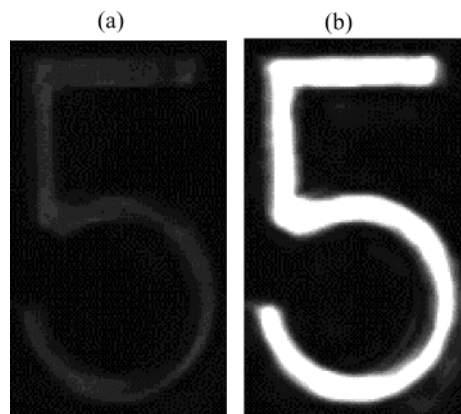


Figure 23. Amplification of image of number 5 from the Air Force resolution test chart (68- μm line width) using the PVK/AODCST/BBP/C₆₀ composite. Frame (a), the image in the absence of the reference beam and frame (b), amplified image 33 ms later. Data were recorded at a signal beam intensity $I_{s0} = 0.5$ mW/cm², reference beam intensity $I_{r0} = 1$ W/cm², and applied electric field of 68 V/ μm . Reprinted from ref 14 with permission. Copyright 2000 American Institute of Physics.

In the last study, the LC cell was coated with a 100 nm layer of photoconducting polymer poly(decylthiophene) doped with DR1 and then filled with LC E7.

7.1.2.3. Image Amplification, Novelty Filtering, and Edge Enhancement. One of the most important properties of PR materials is the 2BC effect which enables energy transfer from one beam to another (section 4). Several applications such as image amplification and novelty filtering that take advantage of this effect have been demonstrated in PR polymers.^{14,15} As we discussed in section 4.1.1, in the 2BC experiment in the limit of high beam ratio ($\beta_p = I_{r0}/I_{s0} \gg 1$, where I_{s0} (I_{r0}) is the incident signal (reference) beam intensity), the intensity of the transmitted signal beam I_s is given by $I_s = I_{s0} \exp(\Gamma L)$, where Γ is the 2BC gain coefficient, and L is the interaction length in the sample. Therefore, if in a conventional 2BC geometry (section 4.1.1), an object is inserted in the signal beam path, its image will be enhanced after passage through the sample due to the energy transfer from the reference beam. In ref 14, such an experiment was performed at a wavelength of 647 nm using the high-performance polymer composite PVK/AODCST/BBP/C₆₀. An Air Force resolution chart was inserted in the signal beam path ($I_{s0} = 0.5$ mW/cm²), and its image was recorded by a CCD camera (Figure 23a). Then, an electric field of 68 V/ μm was applied and the reference beam of $I_{r0} = 1$ W/cm² was launched. After 33 ms, the image amplification factor (I_s/I_{s0}) reached 9.4 (Figure 23b).

Interestingly, the identical optical setup was also used for novelty filtering (image differentiation) experiments, in which only moving objects are visualized.⁵ Because of the dynamical nature of this effect, only the objects that move with a speed faster than PR response speed of the material are detected. As discussed in section 4.1.1, reversing the direction of applied electric field leads to reversed direction of energy transfer. In the setup for the novelty filtering demonstration, the polarity of the applied field was

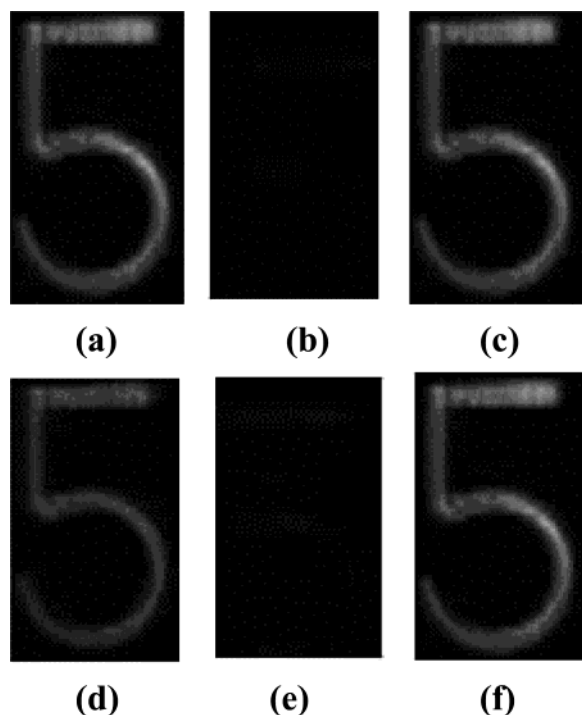


Figure 24. Demonstration of novelty filter effect using the PVK/AODCST/BBP/C₆₀ composite. Frames: (a) Image with the reference beam off. (b) Image after the reference beam is on and steady state is reached; the output is dark. (c) After a sudden movement of the data mask, the image is visible. (d) Fading image after 1/30 s. (e) Back to a dark output after 4/30 s. (f) After the sudden movement of the data mask, the image is visible again. The frames were recorded at signal beam intensity $I_{s0} = 0.45$ mW/cm², reference beam intensity $I_{r0} = 1$ W/cm², and applied electric field of 55 V/μm. Reprinted from ref 14 with permission. Copyright 2000 American Institute of Physics.

simply reversed compared to the configuration for image amplification, the electric field of 55 V/μm was applied, and the intensities of the signal I_{s0} and reference I_{r0} beams were ~ 0.45 mW/cm² and ~ 1 W/cm², respectively. The resulting effect in steady-state is suppression of the transmitted image, which is eliminated when the image moves. The series of images shown in Figure 24 demonstrates detection of a moving object by novelty filtering. In frame (a), the reference beam was off, and thus the image of number 5 was visible. When the reference beam was turned on, the image started to fade away due to the energy transfer from the signal beam to the reference beam (i.e., suppression) and appeared almost dark when steady state was reached (frame (b) of Figure 24). The image reappeared if the object mask was suddenly moved a fraction of a millimeter, as seen in frame (c), and then faded back to a dark image as shown in frames (d) and (e), respectively. If the target was moved again, the image as shown in frame (f) appeared again and again faded away with time. A novelty filter operating by analogous principle in the near-IR wavelength region was demonstrated using PVK/Lemke-E/ECZ/TNFM polymer composite at 780 nm.¹⁵

Another type of image processing that involves a special type of image intensity filtering, namely, edge enhancement, was also demonstrated in PR organic materials.^{364,367} In ref 367, a mesogenic composite

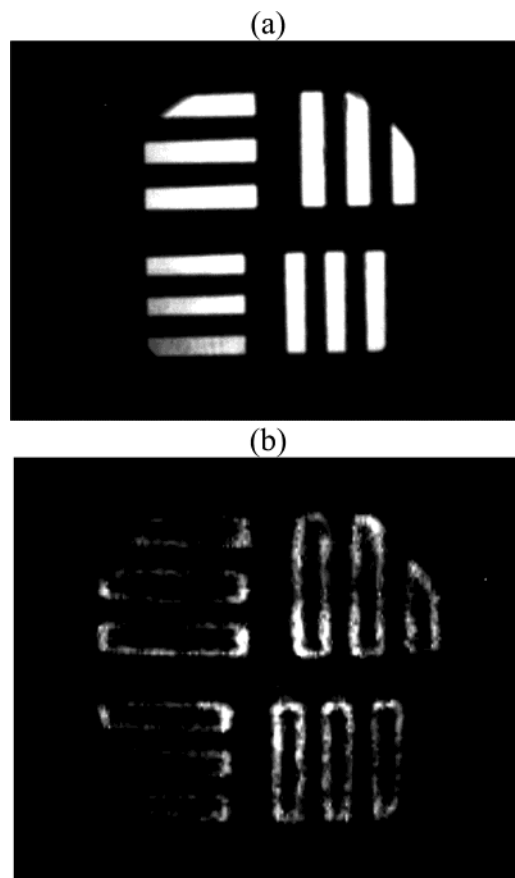


Figure 25. Demonstration of the edge enhancement effect using mesogenic composite Cop1/E7/TNF. (a) With the ratio between the signal and reference beam intensities $I_{s0}/I_{r0} = 0.1$, the exact replica of the object is produced; (b) with the beam ratio $I_{s0}/I_{r0} = 20$, the edge enhanced image is obtained. Reprinted from ref 367 with permission. Copyright 2001 American Institute of Physics.

containing copolymer Cop1 (Figure 18b), nematic LC mixture E7, and TNF was used as a recording medium. The image of an object was recorded in the standard 2BC geometry at a wavelength of 532 nm and applied electric field of 0.2 V/μm, after which it was read out with a 633 nm light. Depending on the ratio between the signal and reference beam intensities (I_{s0}/I_{r0}), either an exact replica of the object (Figure 25a, $I_{s0}/I_{r0} = 0.1$) or an edge-enhanced image (Figure 25b, $I_{s0}/I_{r0} = 20$) were obtained. When $I_{s0}/I_{r0} \gg 1$, the edge-enhanced image results because the diffraction efficiency is maximized in places where two optical fields of the same intensity interfere, i.e., at the edges where the intensity of the signal beam is the lowest and closest to that of the reference beam.

Another method of producing an edge enhancement effect was demonstrated in ref 364. In this work, the image was recorded in a PVK/PNP/ECZ/TNF polymer composite using a standard 2BC geometry, with the signal beam passing through an object mask, and the edge enhanced image appearing at the position of a higher diffraction order.

7.1.2.4. Imaging Through Scattering Media. Optical imaging through highly scattering media in the near-IR part of the spectrum has received particular attention because of its potential applications in medical diagnostics benefiting from the biological

tissue transparency window at wavelengths of 700–900 nm. Although other very successful medical imaging techniques, such as X-ray computed tomography, magnetic resonance imaging, and ultrasound, have been developed, they are associated with potential health hazards in some cases, often have low resolution, and there is a need for alternatives. High-resolution optical imaging of biological samples is made complicated by severe scattering of optical radiation in tissue due to refractive index inhomogeneities. Illumination of tissue in the transmission geometry yields several kinds of signals: light that is transmitted through the medium without scattering (ballistic light), collinear with it weakly scattered (snake) light, and highly scattered (diffuse) light.³⁶⁸ While ballistic and snake light provide useful information about the tissue, diffuse light, which emerges from the medium in arbitrary directions and at times later than the ballistic and snake light, bears hard-to-extract information and reduces signal-to-noise ratio.³⁶⁹ One of the methods proposed for extraction of only the ballistic light from the background of scattered light was time-gated holographic imaging (TGHI), which was first utilized in PR inorganic crystals^{370,371} and later in polymers.^{163,368} In this technique, either a short-pulse laser or a low-coherence laser diode was used as a light source, and a hologram was formed between the ballistic light of an object beam and a reference beam. Signal filtering was then achieved by adjusting the relative time delay between the object and the reference beams. When short laser pulses were used in the recording scheme, a hologram of the object was formed by adjusting the temporal overlap between the ballistic light and the reference pulse, and after many pulses the grating is recorded. In this case, the diffuse light delayed with respect to the ballistic light did not temporally overlap with the reference pulse and therefore did not participate in a hologram formation. The information recorded by the ballistic light was then reconstructed by reading out the hologram in the FWM geometry. When low-coherence continuous wave (cw) lasers or laser diodes were used for the recording, the hologram was formed only when the path length of the two recording beams was the same within the coherence length of the laser source. Similar to the previous case of a pulsed laser source, in this case, the delayed scattered light did not interfere with the reference beam and therefore did not contribute to the hologram formation. In a recent study, TGHI through a scattering medium was demonstrated using the PVK/DHADC-MPN/ECZ/TNFM polymer composite as a recording medium and both the pulsed and cw modes of a Ti:Sapphire laser at 830 nm as a light source.³⁶⁸ In this experiment, a signal beam passed through an object mask (Air Force test chart) followed by a 1 cm cell filled with 0.06% suspension of 0.548 μm polystyrene spheres in water, which provided an effective optical density of ~ 4.0 (equivalent to 9 scattering mean free paths) due to scattering. The image of the object was recorded in a 105- μm -thick film and successfully reconstructed using the FWM geometry and an applied electric field of 52 V/ μm .

Recent progress in the development of near-IR sensitive PR materials (section 6.6) will open a door to a variety of additional applications related to medical imaging.

7.1.3. Nondestructive Testing

Laser-based ultrasound (LBU) is a promising non-destructive technique for remote sensing, inspection, and manufacturing diagnostics for many industrial applications.³⁷² In contrast to piezoelectric transducer-based systems, the LBU method allows for remote generation of surface vibrations in surfaces of complex geometry as well as in hazardous and high-temperature environments. On the detection side of LBU, the most common vibration detection devices are laser interferometers, which are used to measure the small displacements produced when an ultrasonic wave reaches and distorts a surface. One of the recent approaches utilized real-time holography, in particular, two-wave mixing, in a PR material to combine a signal beam, distorted after reflection from the test surface in motion, with a plane-wave reference beam with matching of the signal and reference wave fronts for homodyne detection^{373,374} (Figure 26a). The hologram in the PR material acted as an adaptive beam splitter, which combined the two beams with exact wave front matching, thus allowing efficient coherent detection. Thinking of this in hologram language, the material records the interference pattern between the reference and the speckled signal beams, which is ideally suited to diffract the reference beam in the direction of the transmitted signal beam with an identical wave front. Slow variations in the wave front of the signal beam resulting from motion of the test surface (workpiece in Figure 26a) and dynamic turbulence in the propagation path were compensated by the real-time hologram and did not interfere with the quality of the wave front overlap of the output beams. A useful figure of merit for two-wave mixing-based homodyne detection is the noise-equivalent minimum surface displacement amplitude defined as follows:³⁷⁴

$$\delta = \frac{\lambda}{4\pi} \sqrt{\frac{hc \exp[\alpha L/2]}{2\eta\lambda \sin[\gamma_I L]}} \quad (11)$$

where λ is the optical wavelength, η is the quantum efficiency of the detector, α is the absorption coefficient, γ_I is the *in-phase* 2BC gain coefficient (i.e., arising from 0 degree phase-shifted index modulation), and L is an interaction length in the PR material.

PR crystals and multiple quantum wells have been previously used as adaptive beam splitters for homodyne detection of ultrasonic surface displacements.^{373,375} Recently, a homodyne detection system based on the PR polymer composite PVK/7-DCST/BBP/C₆₀ was demonstrated.³⁷⁴ At 676 nm, the noise-equivalent minimum surface displacement amplitude (δ) given by eq 11 was found to be $\delta = 7.2 \times 10^{-8}$ nm (W/Hz)^{1/2}, a value within a factor of 3 of the ideal value possible for an ideal homodyne detector. This PR polymer-based homodyne receiver was utilized to detect single ultrasonic pulses generated by a 5 MHz

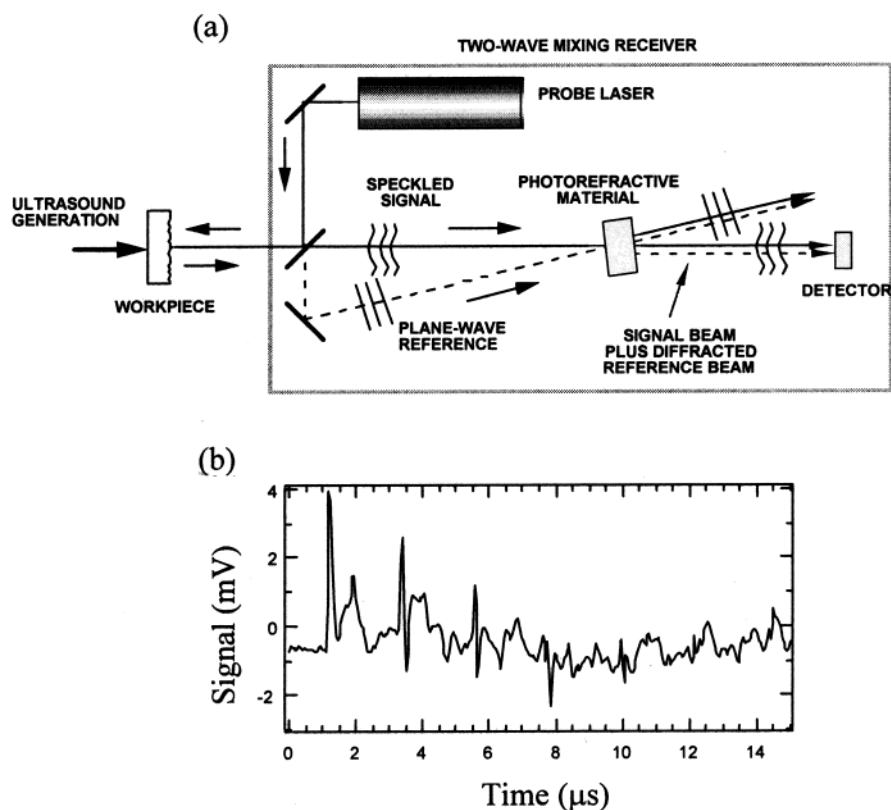


Figure 26. (a) Schematic diagram of a laser ultrasonic receiver based on two-wave mixing. (b) Ultrasonic signal detected with homodyne receiver utilizing two-wave mixing in the PVK/7-DCST/BBP/C₆₀ polymer composite. Reprinted from ref 374 with permission. Copyright 1999 Elsevier.

wideband piezoelectric transducer bonded to a quartz mirror. The ultrasonic wave distorting the front surface of the mirror was sensed using a 15 mW laser diode at 690 nm. In the detected output signal shown in Figure 26b, the transmitted wave with its various echoes could be readily identified, which demonstrated the feasibility of PR polymers to remotely detect surface displacements with good signal-to-noise ratio, although spurious vibrations were only suppressed below ~ 10 Hz. Further improvement of the speed of PR polymer materials would have the effect of pushing the high-pass characteristic of this system to more useful higher frequencies.

The applications possible in PR organic materials are by no means limited to those considered in this section. Various properties leading to other applications in image processing, all-optical light modulation, optical limiting, switching and computing, which were not described here, have been studied in PR polymers, organic glasses, and LCs.^{16,257,339,360,376}

7.2. Novel Optical Effects

Recently, various space-charge-field-related effects were observed in PR polymers and organic glasses. These effects are awaiting theoretical description and can be further explored for use in applications and as diagnostic tools in materials characterization.

7.2.1. Spatial Solitons

The self-trapping of light and the formation of optical spatial solitons have attracted considerable interest, with experimental demonstrations and theo-

retical investigations carried out in diverse NLO material systems such as inorganic PR crystals, saturable Kerr-like nonlinear media, LCs, etc.^{377–380} Recently, optical spatial solitons were theoretically predicted^{381–383} and experimentally demonstrated³⁸⁴ in PR organic materials. In ref 384, a 780 nm collimated beam was focused with a cylindrical lens onto the input face of a 120- μm -thick sample of the PR high performance organic glass DCDHF-6/DCDHF-6-C7M/C₆₀.^{69,104} As shown in Figure 27a, the beam propagated along the z -direction through the 2.5-mm-long film, while a dc electric field was applied between ITO electrodes along the x -direction. Behind the sample, a CCD camera together with an imaging lens was used to monitor the beam profile in the x - y plane directly at the input/output faces of the sample. With such a setup, self-focusing and self-trapping of light were observed when the beam was polarized in the y -direction (i.e., perpendicular to the bias field), while self-defocusing was obtained if the polarization was switched to the x -direction (i.e., parallel with the bias field). Typical experimental results are illustrated in Figure 27b. The beam with power of ~ 24 mW was focused to 12 μm fwhm (in the x -direction) at the input face of the sample (frame (1) in the case of the y -polarized beam and frame (4) in the case of the x -polarized beam). Without the bias electric field, the beam diffracted to about 55 μm after 2.5 mm of linear propagation through the sample (frame (2) and frame (5) for y - and x -polarized beams, respectively). After the bias dc field (\mathbf{E}_0) of 16 V/ μm was applied, self-focusing was observed in the case of y -polarized

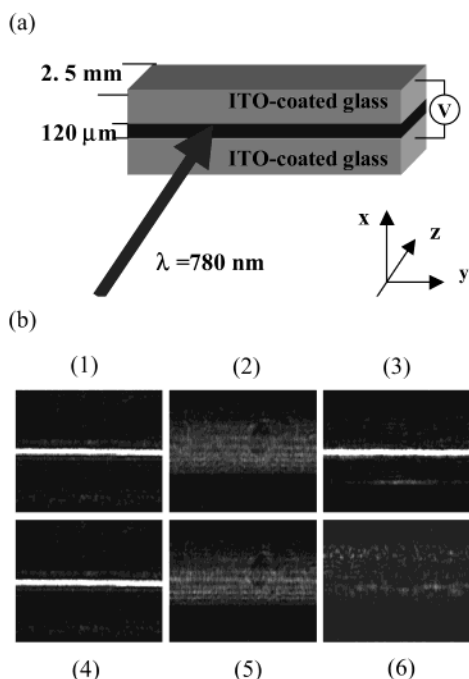


Figure 27. (a) Experimental geometry used for observation of spatial solitons in PR organic glass DCDHF-6/DCDHF-6-C7M/C₆₀. (b) Image of the beam at frame (1) sample input (original y -polarized beam); (2) sample output ($E_0 = 0$; linearly diffracted y -polarized beam); (3) sample output ($E_0 = 16 \text{ V}/\mu\text{m}$, self-trapped y -polarized beam); (4) sample input (original x -polarized beam); (5) sample output ($E_0 = 0$, linearly diffracted x -polarized beam); (6) sample output ($E_0 = 16 \text{ V}/\mu\text{m}$, defocused x -polarized beam). Reprinted from ref 384 with permission. Copyright 2003 American Institute of Physics.

beam (i.e., when the beam was polarized perpendicular to the bias field), with the strength of focusing increasing gradually. In about 162 s, self-trapping of the y -polarized beam into an optical soliton was realized, as the beam reached its original size (frame (3)). The soliton was stable during a period of time of more than 100 s, after which the beam size started to increase slowly while the electric field was still applied. However, the focused beam did not “relax” completely to its original width of linear diffraction even after 1 h. In the case of the x -polarized beam (i.e., when the beam polarization was parallel to the applied field direction) with all other experimental conditions remaining the same, self-defocusing was observed instead of self-focusing. In this case, the beam width increased from linearly diffracted size of $55 \mu\text{m}$ (frame (5)) to about $80 \mu\text{m}$ in 162 s after the dc field of $16 \text{ V}/\mu\text{m}$ was applied (frame (6)). Self-focusing to defocusing switching did not occur with reversal of polarity of applied electric field. The strength of the effect depended strongly on the electric field, and the soliton formation speed depended on both electric field and incident beam power. The mechanism of the effect was determined to be a refractive index change due to space-charge field formation followed by chromophore reorientation in the illuminated part of the sample which created a waveguide-like structure.³⁸⁴ Recently, it was demonstrated that in the DCDHF-6/DCDHF-6-C7M/C₆₀ glass the optically induced (with a beam at the wavelength of $\lambda = 780 \text{ nm}$) waveguide could

efficiently guide another (probe) beam (e.g., at the wavelength of $\lambda = 960 \text{ nm}$).³⁸⁵ This demonstration may lead to a number of potential future applications such as optical couplers, switches, logic gates, etc.

7.2.2. Other Space-Charge Field Related Effects

It is known that in PR materials the space-charge field can form even in the presence of only one light beam due to the (Gaussian) transverse intensity pattern of the beam; the existence of spatial solitons in a PR medium is one of the indications of this fact. However, the manifestations of the space-charge field and its contribution to various physical effects are not well understood and may take different forms, as we consider in this section. For example, in the high-performance methine dye-based PR organic glass described in section 6.6, an effect of periodically pulsating self-focusing was observed.¹⁷¹ The sample used was a thin film squeezed between two ITO glass slides. The light of 780 nm with intensity of $2.87 \text{ W}/\text{cm}^2$ was obliquely incident on the sample with electric field applied, and the near-field pattern of the output beam, characterized as a series of bright and dark rings, was projected on a screen. It was found that the size of the first bright ring increased monotonically with increasing applied field. After a certain threshold (around $\sim 90 \text{ V}/\mu\text{m}$ at $2.87 \text{ W}/\text{cm}^2$), the size of the rings expanded in an accelerating fashion followed by collapse to a nondefocused pattern. The effect was explained by self-modulation of the refractive index by the optical field and was found to limit the 2BC gain coefficient in this material.¹⁷¹

In several PR polymers, a light-induced antiguiding structure (i.e., the refractive index of the illuminated part of the sample is lower than that of the nonilluminated part) was observed and probed by second harmonic generation (SHG) techniques.^{386–388} In one of these studies,³⁸⁷ the sample was a thin film ($\sim 25 \mu\text{m}$) of a PR polymer composite containing 46.9% of PVK, 1.4% of TNF, 14.7% of NLO chromophore (4-methoxy-4'-nitrostilbene), and 37.2% of a plasticizer (1,3-bis(N -carbazolyl)-propane) cast on a substrate that had aluminum in-plane electrodes with a gap of $\sim 200 \mu\text{m}$. Two beams of $\sim 90 \mu\text{m}$ diameter were collinearly incident on the gap area—one beam (pump) originated from a 633 nm cw HeNe laser, and another one (fundamental)—from a 1047 nm pulsed Nd:YLF laser. The PR polymer did not exhibit significant absorption at 1047 nm , but was sensitive to both pump (633 nm) and SHG (523.5 nm) wavelengths (e.g., $\alpha_{633} \sim 60 \text{ cm}^{-1}$). The experiment was performed at a temperature of $50 \text{ }^\circ\text{C}$, which was determined to be optimal for the electric-field poling of the NLO chromophores in this composite. During the poling process in the external electric field of $\sim 15 \text{ V}/\mu\text{m}$, the build-up of the power of second harmonic light, generated in the sample by the 1047 nm fundamental light in the absence of the pump beam, was monitored with a photomultiplier. When the SHG power reached a plateau, indicating the completion of the chromophore alignment process, the pump beam with a power of $\sim 0.5 \text{ mW}$ was unblocked (with the electric field kept on), and a SHG power increase by a factor of 4 was observed. When the pump beam

was blocked again, the SHG power decreased to its previous level. SHG enhancement depended on the pump power and applied electric field and was explained by a space-charge field created by the pump beam that led to antiguiding formation.³⁸⁹

In another study,¹³⁴ a similar SHG enhancement was observed, but in a completely different experimental geometry. In this work, a thin film of a low- T_g PR polymer composite containing PVK, BBP, C₆₀, and 5CB or AODCST was squeezed between two ITO glass slides (as in a standard PR sample). An electric field was applied, and light at a wavelength of ~ 780 nm from a mode-locked Ti:Sapphire laser (fundamental beam) was obliquely incident on the sample. The SHG generated in the sample due to chromophore orientation in the electric field was detected using a photomultiplier and a lock-in detection scheme. When another beam (at $\lambda = 633$ nm from a HeNe laser) with a diameter much larger than that of the fundamental beam was incident on the sample, the SHG increased. The SHG enhancement depended on HeNe beam power and applied electric field. The results were explained by changes in local electric field induced by photoconductivity.¹³⁴

The last example of space-charge field-related effects we consider in this section is a study in which Joo et al. attempted to evaluate the space-charge field created during PR grating formation by measuring electric field-induced birefringence during the FWM experiment.³⁹⁰ The PR grating was written in a PSX/DB-IP-DC/TNF polymer composite at an electric field of 30 V/ μm and total light intensity of 60 mW/cm² at 633 nm. The diffraction efficiency was measured in a standard FWM geometry using a read-out beam of the same wavelength and a light intensity of 0.06 mW/cm². An additional probe beam of the same wavelength and intensity of 0.1 mW/cm², polarized at +45° with respect to the incidence plane, was incident on the sample at an angle far enough from the Bragg angle to not be diffracted by the grating. The transmitted probe beam intensity passing through an analyzer set at -45° with respect to the incidence plane was recorded. Similar to a conventional transmission ellipsometry experiment (section 4.2.2), when no electric field was applied, no transmitted signal was observed because the beam passed through crossed polarizers. After an electric field was applied (with the absence of the writing beams), a transmission due to birefringent chromophores reoriented in the electric field was detected. As the writing beams were unblocked, creating a PR grating which was monitored by measuring diffraction efficiency, the transmission increased. From the amplitude of the transmitted signal increase, the space-charge field was calculated. While it is not straightforward to accurately determine space-charge field of the PR grating by this method due to the complicated geometry, photoconductivity issues, etc., this effect as well as others described in this section could be further studied and employed for sensing local electric fields.

To summarize section 7, many applications originally envisioned for PR inorganic crystals have been demonstrated in real PR polymer composites, organic

glasses, and LCs. In addition, a number of recent studies showed the possibility of developing novel applications as well as the need for theoretical modeling of the observed effects in order to gain valuable insights into the precise details of space-charge field formation in PR organic materials.

8. Conclusions and Outlook

Over the past years, tremendous progress has occurred in both the physical understanding of the PR effect in organic materials and in the development of high performance materials. Physical models of various processes contributing to the PR effect such as charge generation, transport, trapping, and NLO response have been developed and successfully applied to real materials. The composition of the PR polymer composites has been examined in detail and schemes for optimizing the various constituents for certain applications have been proposed. Synthetic efforts have resulted in a broad array of materials with outstanding 2BC gain coefficients and 100% diffraction efficiencies at low electric fields over wide spectral ranges, including the near-IR wavelength region. A number of ways to create thermodynamically stable materials with high optical quality have been proposed. PR response times on the order of milliseconds have been achieved in a variety of materials, including polymer composites, glasses and LCs. Many of the previously proposed applications have been demonstrated, and novel effects that may lead to new applications and diagnostic techniques have been documented.

Despite all this progress, however, a number of challenges remain. Among them is the need for complex optimization of each material for a particular application due to the inability to maximize both steady-state and dynamic performance at the same time. To be accomplished are the achievement of sub-millisecond response times, the development of an understanding of the illumination history dependence of the PR performance, and the reduction of degradation of optical properties with time. Reliable experimental techniques that directly assess recombination and trapping properties are needed in order to complement other photoconductivity experiments in determining all the parameters contributing to the overall PR performance. Theoretical models, which take into account dark conductivity, charge injection, field dependence, etc., developed in conjunction with experimental studies are required for successful prediction of the material potential for a certain application. Theoretical explanation for the experimentally observed space-charge field effects is needed to understand these complex processes and to be able to utilize them in applications.

Very recently, a surprising result was obtained, which could allow the detailed study of the mechanisms of the PR effect in organic materials on the microscopic level. It was discovered that many of the DCDHF NLO chromophores that form high performance PR organic glasses were highly fluorescent and could be imaged on a single-molecule level in polymers using a standard epi-fluorescence experimental technique.³⁹¹ This means that this class of

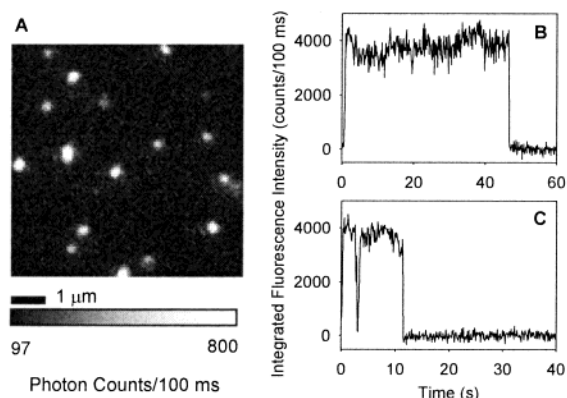


Figure 28. (a) Wide-field image of the fluorescent single molecules of high performance PR dye DCDHF-6 in PMMA matrix. (b), (c) The integrated fluorescence intensity in two individual DCDHF-6 molecules as a function of time. Reprinted from ref 391 with permission. Copyright 2003 American Chemical Society.

dopants has strong fluorescence, weak bottlenecks, and low probability of photochemical damage in order to emit enough photons to allow the observation of a single, individual molecule above background. Figure 28 shows a wide-field microscopic image of single molecules of DCDHF-6 (white spots in Figure 28a) in a PMMA matrix upon excitation by 488 nm light as well as the integrated fluorescence intensity of two individual molecules as a function of time (Figures 28b,c). The fact that a variety of NLO chromophores can now be studied on the single-molecule level could open the door to solving the puzzles of the PR effect in organic materials on the microscopic level. In particular, charge photogeneration, trapping, recombination and electric field-induced reorientation processes, crucial for the PR grating formation, can be explored on microscales, which would lead to refinements of the PR molecular model and further boost the development of this exciting field.

9. Abbreviations

PR	photorefractive
OE	orientational enhancement
2BC	two-beam coupling
FWM	four-wave mixing
PC	phase conjugation
SHG	second harmonic generation
fwhm	full-width at half-maximum
NLO	nonlinear optical
LBU	laser-based ultrasound
TGHI	time-gated holographic imaging
COANP	2-cyclooctylamino-5-nitropyridine
TCNQ	7,7,8,8-tetracyanoquinodimethane
PVK	poly(<i>N</i> -vinylcarbazole) (Table 1)
PSX	poly[methyl(3-carbazol-9-ylpropyl)siloxane] (Table 1)
DBOP-PPV	poly[1,4-phenylene-1,2-di(4-benzyloxyphenyl)vinylene] (Table 1)
p-PMEH-PPV	poly[<i>o</i> (<i>p</i>)-phenylenevinylene- <i>alt</i> -2-methoxy-5-(2-ethylhexyloxy)- <i>p</i> -phenylenevinylene] (Table 1)
PPT-Cz	poly(<i>p</i> -phenyleneterephthalate) with pendant carbazole groups (Table 1)

PS	polystyrene
PIBM	polyisobutyl methacrylate
PTCB	poly(methyl methacrylate- <i>co</i> -tricyclodecyl methacrylate- <i>co</i> - <i>N</i> -cyclohexylmaleimide- <i>co</i> -benzyl methacrylate)
TFB	poly(9,9'-dioctylfluorene- <i>co</i> - <i>N</i> -(4-butylphenyl)-diphenylamine)
PBPES	poly(4- <i>n</i> -butoxyphenylethylsilane)
PMPS	polymethylphenylsilane
PMMA	poly(methyl methacrylate)
P1	poly(thiophene- <i>p</i> -phenylene) with dicyanomethylenedihydrofuran chromophore (Figure 17c)
Cop1	copolymer containing 4-cyanobenzoate and <i>N</i> -carbazoyl side groups (Figure 18b)
Ru-FFP	poly(phenylenevinylene) with Ruthenium complex (Figure 17a)
P6	copolymer with carbazole and azo-dye side chains (Figure 17b)
SG-Cz	triethoxysilane with carbazole unit
SG-MN	triethoxysilane with NLO chromophore unit
TDPANA-FA	1-(4'-nitrobenzyl)-4,4-(<i>N,N</i> -diphenyl-4-methylphenylamino) piperidine-paraformaldehyde'
BisA-NPDA	bisphenol A-diglycidyl ether 4-nitro-1,2-phenylenediamine
SCLP	side-chain liquid crystalline polymer poly(methyl methacrylate) with 4-cyanophenyl benzoate side group (Figure 18a)
DEH	diethylaminobenzaldehyde-diphenylhydrazone
TTA	tri-tolylamine
TPD	<i>N,N</i> -bis(4-methylphenyl)- <i>N,N</i> -bis(phenyl)-benzidine
DTNBI	(1,3-dimethyl-2,2-tetramethylene-5-nitrobenzimidazole)
DEANST	4- <i>N,N</i> -diethylamino- β -nitrostyrene
FDEANST	3-fluoro-4-(<i>N,N</i> -diethylamino)- β -nitrostyrene
DR1	Disperse red 1
FTCN	fluorinated cyano-tolane chromophore
DCST	dicyanostyrene
AODCST	2-[4-bis(2-methoxyethyl)amino]benzylidene]malononitrile] (Table 1)
PDCST	4-piperidinobenzylidenemalononitrile
7-DCST	4-(azepan-1-yl)benzylidenemalononitrile
DDCST	diethylaminodicyanostyrene
MPDCST	methylpiperidinodicyanostyrene
ATOP	1-alkyl-5-[2-(5-dialkylaminothienyl)methylene]-4-alkyl-[2,6-dioxo-1,2,5,6-tetrahydropyridine]-3-carbonitrile (Table 1, Figure 16)
IDOP	1-alkyl-5-[2-(1,3-dihydro-1-alkyl-3,3-dimethyl-2- <i>H</i> indol-2-ylidene)ethylidene]-4-alkyl-2,6-dioxo-1,2,5,6-tetrahydropyridine-3-carbonitrile (Figure 16)
DCDHF-6	2-dicyanomethylen-3-cyano-5,5-dimethyl-4-(4'-dihexylaminophenyl)-2,5-dihydrofuran (Table 1)
DCDHF-6-C7M	3-cyano-2-dicyanomethylen-4-{4'-[<i>N,N</i> -(dihexyl)aminophenyl]}-1-oxaspiro[4,7]-dodec-3-ene (Figure 16)
DCDHF-8	2-dicyanomethylen-3-cyano-5,5-dimethyl-4-(4'-dioctylaminophenyl)-2,5-dihydrofuran (Figure 19b)
TH-DCDHF-6V	1-(3-cyano-2-dicyanomethylen-5,5-dimethyl-2,5-dihydrofuran-4-yl)-2-[5-(<i>N,N</i> -dihexyl)aminothien-2-yl]ethene (Figure 19b)
EHCN	9-(2-ethyl-hexyl)-3-[2-(4-nitro-phenyl)-vinyl]-9 <i>H</i> -carbazole (Figure 16)

DHADC-MPN	2, <i>N,N</i> -dihexylamino-7-dicyanomethylidene-3,4,5,6,10-pentahydronaphthalene (Table 1)
2BNCM	<i>N</i> -2-butyl-2,6-dimethyl-4 <i>H</i> -pyridone-4-ylidenecyanomethyl acetate (Figure 16)
DB-IP-DC	2-{3-[(<i>E</i>)-2-(dibutyl-amino)ethen-1-yl]-5,5-dimethylcyclohex-2-enylidene}-malononitrile (Table 1)
PNP	(<i>S</i>)-(-)- <i>N</i> -(5-nitro-2-pyridyl)prolinol
DCVDEA	4-(dicyanovinyl)- <i>N,N</i> -diethylaniline (Table 1)
DMNPAA	2,5-dimethyl-(4- <i>p</i> -nitrophenylazo)anisole (Table 1)
MNPAA	3-methoxy-(4- <i>p</i> -nitrophenylazo)anisole (Table 1)
DMHNAB	2,5-dimethyl-4-(2-hydroxyethoxy)-4'-nitroazobenzene (Table 1)
BDMNPAB	1- <i>n</i> -butoxy-2,5-dimethyl-(4- <i>p</i> -nitrophenylazo)benzene (Table 1)
LEMKE-E	(3-(2-(4-(<i>N,N</i> -diethylamino)phenyl)ethenyl)-5,5-dimethyl-1,2-cyclohexenylidene)-propanedinitrile (Table 1)
DRDCTA	4,4'-di(<i>N</i> -carbazolyl)-4''-(2- <i>N</i> -ethyl-4-[2-(4-nitrophenyl)-1-azo]anilinoethoxy)-triphenylamine (Figure 16)
Cz-C6-THDC	2-(5-[4-[6-(9-ethyl-9 <i>H</i> -carbazol-3-yl)-6-methoxy-hexyl]-piperazin-1-yl]-thiophen-2-yl ethylene)-malononitrile (Figure 16)
EPNA	4-(diethylamino)nitrobenzene
F0-F4, C1-C9	fluorinated styrene derivatives (Figure 11)
Ch C	NLO chromophore similar to Lemke-E (Table 1)
M0	2-dicyanomethylene-3-cyano-5,5-dimethyl-4-(1'-ethylene-4'(bis(2-ethylhexyl)aminophenyl)-2,5-hydrofuran
M1	several dicyanomethylenedihydrofuran chromophores attached to a backbone
6OCB	4-hexyloxy-4'-cyanobiphenyl
8OCB	4'-(<i>n</i> -octyloxy)-4-cyanobiphenyl
5CB	4'-(<i>n</i> -pentyloxy)-4-cyanobiphenyl
E7, E44, E49, TL202	mixtures of liquid crystals available from Merck
E869	liquid crystal S _C * 15 °C S _A * 69 °C N* 82 °C I
DO3	4-(4-nitrophenylazo)aniline
DIP	diphenylisophthalate
BBP	butyl benzyl phthalate (Table 1)
DPP	diphenyl phthalate (Table 1)
DOP	diisooctylphthalate (Table 1)
ECZ	<i>N</i> -ethylcarbazole (Table 1)
TCP	tricesyl phosphate
PEG	poly(ethylene glycol)
EHMPA	<i>N</i> -(2-ethylhexyl)- <i>N</i> -(3-methylphenyl)-aniline (Table 1)
TNF	2,4,7-trinitro-9-fluorenone (Table 1)
TNFM	(2,4,7-trinitro-9-fluorenylidene)malononitrile (Table 1)
PCBM	[6,6]-phenyl-C ₆₁ -butyric acid methyl ester (Table 1)
NI	<i>N,N</i> -di(<i>n</i> -octyl)-1,4,5,8-naphthalenediimide
TBPAH	tri-(4-bromophenyl)-aminium hexachloroantimonate

10. Acknowledgment

This work was supported in part by the Air Force Office of Scientific Research Grant No. F49620-00-1-0038. O.O. thanks the Killam Trusts for the Killam Memorial Fellowship Award. The authors owe a debt

of gratitude to our synthetic colleague, Robert J. Twieg, who provided many of the compounds studied in our laboratories, and to our many coauthors, postdocs, graduate students, and other collaborators over the past 14 years.

11. References

- (1) Eichler, H. J.; Günter, P.; Pohl, D. W. *Laser-Induced Dynamic Gratings*; Springer-Verlag: Berlin/Heidelberg, 1986.
- (2) Ashkin, A.; Boyd, G. D.; Dziedzic, J. M.; Smith, R. G.; Ballman, A. A.; Levinstein, J. J.; Nassau, K. *Appl. Phys. Lett.* **1966**, *9*, 72.
- (3) *Photorefractive Effects and Materials*; Gunter, P., Huignard, J. P., Eds.; Springer-Verlag: New York, 1988; Vol. 61-62.
- (4) Yeh, P. *Introduction to Photorefractive Nonlinear Optics*; John Wiley: New York, 1993.
- (5) Solymar, L.; Webb, D. J.; Grunnet-Jepsen, A. *The Physics and Applications of Photorefractive Materials*; Clarendon Press: Oxford, 1996.
- (6) *Nonlinear Optical Properties of Organic Molecules and Crystals*; Chemla, D. S., Zyss, J., Eds.; Academic Press: Orlando, 1987; Vols. 1 and 2.
- (7) *Photochromism*; Brown, G. H., Ed.; Wiley-Interscience: New York, 1971; Vols. I-III.
- (8) Valley, G. C. *J. Opt. Soc. Am. B-Opt. Phys.* **1984**, *1*, 868.
- (9) Khoo, I. C.; Liu, T. H. *IEEE J. Quantum Electron.* **1987**, *23*, 171.
- (10) Sanchez, F.; Kayoun, P. H.; Huignard, J. P. *J. Appl. Phys.* **1988**, *64*, 26.
- (11) Lee, J. W.; Mun, J.; Yoon, C. S.; Lee, K. S.; Park, J. K. *Adv. Mater.* **2002**, *14*, 144.
- (12) Mun, J.; Lee, J. W.; Park, J. K.; Lee, K. S.; Yoon, C. S. *Opt. Mater.* **2003**, *21*, 379.
- (13) Grunnet-Jepsen, A.; Thompson, C. L.; Moerner, W. E. *Science* **1997**, *277*, 549.
- (14) Goonesekera, A.; Wright, D.; Moerner, W. E. *Appl. Phys. Lett.* **2000**, *76*, 3358.
- (15) Hendrickx, E.; Van Steenwinckel, D.; Persoons, A. *Appl. Opt.* **2001**, *40*, 1412.
- (16) Gubler, U.; He, M.; Wright, D.; Roh, Y.; Twieg, R.; Moerner, W. E. *Adv. Mater.* **2002**, *14*, 313.
- (17) Sutter, K.; Gunter, P. *J. Opt. Soc. Am. B-Opt. Phys.* **1990**, *7*, 2274.
- (18) Sutter, K.; Hulliger, J.; Gunter, P. *Solid State Commun.* **1990**, *74*, 867.
- (19) Sutter, K.; Hulliger, J.; Schlessler, R.; Gunter, P. *Opt. Lett.* **1993**, *18*, 778.
- (20) Ducharme, S.; Scott, J. C.; Twieg, R. J.; Moerner, W. E. *Phys. Rev. Lett.* **1991**, *66*, 1846.
- (21) Moerner, W. E.; Silence, S. M. *Chem. Rev.* **1994**, *94*, 127.
- (22) Moerner, W. E.; Grunnet-Jepsen, A.; Thompson, C. L. *Annu. Rev. Mater. Sci.* **1997**, *27*, 585.
- (23) Kippelen, B.; Peyghambarian, N. In *Polymers for Photonic Applications II*, 2003; Vol. 161.
- (24) Zilker, S. J. *ChemPhysChem* **2000**, *1*, 72.
- (25) Yu, L. P. *J. Polym. Sci. A: Polym. Chem.* **2001**, *39*, 2557.
- (26) Wiederrecht, G. P. *Annu. Rev. Mater. Res.* **2001**, *31*, 139.
- (27) Wurthner, F.; Wortmann, R.; Meerholz, K. *ChemPhysChem* **2002**, *3*, 17.
- (28) Valley, G. C.; Klein, M. B.; Mullen, R. A.; Rytz, D.; Wechsler, B. *Annu. Rev. Mater. Sci.* **1988**, *18*, 165.
- (29) Silence, S. M.; Walsh, C. A.; Scott, J. C.; Moerner, W. E. *Appl. Phys. Lett.* **1992**, *61*, 2967.
- (30) Zhang, Y.; Cui, Y. P.; Prasad, P. N. *Phys. Rev. B* **1992**, *46*, 9900.
- (31) Okamoto, K.; Nomura, T.; Park, S. H.; Ogino, K.; Sato, H. *Chem. Mater.* **1999**, *11*, 3279.
- (32) Wang, L. M.; Ng, M. K.; Yu, L. P. *Phys. Rev. B* **2000**, *62*, 4973.
- (33) Sohn, J.; Hwang, J.; Park, S. Y.; Noh, Y. Y.; Kim, J. J. *Appl. Phys. Lett.* **2002**, *81*, 190.
- (34) You, W.; Hou, Z.; Yu, L. P. *Adv. Mater.* **2004**, *16*, 356.
- (35) Nelson, J. *Curr. Opin. Solid State Mater. Sci.* **2002**, *6*, 87.
- (36) Peumans, P.; Yakimov, A.; Forrest, S. R. *J. Appl. Phys.* **2003**, *93*, 3693.
- (37) Nunzi, J. M. *C. R. Phys.* **2002**, *3*, 523.
- (38) Brabec, C. J.; Sariciftci, N. S.; Hummelen, J. C. *Adv. Funct. Mater.* **2001**, *11*, 15.
- (39) Nozik, A. J. *Phys. E* **2002**, *14*, 115.
- (40) Li, L.; Chittibabu, K. G.; Chen, Z.; Chen, J. I.; Marturunkakul, S.; Kumar, J.; Tripathy, S. K. *Opt. Commun.* **1996**, *125*, 257.
- (41) Mecher, E. H.; Brauchle, C.; Horhold, H. H.; Hummelen, J. C.; Meerholz, K. *PCCP Phys. Chem. Chem. Phys.* **1999**, *1*, 1749.
- (42) Mecher, E.; Gallego-Gomez, F.; Tillmann, H.; Horhold, H. H.; Hummelen, J. C.; Meerholz, K. *Nature* **2002**, *418*, 959.
- (43) Suh, D. J.; Park, O. O.; Ahn, T.; Shim, H. K. *Opt. Mater.* **2003**, *21*, 365.
- (44) Borsenberger, P.; Weiss, D. S. *Organic Photoreceptors for Imaging Systems*; Dekker: New York, 1993.

- (45) Martens, H. C. F.; Blom, P. W. M.; Schoo, H. F. M. *Phys. Rev. B* **2000**, *61*, 7489.
- (46) Grunnet-Jepsen, A.; Wright, D.; Smith, B.; Bratcher, M. S.; DeClue, M. S.; Siegel, J. S.; Moerner, W. E. *Chem. Phys. Lett.* **1998**, *291*, 553.
- (47) Daubler, T. K.; Bittner, R.; Meerholz, K.; Cimrova, V.; Neher, D. *Phys. Rev. B* **2000**, *61*, 13515.
- (48) Ostroverkhova, O.; Singer, K. D. *J. Appl. Phys.* **2002**, *92*, 1727.
- (49) Van Steenwinckel, D.; Hendrickx, E.; Persoons, A. *J. Chem. Phys.* **2001**, *114*, 9557.
- (50) Jakob, T.; Schlöter, S.; Hofmann, U.; Grasruck, M.; Schreiber, A.; Haarer, D. *J. Chem. Phys.* **1999**, *111*, 10633.
- (51) Moerner, W. E.; Silence, S. M.; Hache, F.; Björklund, G. C. *J. Opt. Soc. Am. B* **1994**, *11*, 320.
- (52) Wortmann, R.; Poga, C.; Twieg, R. J.; Geletneky, C.; Moylan, C. R.; Lundquist, P. M.; DeVoe, R. G.; Cotts, P. M.; Horn, H.; Rice, J. E.; Burland, D. M. *J. Chem. Phys.* **1996**, *105*, 10637.
- (53) Kogelnik, H. *Bell Syst. Tech. J.* **1969**, *48*, 2909.
- (54) Kukhtarev, N. V.; Markov, V. B.; Odulov, S. G.; Soskin, M. S.; Vinetskii, V. L. *Ferroelectrics* **1979**, *22*, 949.
- (55) Twarowski, A. *J. Appl. Phys.* **1989**, *65*, 2833.
- (56) Schildkraut, J. S.; Buettner, A. V. *J. Appl. Phys.* **1992**, *72*, 1888.
- (57) Schildkraut, J. S.; Cui, Y. P. *J. Appl. Phys.* **1992**, *72*, 5055.
- (58) Cui, Y. P.; Swedek, B.; Cheng, N.; Zieba, J.; Prasad, P. N. *J. Appl. Phys.* **1999**, *85*, 38.
- (59) Yuan, B. H.; Sun, X. D.; Hou, C. F.; Li, Y.; Zhou, Z. X.; Jiang, Y. Y.; Li, C. F. *J. Appl. Phys.* **2000**, *88*, 5562.
- (60) Yuan, B. H.; Sun, X. D.; Jiang, Y. Y.; Hou, C. F.; Zhou, Z. X. *J. Mod. Opt.* **2001**, *48*, 1161.
- (61) Yuan, B. H.; Sun, X. D.; Zhou, Z. X.; Li, Y.; Jiang, Y. Y.; Hou, C. F. *J. Appl. Phys.* **2001**, *89*, 5881.
- (62) Pope, M.; Swenberg, C. E. *Electronic Processes in Organic Crystals and Polymers*; Oxford University Press: New York, 1999.
- (63) Ostroverkhova, O. Ph.D. Thesis, Case Western Reserve University, 2001.
- (64) Hendrickx, E.; Zhang, Y. D.; Ferrio, K. B.; Herlocker, J. A.; Anderson, J.; Armstrong, N. R.; Mash, E. A.; Persoons, A. P.; Peyghambarian, N.; Kippelen, B. *J. Mater. Chem.* **1999**, *9*, 2251.
- (65) Herlocker, J. A.; Fuentes-Hernandez, C.; Ferrio, K. B.; Hendrickx, E.; Blanche, P. A.; Peyghambarian, N.; Kippelen, B.; Zhang, Y.; Wang, J. F.; Marder, S. R. *Appl. Phys. Lett.* **2000**, *77*, 2292.
- (66) Kulikovskiy, L.; Neher, D.; Mecher, E.; Meerholz, K.; Horhold, H. H.; Ostroverkhova, O. *Phys. Rev. B* **2004**, *69*, 125216.
- (67) Marc, N.; Moisan, J. Y.; Wölffer, N.; Andre, B.; Lever, R. *Philos. Mag. B* **1996**, *74*, 81.
- (68) Marc, N.; Moisan, J. Y.; Andre, B.; Lever, R. *Philos. Mag. B* **1996**, *73*, 779.
- (69) Ostroverkhova, O.; Moerner, W. E.; He, M.; Twieg, R. J. *ChemPhysChem* **2003**, *4*, 732.
- (70) Liphardt, M.; Goonesekera, A.; Ducharme, S.; Takacs, J. M.; Zhang, L. *J. Opt. Soc. Am. B* **1996**, *13*, 2252.
- (71) Grunnet-Jepsen, A.; Thompson, C. L.; Twieg, R. J.; Moerner, W. E. *J. Opt. Soc. Am. B* **1998**, *15*, 901.
- (72) Grunnet-Jepsen, A.; Thompson, C. L.; Twieg, R. J.; Moerner, W. E. *Appl. Phys. Lett.* **1997**, *70*, 1515.
- (73) Meerholz, K.; Bittner, R.; Brauchle, C. *J. Inf. Record.* **1996**, *22*, 475.
- (74) Meerholz, K.; Mecher, E.; Bittner, R.; De Nardin, Y. *J. Opt. Soc. Am. B* **1998**, *15*, 2114.
- (75) Prasad, P. N.; Williams, D. J. *Introduction to Nonlinear Optical Effects in Molecules & Polymers*; John Wiley & Sons: New York, 1991.
- (76) Wu, J. W. *J. Opt. Soc. Am. B* **1991**, *8*, 142.
- (77) Pedersen, T. G.; Jespersen, K.; Johansen, P. M. *Opt. Mater.* **2001**, *18*, 95.
- (78) Baskin, J. S.; Zewail, A. H. *J. Phys. Chem. A* **2001**, *105*, 3680.
- (79) Stahelin, M.; Burland, D. M.; Ebert, M.; Miller, R. D.; Smith, B. A.; Twieg, R. J.; Volksen, W.; Walsh, C. A. *Appl. Phys. Lett.* **1992**, *61*, 1626.
- (80) Dureiko, R. D.; Schuele, D. E.; Singer, K. D. *J. Opt. Soc. Am. B* **1998**, *15*, 338.
- (81) Hall, D. B.; Dhinojwala, A.; Torkelson, J. *Phys. Rev. Lett.* **1997**, *79*, 103.
- (82) Pretre, P.; Meier, U.; Stalder, U.; Bosshard, C.; Gunter, P.; Kaatz, P.; Weder, C.; Neuenschwander, P.; Suter, U. W. *Macromolecules* **1998**, *31*, 1947.
- (83) Ribierre, J. C.; Mager, L.; Fort, A.; Mery, S. *Macromolecules* **2003**, *36*, 2516.
- (84) Walsh, C. A.; Moerner, W. E. *J. Opt. Soc. Am. B* **1992**, *9*, 1642.
- (85) Grunnet-Jepsen, A.; Thompson, C. L.; Moerner, W. E. *J. Opt. Soc. Am. B* **1998**, *15*, 905.
- (86) Hall, J. E.; Higgins, D. A. *Rev. Sci. Instrum.* **2002**, *73*, 2103.
- (87) Cheben, P.; del Monte, F.; Worsfold, D. J.; Carlsson, D. J.; Grover, C. P.; Mackenzie, J. D. *Nature* **2000**, *408*, 64.
- (88) Douglas, W. E.; Kuzhelev, A. S.; Yurasova, I. V.; Antipov, O. L.; Klapshina, L. G.; Semenov, V. V.; Domrachev, G. A.; Lopatina, T. I.; Guy, D. M. H. *PCCP Phys. Chem. Chem. Phys.* **2002**, *4*, 109.
- (89) Peng, Z. H.; Gharavi, A. R.; Yu, L. P. *J. Am. Chem. Soc.* **1997**, *119*, 4622.
- (90) Darracq, B.; Canva, M.; Chaput, F.; Boilot, J. P.; Riehl, D.; Levy, Y.; Brun, A. *Appl. Phys. Lett.* **1997**, *70*, 292.
- (91) Cipparrone, G.; Mazzulla, A.; Pagliusi, P. *Opt. Commun.* **2000**, *185*, 171.
- (92) Kwon, O. P.; Montemezzani, G.; Gunter, P.; Lee, S. H. *Appl. Phys. Lett.* **2004**, *84*, 43.
- (93) Wright, D.; Diaz-Garcia, M. A.; Casperson, J. D.; DeClue, M.; Moerner, W. E.; Twieg, R. J. *Appl. Phys. Lett.* **1998**, *73*, 1490.
- (94) Kwon, O. P.; Lee, S. H.; Montemezzani, G.; Gunter, P. *Adv. Function. Mater.* **2003**, *13*, 434.
- (95) Lee, S. H.; Montemezzani, G.; Gunter, P. *J. Opt. Soc. Am. B* **2003**, *20*, 2307.
- (96) Hayasaki, Y.; Ishikura, N.; Yamamoto, H.; Nishida, N. *Rev. Sci. Instrum.* **2003**, *74*, 3693.
- (97) Ratnam, K.; Banerjee, P. P. *Opt. Commun.* **1994**, *107*, 522.
- (98) Pedersen, H. C.; Johansen, P. M.; Pedersen, T. G. *Opt. Commun.* **2001**, *192*, 377.
- (99) Zha, M. Z.; Amrhein, P.; Gunter, P. *IEEE J. Quant. Electron.* **1990**, *26*, 788.
- (100) Grunnet-Jepsen, A.; Thompson, C. L.; Moerner, W. E. *Opt. Lett.* **1997**, *22*, 874.
- (101) Liphardt, M.; Ducharme, S. *J. Opt. Soc. Am. B* **1998**, *15*, 2154.
- (102) Zhang, J.; Singer, K. D. *Appl. Phys. Lett.* **1998**, *72*, 2948.
- (103) Van Steenwinckel, D.; Hendrickx, E.; Samyn, C.; Engels, C.; Persoons, A. *J. Mater. Chem.* **2000**, *10*, 2692.
- (104) Ostroverkhova, O.; Gubler, U.; Wright, D.; Moerner, W. E.; He, M.; Twieg, R. *Adv. Function. Mater.* **2002**, *12*, 621.
- (105) Bittner, R.; Meerholz, K.; Steckman, G.; Psaltis, D. *Appl. Phys. Lett.* **2002**, *81*, 211.
- (106) Trofimov, G.; Stepanov, S. *Sov. Phys. Solid State* **1986**, *28*, 1559.
- (107) Bittner, R.; Meerholz, K.; Stepanov, S. *Appl. Phys. Lett.* **1999**, *74*, 3723.
- (108) Horowitz, M.; Fischer, B.; Barad, Y.; Silberberg, Y. *Opt. Lett.* **1996**, *21*, 1120.
- (109) Kawata, Y.; Ishitobi, H.; Kawata, S. *Opt. Lett.* **1998**, *23*, 756.
- (110) Blanche, P. A.; Kippelen, B.; Schülzgen, A.; Fuentes-Hernandez, C.; Ramos-Ortiz, G.; Wang, J. F.; Hendrickx, E.; Peyghambarian, N. *Opt. Lett.* **2002**, *27*, 19.
- (111) Kippelen, B.; Blanche, P. A.; Schülzgen, A.; Fuentes-Hernandez, C.; Ramos-Ortiz, G.; Wang, J. F.; Peyghambarian, N.; Marder, S. R.; Leclercq, A.; Beljonne, D.; Bredas, J. L. *Adv. Function. Mater.* **2002**, *12*, 615.
- (112) Lee, H. J.; Sohn, J.; Hwang, J.; Park, S. Y. *Chem. Mater.* **2004**, *16*, 456.
- (113) Borsenberger, P. M.; Weiss, D. S. *Organic Photoreceptors for Xerography*; Marcel Dekker: New York, 1998.
- (114) Wada, T.; Zhang, Y. D.; Aoyama, T.; Sasabe, H. *Proc. Jpn. Acad. Ser. B* **1997**, *73*, 165.
- (115) Daubler, T. K.; Cimrova, V.; Pfeiffer, S.; Horhold, H. H.; Neher, D. *Adv. Mater.* **1999**, *11*, 1274.
- (116) Winiarz, J. G.; Zhang, L. M.; Lal, M.; Friend, C. S.; Prasad, P. N. *Chem. Phys.* **1999**, *245*, 417.
- (117) Hendrickx, E.; Kippelen, B.; Thayumanavan, S.; Marder, S. R.; Persoons, A.; Peyghambarian, N. *J. Chem. Phys.* **2000**, *112*, 9557.
- (118) Goonesekera, A.; Ducharme, S.; Takacs, J. M.; Zhang, L. *J. Chem. Phys.* **1997**, *107*, 8709.
- (119) Goonesekera, A.; Ducharme, S. *J. Appl. Phys.* **1999**, *85*, 6506.
- (120) Malliaras, G. G.; Krasnikov, V. V.; Bolink, H. J.; Hadziioannou, G. *Phys. Rev. B* **1995**, *52*, 14324.
- (121) Zilker, S. J.; Grasruck, M.; Wolff, J.; Schlöter, S.; Leopold, A.; Kol'chenko, M. A.; Hofmann, U.; Schreiber, A.; Strohrriegel, P.; Hohle, C.; Haarer, D. *Chem. Phys. Lett.* **1999**, *306*, 285.
- (122) Bartkiewicz, S.; Miniewicz, A.; Sahaoui, B.; Kajzar, F. *Appl. Phys. Lett.* **2002**, *81*, 3705.
- (123) Juska, G.; Arlauskas, K.; Viliunas, M.; Kocka, J. *Phys. Rev. Lett.* **2000**, *84*, 4946.
- (124) Juska, G.; Arlauskas, K.; Viliunas, M.; Genevicius, K.; Osterbacka, R.; Stubb, H. *Phys. Rev. B* **2000**, *62*, R16235.
- (125) Juska, G.; Genevicius, K.; Arlauskas, K.; Osterbacka, R.; Stubb, H. *Phys. Rev. B* **2002**, *65*, 233208.
- (126) Karl, N. *Synth. Met.* **2003**, *133–134*, 649.
- (127) Bauml, G.; Schlöter, S.; Hofmann, U.; Haarer, D. *Synth. Met.* **1998**, *97*, 165.
- (128) Kuzyk, M. In *Characterization Techniques and Tabulations for Organic Nonlinear Optical Materials*; Kuzyk, M., Dirk, C., Eds.; Marcel Dekker: New York, 1998; Vol. 60.
- (129) Herlocker, J. A.; Ferrio, K. B.; Hendrickx, E.; Guenther, B. D.; Mery, S.; Kippelen, B.; Peyghambarian, N. *Appl. Phys. Lett.* **1999**, *74*, 2253.
- (130) Bittner, R.; Daubler, T. K.; Neher, D.; Meerholz, K. *Adv. Mater.* **1999**, *11*, 123.

- (131) Wright, D.; Gubler, U.; Roh, Y.; Moerner, W. E.; He, M.; Twieg, R. *J. Appl. Phys. Lett.* **2001**, *79*, 4274.
- (132) Binks, D. J.; Khand, K.; West, D. P. *J. Opt. Soc. Am. B* **2001**, *18*, 308.
- (133) Moylan, C. R.; Miller, R. D.; Twieg, R. J.; Lee, V. Y. *Polym. Second-Order Nonlinear Opt.* **1995**, *601*, 66.
- (134) Ostroverkhova, O.; Stickerath, A.; Singer, K. D. *J. Appl. Phys.* **2002**, *91*, 9481.
- (135) Sandalphon; Kippelen, B.; Meerholz, K.; Peyghambarian, N. *Appl. Opt.* **1996**, *35*, 2346.
- (136) Sandalphon; Wang, J. F.; Kippelen, B.; Peyghambarian, N. *Appl. Phys. Lett.* **1997**, *71*, 873.
- (137) Hoechstetter, K.; Schloter, S.; Hofmann, U.; Haarer, D. *J. Chem. Phys.* **1999**, *110*, 4944.
- (138) Jespersen, K.; Pedersen, T. G.; Johansen, P. M. *J. Opt. Soc. Am. B* **2003**, *20*, 2179.
- (139) Onsager, L. *Phys. Rev.* **1938**, *54*, 554.
- (140) Noolandi, J.; Hong, K. M. *J. Chem. Phys.* **1979**, *70*, 3230.
- (141) Braun, C. L. *J. Chem. Phys.* **1984**, *80*, 4157.
- (142) Marcus, R. A. *Annu. Rev. Phys. Chem.* **1964**, *86*, 622.
- (143) Wang, Y.; Suna, A. *J. Phys. Chem. B* **1997**, *101*, 5627.
- (144) Kavarnos, G. J. *Fundamentals of Photoinduced Electron Transfer*; VCH Publishers: New York, 1993.
- (145) Kraabel, B.; McBranch, D.; Sariciftci, N. S.; Moses, D.; Heeger, A. *J. Phys. Rev. B* **1994**, *50*, 18543.
- (146) Moses, D.; Okumoto, H.; Comoretto, D.; Lee, C. H.; Heeger, A. J.; T., O.; Noguchi, T. *Synth. Met.* **1997**, *84*, 539.
- (147) Ueda, T.; Fujisawa, R.; Fukumura, H.; Itaya, A.; Masuhara, H. *J. Phys. Chem.* **1995**, *99*, 3629.
- (148) Ruseckas, A.; Gulbinas, V.; Sundstrom, V.; Undzenas, A.; Valkunas, L. *J. Phys. Chem. B* **1998**, *102*, 7365.
- (149) Abramavicius, D.; Gulbinas, V.; Valkunas, L. *Synth. Met.* **2000**, *109*, 39.
- (150) Moses, D.; Dogariu, A.; Heeger, A. J. *Synth. Met.* **2001**, *116*, 19.
- (151) Schloter, S.; Schreiber, A.; Grasruck, M.; Leopold, A.; Kolchenko, M.; Pan, J.; Hohle, C.; Strohhriegl, P.; Zilker, S. J.; Haarer, D. *Appl. Phys. B* **1999**, *68*, 899.
- (152) Vannikov, A. V.; Grishina, A. D.; Shapiro, B. I.; Pereshivko, L. Y.; Krivenko, T. V.; Savel'ev, V. V.; Berendyaev, V. I.; Rychwalski, R. W. *Chem. Phys.* **2003**, *287*, 261.
- (153) Wang, Q.; Wang, L. M.; Yu, J. J.; Yu, L. P. *Adv. Mater.* **2000**, *12*, 974.
- (154) You, W.; Wang, L. M.; Wang, Q.; Yu, L. P. *Macromolecules* **2002**, *35*, 4636.
- (155) Aiello, I.; Dattilo, D.; Ghedini, M.; Bruno, A.; Termine, R.; Golemme, A. *Adv. Mater.* **2002**, *14*, 1233.
- (156) Wang, Y.; Herron, N. *Chem. Phys. Lett.* **1992**, *200*, 71.
- (157) Winiarz, J. G.; Zhang, L. M.; Lal, M.; Friend, C. S.; Prasad, P. N. *J. Am. Chem. Soc.* **1999**, *121*, 5287.
- (158) Winiarz, J.; Prasad, P. *Opt. Lett.* **2002**, *27*, 1330.
- (159) Binks, D. J.; West, D. P.; Norager, S.; O'Brien, P. *J. Chem. Phys.* **2002**, *117*, 7335.
- (160) Ostroverkhova, O.; Gubler, U.; Wright, D.; He, M.; Twieg, R.; Moerner, W. E. SPIE Proceedings, SPIE annual meeting, Seattle, WA, 2002; Vol. 4802, p 21.
- (161) Sohn, J.; Hwang, J.; Park, S. Y.; Lee, J. K.; Lee, J. H.; Chang, J. S.; Lee, G. J.; Zhang, B.; Gong, Q. H. *Appl. Phys. Lett.* **2000**, *77*, 1422.
- (162) Ostroverkhova, O.; Moerner, W. E.; He, M.; Twieg, R. *J. Appl. Phys. Lett.* **2003**, *82*, 3602.
- (163) Kippelen, B.; Marder, S. R.; Hendrickx, E.; Maldonado, J. L.; Guillemet, G.; Volodin, B. L.; Steele, D. D.; Enami, Y.; Sandalphon; Yao, Y. J.; Wang, J. F.; Rockel, H.; Erskine, L.; Peyghambarian, N. *Science* **1998**, *279*, 54.
- (164) Schloter, S.; Hofmann, U.; Strohhriegl, P.; Schmidt, H. W.; Haarer, D. *J. Opt. Soc. Am. B* **1998**, *15*, 2473.
- (165) Chun, H.; Moon, I. K.; Shin, D. H.; Song, S.; Kim, N. *J. Mater. Chem.* **2002**, *12*, 858.
- (166) Hendrickx, E.; Herlocker, J.; Maldonado, J. L.; Marder, S. R.; Kippelen, B.; Persoons, A.; Peyghambarian, N. *Appl. Phys. Lett.* **1998**, *72*, 1679.
- (167) Iftime, G.; Labarthe, F. L.; Natansohn, A.; Rochon, P.; Murti, K. *Chem. Mater.* **2002**, *14*, 168.
- (168) Bratcher, M. S.; DeClue, M. S.; Grunnet-Jepsen, A.; Wright, D.; Smith, B. R.; Moerner, W. E.; Siegel, J. S. *J. Am. Chem. Soc.* **1998**, *120*, 9680.
- (169) Wright, D.; Gubler, U.; Moerner, W. E.; DeClue, M.; Siegel, J. S. *J. Phys. Chem. B* **2003**, *107*, 4732.
- (170) Wurthner, F.; Yao, S.; Schilling, J.; Wortmann, R.; Redi-Abshiro, M.; Mecher, E.; Gallego-Gomez, F.; Meerholz, K. *J. Am. Chem. Soc.* **2001**, *123*, 2810.
- (171) Wang, L. M.; Ng, M. K.; Yu, L. P. *Appl. Phys. Lett.* **2001**, *78*, 700.
- (172) Hou, Z.; You, W.; Yu, L. P. *Appl. Phys. Lett.* **2003**, *82*, 3385.
- (173) Bässler, H. *Phys. Status Solidi B* **1993**, *175*, 15.
- (174) Blom, P. W. M.; Vissenberg, M. *Mater. Sci. Eng. R* **2000**, *27*, 53.
- (175) Visser, S. A.; Gruenbaum, W. T.; Magin, E. H.; Borsenberger, P. M. *Chem. Phys.* **1999**, *240*, 197.
- (176) Borsenberger, P. M.; Magin, E. H.; Sinicropi, J. A.; Lin, L. B. *Jpn. J. Appl. Phys. Part 1* **1998**, *37*, 166.
- (177) Young, R. H.; Rule, N. G. *Phys. Rev. Lett.* **1994**, *72*, 388.
- (178) Seki, K.; Tachiya, M. *Phys. Rev. B* **2002**, *65*, 014305.
- (179) Van der Auweraer, M.; De Schryver, F. C.; Borsenberger, P. *Chem. Phys.* **1994**, *186*, 409.
- (180) Malliaras, G. G.; Krasnikov, V. V.; Bolink, H. J.; Hadziioannou, G. *Appl. Phys. Lett.* **1995**, *66*, 1038.
- (181) West, D. P.; Rahn, M. D.; Im, C.; Bassler, H. *Chem. Phys. Lett.* **2000**, *326*, 407.
- (182) Borsenberger, P. M.; Gruenbaum, W. T.; Magin, E. H.; Visser, S. A. *Phys. Status Solidi A* **1998**, *166*, 835.
- (183) Malliaras, G. G.; Angerman, H.; Krasnikov, V. V.; tenBrinke, G.; Hadziioannou, G. *J. Phys. D* **1996**, *29*, 2045.
- (184) Hofmann, U.; Grasruck, M.; Leopold, A.; Schreiber, A.; Schloter, S.; Hohle, C.; Strohhriegl, P.; Haarer, D.; Zilker, S. J. *J. Phys. Chem. B* **2000**, *104*, 3887.
- (185) Choudhury, K. R.; Winiarz, J.; Samoc, M.; Prasad, P. N. *Appl. Phys. Lett.* **2003**, *82*, 406.
- (186) Hofmann, U.; Schreiber, A.; Haarer, D.; Zilker, S. J.; Bacher, A.; Bradley, D. D. C.; Redecker, M.; Inbasekaran, M.; Wu, W. W.; Woo, E. P. *Chem. Phys. Lett.* **1999**, *311*, 41.
- (187) Thelakkat, M. *Macromolec. Mater. Eng.* **2002**, *287*, 442.
- (188) Funahashi, M.; Hanna, J. *Appl. Phys. Lett.* **2000**, *76*, 2574.
- (189) Kreouzis, T.; Scott, K.; Donovan, K. J.; Boden, N.; Bushby, R. J.; Lozman, O. R.; Liu, Q. *Chem. Phys.* **2000**, *262*, 489.
- (190) Shiyanovskaya, I.; Singer, K. D.; Twieg, R. J.; Sukhomlinova, L.; Gettewert, V. *Phys. Rev. E* **2002**, *65*, 041715.
- (191) Percec, V.; Glodde, M.; Bera, T. K.; Miura, Y.; Shiyanovskaya, I.; Singer, K. D.; Balagurusamy, V. S. K.; Heiney, P. A.; Schnell, I.; Rapp, A.; Spiess, H. W.; Hudson, S. D.; Duan, H. *Nature* **2002**, *419*, 384.
- (192) Bushby, R. J.; Lozman, O. R. *Curr. Opin. Solid State Mater. Sci.* **2002**, *6*, 569.
- (193) Wiederrecht, G. P.; Niemczyk, M. P.; Svec, W. A.; Wasielewski, M. R. *Chem. Mater.* **1999**, *11*, 1409.
- (194) Kokil, A.; Shiyanovskaya, I.; Singer, K. D.; Weder, C. *J. Am. Chem. Soc.* **2002**, *124*, 9989.
- (195) Ogino, K.; Park, S. H.; Sato, H. *Appl. Phys. Lett.* **1999**, *74*, 3936.
- (196) Strohhriegl, P.; Grazulevicius, J. V. *Adv. Mater.* **2002**, *14*, 1439.
- (197) Dimitrakopoulos, C. D.; Malenfant, P. R. L. *Adv. Mater.* **2002**, *14*, 99.
- (198) Kippelen, B.; Meyers, F.; Peyghambarian, N.; Marder, S. R. *J. Am. Chem. Soc.* **1997**, *119*, 4559.
- (199) Moylan, C. R.; Wortmann, R.; Twieg, R. J.; McComb, I. H. *J. Opt. Soc. Am. B* **1998**, *15*, 929.
- (200) Hendrickx, E.; Guenther, B. D.; Zhang, Y.; Wang, J. F.; Staub, K.; Zhang, Q.; Marder, S. R.; Kippelen, B.; Peyghambarian, N. *Chem. Phys.* **1999**, *245*, 407.
- (201) Wortmann, R.; Glania, C.; Kramer, P.; Lukaszuk, K.; Matschiner, R.; Twieg, R. J.; You, F. *Chem. Phys.* **1999**, *245*, 107.
- (202) Barzoukas, M.; Blanchard-Desce, M. *J. Chem. Phys.* **2000**, *112*, 2036.
- (203) Schaeerlaekens, M.; Hendrickx, E.; Hameurlaine, A.; Dehaen, W.; Persoons, A. *Chem. Phys.* **2002**, *277*, 43.
- (204) Hendrickx, E.; Volodin, B. L.; Steele, D. D.; Maldonado, J. L.; Wang, J. F.; Kippelen, B.; Peyghambarian, N. *Appl. Phys. Lett.* **1997**, *71*, 1159.
- (205) Meerholz, K.; Bittner, R.; DeNardin, Y.; Brauchle, C.; Hendrickx, E.; Volodin, B. L.; Kippelen, B.; Peyghambarian, N. *Adv. Mater.* **1997**, *9*, 1043.
- (206) Meerholz, K.; DeNardin, Y.; Bittner, R.; Wortmann, R.; Wurthner, F. *Appl. Phys. Lett.* **1998**, *73*, 4.
- (207) Wurthner, F.; Yao, C.; Debaeremaeker, T.; Wortmann, R. *J. Am. Chem. Soc.* **2002**, *124*, 9431.
- (208) He, M.; Twieg, R.; Ostroverkhova, O.; Gubler, U.; Wright, D.; Moerner, W. E. SPIE Proceedings, SPIE annual meeting, Seattle, WA, 2002; Vol. 4802, p 9.
- (209) Diaz-Garcia, M. A.; Wright, D.; Casperson, J. D.; Smith, B.; Glazer, E.; Moerner, W. E.; Sukhomlinova, L. I.; Twieg, R. J. *Chem. Mater.* **1999**, *11*, 1784.
- (210) Van Steenwinckel, D.; Hendrickx, E.; Persoons, A.; Van den Broeck, K.; Samyn, C. *J. Chem. Phys.* **2000**, *112*, 11030.
- (211) Bolink, H. J.; Krasnikov, V. V.; Malliaras, G. G.; Hadziioannou, G. *J. Phys. Chem.* **1996**, *100*, 16356.
- (212) Thelakkat, M.; Ostrauskaite, J.; Leopold, A.; Bausinger, R.; Haarer, D. *Chem. Phys.* **2002**, *285*, 133.
- (213) Bai, Y.; Chen, X.; Wan, X.; Zhou, Q. F.; Liu, H.; Zhang, B.; Gong, Q. *Appl. Phys. B* **2001**, *73*, 35.
- (214) Bai, Y.; Chen, X.; Wan, X.; Zhou, Q. F.; Liu, H.; Zhang, B.; Gong, Q. *Appl. Phys. Lett.* **2002**, *80*, 10.
- (215) Chen, Z. J.; Wang, F.; Huang, Z. W.; Gong, Q. H.; Chen, Y. W.; Zhang, Z. J.; Chen, H. Y. *J. Phys. D* **1998**, *31*, 2245.
- (216) Van Steenwinckel, D.; Engels, C.; Gubbelsmans, E.; Hendrickx, E.; Samyn, C.; Persoons, A. *Macromolecules* **2000**, *33*, 4074.
- (217) Engels, C.; Van Steenwinckel, D.; Hendrickx, E.; Schaeerlaekens, M.; Persoons, A.; Samyn, C. *J. Mater. Chem.* **2002**, *12*, 951.
- (218) Bittner, R.; Brauchle, C.; Meerholz, K. *Appl. Opt.* **1998**, *37*, 2843.

- (219) Wang, F.; Chen, Z. J.; Zhang, B.; Gong, Q. H.; Wu, K. W.; Wang, X. S.; Zhang, B. W.; Tang, F. Q. *Appl. Phys. Lett.* **1999**, *75*, 3243.
- (220) Swedek, B.; Cheng, N.; Cui, Y. P.; Zieba, J.; Winiarz, J.; Prasad, P. N. *J. Appl. Phys.* **1997**, *82*, 5923.
- (221) Wu, S. Z.; Zeng, F.; Li, F. X.; Zhu, Y. L.; Zhao, H. P. *J. Polym. Sci., Part B* **1999**, *37*, 3302.
- (222) Hwang, J.; Seo, J.; Sohn, J.; Park, S. Y. *Opt. Mater.* **2003**, *21*, 359.
- (223) Wolff, J.; Schloter, S.; Hofmann, U.; Haarer, D.; Zilker, S. J. *J. Opt. Soc. Am. B* **1999**, *16*, 1080.
- (224) Mecher, E.; Gallego-Gomez, F.; Meerholz, K.; Tillmann, H.; Horhold, H. H.; Hummelen, J. C. *ChemPhysChem* **2004**, *5*, 277.
- (225) Ribierre, J. C.; Cheval, G.; Huber, F.; Mager, L.; Fort, A.; Muller, R.; Mery, S.; Nicoud, J. F. *J. Appl. Phys.* **2002**, *91*, 1710.
- (226) Wortmann, R.; Redi-Abshiro, M.; Rosch, U.; Yao, S.; Wurthner, F. SPIE Proceedings, SPIE annual meeting, Seattle, WA, 2002; Vol. 4802, p 1.
- (227) Mecher, E.; Bittner, R.; Brauchle, C.; Meerholz, K. *Synth. Met.* **1999**, *102*, 993.
- (228) Silence, S. M.; Bjorklund, G. C.; Moerner, W. E. *Opt. Lett.* **1994**, *19*, 1822.
- (229) Bauml, G.; Schloter, S.; Hofmann, U.; Haarer, D. *Opt. Commun.* **1998**, *154*, 75.
- (230) Kador, L.; Bausinger, R.; Leopold, A.; Haarer, D.; Kohler, W. J. *Phys. Chem. A* **2004**, *108*, 1640.
- (231) Leopold, A.; Bausinger, R.; Haarer, D.; Ostrauskaite, J.; Thelakkat, M. SPIE Proceedings, SPIE annual meeting, Seattle, WA, 2002; Vol. 4802, p 33.
- (232) Zilker, S. J.; Hofmann, U. *Appl. Opt.* **2000**, *39*, 2287.
- (233) Meerholz, K.; Bittner, R.; De Nardin, Y. *Opt. Commun.* **1998**, *150*, 205.
- (234) Leahy, M. R.; McGee, D. J. *Opt. Commun.* **2001**, *187*, 277.
- (235) Wang, F.; Chen, Z. J.; Gong, Q. H.; Chen, Y. W.; Chen, H. Y. *J. Opt. Soc. Am. B* **1999**, *16*, 366.
- (236) Wang, F.; Zhang, B.; Gong, Q.; Chen, Y.; Chen, H. *Appl. Phys. B* **1999**, *68*, 907.
- (237) Bittner, R.; Brauchle, C.; Meerholz, K. *J. Inf. Rec.* **1998**, *24*, 469.
- (238) Matsushita, K.; Banerjee, P. P.; Ozaki, S.; Miyazaki, D. *Opt. Lett.* **1999**, *24*, 593.
- (239) Zhang, Y. D.; Wada, T.; Sasabe, H. *J. Mater. Chem.* **1998**, *8*, 809.
- (240) Grazulevicius, J. V.; Stroehriegel, P.; Pielichowski, J.; Pielichowski, K. *Prog. Polym. Sci.* **2003**, *28*, 1297.
- (241) Yesodha, S. K.; Pillai, C. K.; Tsutsumi, N. *Prog. Polym. Sci.* **2004**, *29*, 45.
- (242) Suh, D. J.; Park, O. O.; Ahn, T.; Shim, H. K. *Jpn. J. Appl. Phys. Part 2* **2002**, *41*, L428.
- (243) Haarer, D.; Meyer, H.; Stroehriegel, P. *Makromolekul. Chem.-Macromolekul. Chem. Phys.* **1991**, *192*, 617.
- (244) Silence, S. M.; Scott, J. C.; Hache, F.; Ginsburg, E. J.; Jenkner, P. K.; Miller, R. D.; Twieg, R. J.; Moerner, W. E. *J. Opt. Soc. Am. B* **1993**, *10*, 2306.
- (245) Nishida, F.; Kushibiki, N.; Tomita, Y. *Appl. Phys. Lett.* **1998**, *73*, 2555.
- (246) Park, S. H.; Ogino, K.; Sato, H. *Synth. Met.* **2000**, *113*, 135.
- (247) Joo, W. J.; Kim, N. J.; Chun, H.; Moon, I. K.; Kim, N. *Polymer* **2001**, *42*, 9863.
- (248) Chun, H.; Moon, I. K.; Shin, D. H.; Kim, N. *Chem. Mater.* **2001**, *13*, 2813.
- (249) Lundquist, P. M.; Wortmann, R.; Geletneky, C.; Twieg, R. J.; Jurich, M.; Lee, V. Y.; Moylan, C. R.; Burland, D. M. *Science* **1996**, *274*, 1182.
- (250) He, M.; Twieg, R. J.; Gubler, U.; Wright, D.; Moerner, W. E. *Chem. Mater.* **2003**, *15*, 1156.
- (251) Sohn, J.; Hwang, J.; Park, S. Y.; Lee, G. J. *Jpn. J. Appl. Phys., Part 1* **2001**, *5A*, 3301.
- (252) Chun, H.; Kim, N. J.; Joo, W. J.; Han, J. W.; Oh, C. H.; Kim, N. *Synth. Met.* **2002**, *129*, 281.
- (253) Yu, L. P.; Chan, W. K.; Bao, Z. N.; Cao, S. X. F. *J. Chem. Soc.-Chem. Commun.* **1992**, 1735.
- (254) Ng, M. K.; Wang, L. M.; Yu, L. P. *Chem. Mater.* **2000**, *12*, 2988.
- (255) Schloter, S.; Hofmann, U.; Hoechstetter, K.; Bauml, G.; Haarer, D.; Ewert, K.; Eisenbach, C. D. *J. Opt. Soc. Am. B* **1998**, *15*, 2560.
- (256) Chang, C. J.; Whang, W. T.; Hsu, K. Y. *J. Appl. Polym. Sci.* **1999**, *74*, 1321.
- (257) Chen, Y. W.; Chen, Z. J.; Gong, Q. H.; Schroers, M. *Mater. Lett.* **2003**, *57*, 2271.
- (258) Li, W. J.; Gharavi, A.; Wang, Q.; Yu, L. P. *Adv. Mater.* **1998**, *10*, 927.
- (259) You, W.; Cao, S.; Hou, Z.; Yu, L. P. *Macromolecules* **2003**, *36*, 7014.
- (260) Chidichimo, G.; Arabia, G.; Golemme, A.; Doane, J. W. *Liq. Cryst.* **1989**, *5*, 1443.
- (261) Doane, J. W.; Golemme, A.; West, J. L.; Whitehead, J. B.; Wu, B. G. *Mol. Cryst. Liq. Cryst.* **1988**, *165*, 511.
- (262) Golemme, A.; Volodin, B. L.; Kippelen, E.; Peyghambarian, N. *Opt. Lett.* **1997**, *22*, 1226.
- (263) Ono, H.; Kawatsuki, N. *Opt. Lett.* **1997**, *22*, 1144.
- (264) Klein, W. R.; Cook, B. D. *IEEE Trans. Sonics Ultrason.* **1967**, *SU-14*, 123.
- (265) Golemme, A.; Kippelen, B.; Peyghambarian, N. *Appl. Phys. Lett.* **1998**, *73*, 2408.
- (266) Cipparrone, G.; Mazzulla, A.; Nicoletta, F. P.; Lucchetti, L.; Simoni, F. *Opt. Commun.* **1998**, *150*, 297.
- (267) Van Steenwinckel, D.; Hendrickx, E.; Persoons, A. *Chem. Mater.* **2001**, *13*, 1230.
- (268) Yoshimoto, N.; Morino, S.; Nakagawa, M.; Ichimura, K. *Opt. Lett.* **2002**, *27*, 182.
- (269) Ono, H.; Shimokawa, H.; Emoto, A.; Kawatsuki, N. *J. Appl. Phys.* **2003**, *94*, 23.
- (270) Termine, R.; Golemme, A. *Opt. Lett.* **2001**, *26*, 1001.
- (271) Ono, H.; Kawatsuki, N. *Jpn. J. Appl. Phys., Part 1* **1997**, *36*, 6444.
- (272) Cipparrone, G.; Mazzulla, A.; Pagliusi, P.; Sukhov, A. V.; Ushakov, R. F. *J. Opt. Soc. Am. B* **2001**, *18*, 182.
- (273) Simoni, F.; Cipparrone, G.; Mazzulla, A.; Pagliusi, P. *Chem. Phys.* **1999**, *245*, 429.
- (274) Golemme, A.; Kippelen, B.; Peyghambarian, N. *Chem. Phys. Lett.* **2000**, *319*, 655.
- (275) Ono, H.; Shimokawa, H.; Emoto, A.; Kawatsuki, N. *Polymer* **2003**, *44*, 7971.
- (276) Hall, J. E.; Higgins, D. A. *J. Phys. Chem. B* **2003**, *107*, 14211.
- (277) Rudenko, E. V.; Sukhov, A. V. *J. Exp. Theor. Phys.* **1994**, *78*, 875.
- (278) Rudenko, E. V.; Sukhov, A. V. *JETP Lett.* **1994**, *59*, 142.
- (279) Khoo, I. C.; Li, H.; Liang, Y. *Optics Lett.* **1994**, *19*, 1723.
- (280) Khoo, I. C. *IEEE J. Quantum Electron.* **1996**, *32*, 525.
- (281) Zhang, G. Q.; Montemezzani, G.; Gunter, P. *J. Appl. Phys.* **2000**, *88*, 1709.
- (282) Jones, D. C.; Cook, G. *Opt. Commun.* **2004**, 232.
- (283) Mehta, P. C.; Rampal, V. V. *Lasers and Holography*; World Scientific Publishing Co.: Singapore, 1993.
- (284) Bartkiewicz, S.; Miniewicz, A.; Kajzar, F.; Zagorska, M. *Appl. Opt.* **1998**, *37*, 6871.
- (285) Wiederrecht, G. P.; Yoon, B. A.; Wasielewski, M. R. *Science* **1995**, *270*, 1794.
- (286) Khoo, I. C.; Guenther, B. D.; Wood, M. V.; Chen, P.; Shih, M. Y. *Opt. Lett.* **1997**, *22*, 1229.
- (287) Lee, W.; Chiu, C. S. *Opt. Lett.* **2001**, *26*, 521.
- (288) Khoo, I. C.; Ding, Y.; Zhang, Y.; Chen, K.; Diaz, A. *Appl. Phys. Lett.* **2003**, *82*, 3587.
- (289) Wiederrecht, G. P.; Wasielewski, M. R. *J. Am. Chem. Soc.* **1998**, *120*, 3231.
- (290) Tabiryan, N. V.; Umetsu, C. *J. Opt. Soc. Am. B* **1998**, *15*, 1912.
- (291) Ono, H.; Kawatsuki, N. *Opt. Commun.* **1998**, *147*, 237.
- (292) Fuller, M. J.; Walsh, C. J.; Zhao, Y. Y.; Wasielewski, M. R. *Chem. Mater.* **2002**, *14*, 952.
- (293) Bartkiewicz, S.; Matczyszyn, K.; Miniewicz, A.; Kajzar, F. *Opt. Commun.* **2001**, *187*, 257.
- (294) Kim, H. W.; Mun, J. H.; Yoon, C. S.; Kim, J. D. *Jpn. J. Appl. Phys., Part 2* **2001**, *40*, L952.
- (295) Termine, R.; De Simone, B. C.; Golemme, A. *Appl. Phys. Lett.* **2001**, *78*, 688.
- (296) Kim, H. W.; Jung, S.; Yoon, C. S.; Kim, J. D. *Appl. Phys. B* **2003**, *77*, 427.
- (297) Kim, H. W.; Choi, K. S.; Mun, J.; Jung, S.; Yoon, C. S.; Kim, J. D. *Opt. Mater.* **2002**, *21*, 657.
- (298) Wiederrecht, G. P.; Wasielewski, M. R. *Appl. Phys. Lett.* **1999**, *74*, 3459.
- (299) Zhang, J.; Ostroverkhov, V.; Singer, K. D.; Reshetnyak, V.; Reznikov, Y. *Opt. Lett.* **2000**, *25*, 414.
- (300) Pagliusi, P.; Cipparrone, G. *J. Appl. Phys.* **2002**, *92*, 4863.
- (301) Pagliusi, P.; Cipparrone, G. *Opt. Lett.* **2003**, *28*, 2369.
- (302) Wiederrecht, G. P.; Yoon, B. A.; Wasielewski, M. R. *Adv. Mat.* **2000**, *12*, 1533.
- (303) Sasaki, T.; Kino, Y.; Shibata, M.; Mizusaki, N.; Katsuragi, A.; Ishikawa, Y.; Yoshimi, T. *Appl. Phys. Lett.* **2001**, *78*, 4112.
- (304) Termine, R.; Golemme, A. *J. Phys. Chem. B* **2002**, *106*, 4105.
- (305) Sasaki, T.; Katsuragi, A.; Ohno, K. *J. Phys. Chem. B* **2002**, *106*, 2520.
- (306) Talarico, M.; Barberio, G.; Pucci, D.; Ghedini, M.; Golemme, A. *Adv. Mater.* **2003**, *15*, 1374.
- (307) Sasaki, T.; Katsuragi, A.; Mochizuki, O.; Nakazawa, Y. *J. Phys. Chem. B* **2003**, *107*, 7659.
- (308) Talarico, M.; Termine, R.; Barberio, G.; Pucci, D.; Ghedini, M.; Golemme, A. *Appl. Phys. Lett.* **2004**, *84*, 1034.
- (309) Sasaki, T.; Goto, M.; Ishikawa, Y.; Yoshimi, T. *J. Phys. Chem. B* **1999**, *103*, 1925.
- (310) Ono, H.; Kawatsuki, N. *J. Appl. Phys.* **1999**, *85*, 2482.
- (311) Ono, H.; Kawamura, T.; Frias, N. M.; Kitamura, K.; Kawatsuki, N.; Norisada, H.; Yamamoto, T. *J. Appl. Phys.* **2000**, *88*, 3853.
- (312) Sanchez, C.; Lebeau, B.; Chaput, F.; Boilot, J. P. *Adv. Mater.* **2003**, *15*, 1969.
- (313) Wang, Y. *Nature* **1992**, *356*, 585.
- (314) Wang, S.; Yang, S.; Yang, C.; Li, Z.; Wang, J.; Ge, W. *J. Phys. Chem. B* **2000**, *104*, 11853.
- (315) Ginger, D. S.; Greenham, N. C. *Phys. Rev. B* **1999**, *59*, 10622.

- (316) Choudhury, K. R.; Samoc, M.; Patra, A.; Prasad, P. N. *J. Phys. Chem. B* **2004**, *108*, 1556.
- (317) Valley, G. C. *J. Appl. Phys.* **1986**, *59*, 3363.
- (318) Wu, C. C.; Liu, T. L.; Hung, W. Y.; Lin, Y. T.; Wong, K. T.; Chen, R. T.; Chen, Y. M.; Chien, Y. Y. *J. Am. Chem. Soc.* **2003**, *125*, 3710.
- (319) Silence, S. M.; Walsh, C. A.; Scott, J. C.; Matray, T. J.; Twieg, R. J.; Hache, F.; Bjorklund, G. C.; Moerner, W. E. *Opt. Lett.* **1992**, *17*, 1107.
- (320) Wright, J. D.; Sommerdijk, N. A. J. M. *Sol-Gel Materials: Chemistry and Applications*; Gordon and Breach Science Publishers: Amsterdam, 2001.
- (321) *Sol-Gel Technology for Thin Films, Fibers, Preforms, Electronics, and Specialty Shapes*; Klein, L. C., Ed.; Noyes Publications: Park Ridge, New Jersey, USA, 1988.
- (322) Burzynski, R.; Casstevens, M. K.; Zhang, Y.; Ghosal, S. *Opt. Eng.* **1996**, *35*, 443.
- (323) Choi, D. H.; Hong, H. T.; Jun, W. G.; Oh, K. Y. *Opt. Mater.* **2003**, *21*, 373.
- (324) Herlocker, J. A.; Fuentes-Hernandez, C.; Wang, J. F.; Peyghambarian, N.; Kippelen, B.; Zhang, Q.; Marder, S. R. *Appl. Phys. Lett.* **2002**, *80*, 1156.
- (325) Zilker, S. J. *ChemPhysChem* **2002**, *2*, 333.
- (326) Steckman, G. J.; Pu, A.; Psaltis, D. *Appl. Opt.* **2001**, *40*, 3387.
- (327) van Heerden, P. J. *Appl. Opt.* **1963**, *2*, 393.
- (328) Lundquist, P. M.; Poga, C.; DeVoe, R. G.; Jia, Y.; Moerner, W. E.; Bernal, M. P.; Coufal, H.; Grygier, R. K.; Hoffnagle, J. A.; Jefferson, C. M.; Macfarlane, R. M.; Shelby, R. M.; Sincerbox, G. T. *Opt. Lett.* **1996**, *21*, 890.
- (329) Poga, C.; Lundquist, P. M.; Lee, V.; Shelby, R. M.; Twieg, R. J.; Burland, D. M. *Appl. Phys. Lett.* **1996**, *69*, 1047.
- (330) Cheng, N.; Swedek, B.; Prasad, P. N. *Appl. Phys. Lett.* **1997**, *71*, 1828.
- (331) Strutz, S. J.; Hayden, L. M. *Appl. Phys. Lett.* **1999**, *74*, 2749.
- (332) Harris, K. D.; Ayachitula, R.; Strutz, S. J.; Hayden, L. M.; Twieg, R. J. *Appl. Opt.* **2001**, *40*, 2895.
- (333) Mok, F. H.; Burr, G. W.; Psaltis, D. *Opt. Lett.* **1996**, *21*, 896.
- (334) Steckman, G. J.; Bittner, R.; Meerholz, K.; Psaltis, D. *Opt. Commun.* **2000**, *185*, 13.
- (335) Chang, C. J.; Whang, W. T.; Hsu, K. Y.; Hsieh, M. L. *J. Polym. Sci., Part B* **1999**, *37*, 1057.
- (336) Chang, C. J.; Whang, W. T.; Hsu, C. C.; Ding, Z. Y.; Hsu, K. Y.; Lin, S. H. *Macromolecules* **1999**, *32*, 5637.
- (337) Rahn, M. D.; West, D. P.; Khand, K.; Shakos, J. D.; Shelby, R. M. *Appl. Opt.* **2001**, *40*, 3395.
- (338) Aoyama, T.; Takabayashi, E.; Zhang, Y.; Sasabe, H.; Wada, T. *IEICE Trans. Electron.* **2002**, *E850C*, 1282.
- (339) Miniewicz, A.; Gniewek, A.; Parka, J. *Opt. Mater.* **2003**, *21*, 605.
- (340) Li, W. J.; Gharavi, A.; Wang, Q.; Yu, L. P. In *Field Responsive Polymers*; Khan, I. M., Harrison, J. S., Eds., American Chemical Society, Washington, DC, 1999; Vol. 726.
- (341) Stankus, J. J.; Silence, S. M.; Moerner, W. E.; Bjorklund, G. C. *Opt. Lett.* **1994**, *19*, 1480.
- (342) Ketchel, B. P.; Wood, G. L.; Anderson, R. J.; Salamo, G. J. *Appl. Phys. Lett.* **1997**, *71*, 7.
- (343) Ketchel, B. P.; Heid, C. A.; Wood, G. L.; Miller, M. J.; Mott, A. G.; Anderson, R. J.; Salamo, G. J. *Appl. Opt.* **1999**, *38*, 6159.
- (344) Gu, M. *Proc. IEEE* **1999**, *87*, 2021.
- (345) Day, D.; Gu, M.; Smallridge, A. *Infrared Holography Opt. Commun.* **2002**, *86*, 75.
- (346) McPhail, D.; Gu, M. *Appl. Phys. Lett.* **2002**, *81*, 1160.
- (347) Kawata, S. *Proc. IEEE* **1999**, *87*, 2009.
- (348) Day, D.; Gu, M.; Smallridge, A. *Infrared Holography Opt. Commun.* **2002**, *86*, 1.
- (349) *Optical Phase Conjugation*; Fischer, R. A., Ed.; Academic Press: New York, 1983.
- (350) Zel'dovich, B. Y.; Popovichev, V. I.; Raguelsky, V. V.; Faizullof, F. S. *Sov. Phys. JETP* **1972**, *15*, 109.
- (351) Hellwarth, R. W. *J. Opt. Soc. Am.* **1977**, *67*, 1.
- (352) Feinberg, J.; Macdonald, K. R. *Top. Appl. Phys.* **1989**, *62*, 151.
- (353) Chiou, A. E. *Proc. IEEE* **1999**, *87*, 2074.
- (354) Ono, H.; Kitamura, K.; Kawatsuki, N.; Norisada, H. *Jpn. J. Appl. Phys., Part 1* **2001**, *40*, 1328.
- (355) Ono, H.; Kitamura, K.; Kawatsuki, N. *Liq. Cryst.* **2002**, *29*, 1339.
- (356) Volodin, B. L.; Kippelen, B.; Meerholz, K.; Kukhtarev, N. V.; Caulfield, H. J.; Peyghambarian, N. *Opt. Lett.* **1996**, *21*, 519.
- (357) Volodin, B. L.; Kippelen, B.; Meerholz, K.; Peyghambarian, N.; Kukhtarev, N. V.; Caulfield, H. J. *J. Opt. Soc. Am. B* **1996**, *13*, 2261.
- (358) Feinberg, J.; Hellwarth, R. W. *Opt. Lett.* **1980**, *5*, 519.
- (359) White, J. O.; Cronin-Golomb, M.; Fischer, B.; Yariv, A. *Appl. Phys. Lett.* **1982**, *40*, 450.
- (360) Halvorson, C.; Kraabel, B.; Heeger, A. J.; Volodin, B. L.; Meerholz, K.; Sandalphon; Peyghambarian, N. *Opt. Lett.* **1995**, *20*, 76.
- (361) Vacar, D.; Heeger, A. J.; Volodin, B.; Kippelen, B.; Peyghambarian, N. *Rev. Sci. Instrum.* **1997**, *68*, 1119.
- (362) Nagayama, N.; Yokoyama, M. *Molec. Cryst. Liq. Cryst. Sci. Technol., Sect. A* **1999**, *327*, 19.
- (363) Sato, T.; Nagayama, N.; Yokoyama, M. *Molec. Cryst. Liq. Cryst.* **2001**, *370*, 115.
- (364) Banerjee, P. P.; Gad, E.; Hudson, T.; McMillen, D.; Abdeldayem, H.; Frazier, D.; Matsushita, K. *Appl. Opt.* **2000**, *39*, 5337.
- (365) Chun, H.; Joo, W. J.; Kim, N. J.; Moon, I. K.; Kim, N. *J. Appl. Polym. Sci.* **2003**, *89*, 368.
- (366) Bartkiewicz, S.; Sikorski, P.; Miniewicz, A. *Opt. Lett.* **1998**, *23*, 1769.
- (367) Ono, H.; Kawamura, T.; Kawatsuki, N.; Norisada, H. *Appl. Phys. Lett.* **2001**, *79*, 895.
- (368) Steele, D. D.; Volodin, B. L.; Savina, O.; Kippelen, B.; Peyghambarian, N.; Rockel, H.; Marder, S. R. *Opt. Lett.* **1998**, *23*, 153.
- (369) Singer, J. R.; Grunbaum, F. A.; Kohn, P.; Zubelli, J. P. *Science* **1990**, *248*, 990.
- (370) Moon, J. A.; Mahon, R.; Duncan, M. D.; Reintjes, J. *Opt. Lett.* **1994**, *19*, 1234.
- (371) Hyde, S. C. W.; Jones, R.; Barry, N. P.; Dainty, J. C.; French, P. M. W.; Kwolek, K. M.; Nolte, D. D.; Melloch, M. R. *IEEE J. Sel. Top. Quantum Electron.* **1996**, *2*, 965.
- (372) Scruby, C. B. *Ultrasonics* **1989**, *27*, 195.
- (373) Lahiri, I.; Pyrak-Nolte, L. J.; Nolte, D. D.; Melloch, M. R.; Kruger, R. A.; Bacher, G. D.; Klein, M. B. *Appl. Phys. Lett.* **1998**, *73*, 1041.
- (374) Klein, M. B.; Bacher, G. D.; Grunnet-Jepsen, A.; Wright, D.; Moerner, W. E. *Opt. Commun.* **1999**, *162*, 79.
- (375) Blouin, A.; Monchalain, J. P. *Appl. Phys. Lett.* **1994**, *65*, 932.
- (376) Khoo, I. C.; Shih, M. Y.; Wood, M. V.; Guenther, B. D.; Chen, P. H.; Simoni, F.; Slussarenko, S. S.; Francescangeli, O.; Lucchetti, L. *Proc. IEEE* **1999**, *87*, 1897.
- (377) Stegeman, G. I.; Segev, M. *Science* **1999**, *286*, 1518.
- (378) Stegeman, G. I. A.; Christodoulides, D. N.; Segev, M. *IEEE J. Sel. Top. Quantum Electron.* **2000**, *6*, 1419.
- (379) Peccianti, M.; De Rossi, A.; Assanto, G.; De Luca, A.; Umerton, C.; Khoo, I. C. *Appl. Phys. Lett.* **2000**, *77*, 7.
- (380) Peccianti, M.; Brzdakiewicz, K. A.; Assanto, G. *Opt. Lett.* **2002**, *27*, 1460.
- (381) Shih, M. F.; Sheu, F. W. *Opt. Lett.* **1999**, *24*, 1853.
- (382) Sheu, F. W.; Shih, M. F. *J. Opt. Soc. Am. B* **2001**, *18*, 785.
- (383) Hou, C. F.; Jiang, Y. Y.; Yuan, B. H.; Sun, X. D.; Du, C. G.; Li, S. Q. *Opt. Mater.* **2002**, *19*, 377.
- (384) Chen, Z. G.; Asaro, M.; Ostroverkhova, O.; Moerner, W. E.; He, M.; Twieg, R. J. *Opt. Lett.* **2003**, *28*, 2509.
- (385) Chen, Z.; Asaro, M.; Sheldon, M.; Ostroverkhova, O.; Moerner, W. E.; He, M.; Twieg, R. CLEO/IQEC, San Francisco, 2004.
- (386) Sassa, T.; Umegaki, S. *Opt. Lett.* **1997**, *22*, 856.
- (387) Sassa, T.; Wada, T.; Sasabe, H. *Opt. Lett.* **2001**, *26*, 995.
- (388) Fujihara, T.; Tokuue, M.; Umegaki, S.; Sassa, T.; Yokoyama, M. *Opt. Mater.* **2003**, *21*, 51.
- (389) Sassa, T.; Umegaki, S. *J. Appl. Phys.* **1998**, *84*, 4071.
- (390) Joo, W. J.; Kim, N. J.; Chun, H.; Moon, I. K.; Oh, C. H. *J. Appl. Phys.* **2002**, *91*, 6471.
- (391) Willets, K. A.; Ostroverkhova, O.; He, M.; Twieg, R. J.; Moerner, W. E. *J. Am. Chem. Soc.* **2003**, *125*, 1174.